Quantitative Modeling of Entangled Polymer Rheology: Experiments, Tube Models and Slip-Link Simulations

by

Priyanka Subhash Desai

A dissertation submitted in partial fulfillment
of the requirements for the degree of
Doctor of Philosophy
(Macromolecular Science and Engineering)
in the University of Michigan
2016

Doctoral Committee:

Professor Ronald G. Larson, Chair
Professor Richard E. Robertson
Professor Michael J. Solomon
Professor Alan S. Wineman

To my beloved grandparents - my life-coaches, whose role in my life was, and remains, monumental

ACKNOWLEDGEMENTS

As I conclude this tremendously gratifying chapter of my life as a PhD student and move on, there are a number of people who deserve to be both acknowledged and thanked, who have inspired me, mentored me, admonished me, without whom this endeavor would not have come to fruition.

Having a teacher to guide us in any path is invaluable. *A guru* is someone who is a "teacher, guide and a master" of certain knowledge and the one who leads the seeker on his journey toward wisdom. I would like to thank Prof. Ron Larson - my advisor, for being my guru. I consider myself to be immensely blessed to have had the great fortune of learning from him. Words would fail to describe the impact he has had in my evolution as a student and as an individual over these last few years. I am deeply indebted to my advisor to have received all of his patient support, ample supervision and guidance, and valuable feedback in both, my scientific and professional undertakings. Thank you, Ron.

I would like to thank Prof. Michael Solomon, Prof. Alan Wineman and Prof. Richard Robertson for serving on my thesis committee and for their constructive questions and insightful suggestions. I also want to acknowledge the extremely cordial and obliging staff in the Macromolecular Science and Engineering as well as the Chemical Engineering department, especially Nonna Hamilton, Adam Mael and Susan Hamlin for catering to my graduate student needs on numerous occasions.

I have been fortunate to have many fruitful collaborations. I would like to deeply acknowledge Prof. Seung Joon Park from Korea Polytechnic University for his invaluable guidance, in both, theory and experimental rheology, while his year-long stay as a visiting professor at the University of Michigan. I also wish to acknowledge Prof. Jay Schieber, from Illinois Institute of Technology and my fellow-PhD collaborator from his lab, Maria Katzarova, for their scientific direction and engaging discussions on slip-link simulations. I am also very

thankful to Prof. Jimmy Mays and his post-doc, Dr. Beom-Goo Kang, from the University of Tennessee and Prof. Nikos Hadjichristidis, from KAUST, Prof. Taihyun Chang and his post-doc, Dr. Sanghoon Lee, for neatly synthesizing and characterizing the invaluable star polymers for our experimental rheology study and model validation. I want to thank Prof. David Venerus and his student, Dan, from the Illinois Institute of Technology, for their hospitality and generous assistance with the RMS-800 rheometer during my brief research stay at IIT, Chicago.

Thanks are due to the immensely dedicated and bright undergraduate and high school students I have had a chance to mentor and learn from, while they contributed to and enhanced my various PhD projects. Especially, Jingyi Li, Qifan Huang, Caleb Steele and Alex Moyer. I wish them great luck and success in their academic lives.

I appreciate the endless support of all the current and past members of the Ron Larson research group – especially, Prateek Jha, Indranil Saha Dalal, Zuowei Wang, Nazish Hoda, Thomas Juhl, Miqiu Kong, Xueming Tang, Lei Jiang, Xue Chen, Ali Salehi, Elnaz Hajizadeh, Ryan Hall. I learnt quite a lot from Prateek and Ali while collaborating with them on the polyelectrolyte complexation and assembly work. Thanks to Indranil (sirji) for teaching me many a things about polymer physics and about *life* and always inspiring me to strive towards things that I enjoy. I truly appreciate your mentorship and friendship. I cherish hearty discussions over coffee breaks with Thomas and Indranil. I want to mention Xueming, Miqiu and Elnaz, my girlfriends in the Larson lab whose company I enjoyed very much. I want to thank Ryan for assisting me with rheology experiments and his lovely grandparents for generously welcoming me into their home in Chicago during our weeklong visit to IIT.

I also had an incredible opportunity to intern at P&G in the summer of 2014. I would like to thank Beth Schubert who is a senior scientist at P&G, who also served as my mentor during my time there. It was great fun to learn from such an accomplished scientist and a great teacher. I also wish to acknowledge my fellow P&G PhD intern cohort and good friends, Kellie, Anand and James.

This list will be incomplete without the mention of some of the genuinely incredible friends I made in Ann Arbor – Prao, Priyam, Avani, KP, Pallavi, Champa, Avanti, Deepika, Prasad, Mallory, Sandro, Philipp, Pauline, Shinchan, Gagan, Ashwin. And my friends from back

home – Deepthi, Jason, Kaustubh, Mugdha, Abhinav, Rhushabh, Kaushik, Smita, Mishra. I appreciate them for all the love, laughter and good times.

My family members deserve my utmost gratitude for their unrelenting trust in me. This thesis a manifestation of their love, support and countless sacrifices. Aai, pappa, aai, baba, Prerana, Sadhana kaku, maushi, all my mamas, my mamis and my cousins – thank you for making me the person I am.

Final words of acknowledgement are saved for someone really special – Sameer, thank you for your steadfast love and all-out support, I love you!

TABLE OF CONTENTS

LIST OF FIGURES

LIST OF TABLES

ABSTRACT

Rheology properties are sensitive indicators of molecular structure and dynamics. The relationship between rheology and polymer dynamics is captured in the constitutive model, which, if accurate and robust, would greatly aid molecular design and polymer processing. This dissertation is thus focused on building accurate and quantitative constitutive models that can help predict linear and non-linear viscoelasticity. In this work, we have used a multi-pronged approach based on the tube theory, coarse-grained slip-link simulations, and advanced polymeric synthetic and characterization techniques, to confront some of the outstanding problems in entangled polymer rheology.

First, we modified simple tube based constitutive equations in extensional rheology and developed functional forms to test the effect of Kuhn segment alignment on a) tube diameter enlargement and b) monomeric friction reduction between subchains. We, then, used these functional forms to model extensional viscosity data for polystyrene (PS) melts and solutions. We demonstrated that the idea of reduction in segmental friction due to Kuhn alignment is successful in explaining the qualitative difference between melts and solutions in extension as revealed by recent experiments on polystyrene (PS) solutions and melts. The idea of tube enlargement due to Kuhn segment orientation, on the other hand, failed when done self-consistently. We also applied a modified friction-based tube model to shear flows of PS melts and solutions to further study the impact of friction reduction in shear flows. We found that shear predictions are insensitive to the inclusion of orientation-dependent frictional effects, which is consistent with experimental observations. Additionally, we also reviewed tube theory based constitutive modeling of polymer melts and solutions under non-linear shear and extensional flows. Particularly, we focused on changes in rheological behavior as the concentration increases from un-entangled dilute, to entangled, to the dense melt. The rheological changes were captured by constitutive equations, prototypes of which are the “FENE-P” model for un-entangled solutions and the “DEMG” model for entangled solutions and melts.

Second, we compiled literature data and used it to develop a universal tube model parameter set namely, the equilibration time τ_e, the plateau modulus G_N^0, and the entanglement molecular weight M_e and prescribed their values and uncertainties for 1,4-polybutadiene by comparing linear viscoelastic G' and G" mastercurves for 1,4-PBds of various branching architectures. The high frequency transition region of the mastercurves superposed very well for all the 1,4-polybutadienes irrespective of their molecular weight and architecture, indicating universality in high frequency behavior of 1,4-polybutadienes. Therefore, all three parameters of the tube model were extracted from this high frequency transition region alone. This removes the freedom to adjust the tube parameters to fit various versions of the tube model to low- and moderate-frequency data, as has been done numerous times in the literature. In this way, tests of these tube models can be made more rigorously, by removing adjustable parameters.

Third, we compared predictions of two of the most advanced versions of the tube model, the Hierarchical model and the BoB (branch-on-branch) model against linear viscoelastic G' and G" data of binary blends of 1,4-PBd star and linear polymer melts. The star was carefully synthesized and characterized by temperature gradient interaction chromatography. We found massive failures of the tube models to predict the terminal relaxation behavior of the star/linear blends. This failure occurred regardless of the choices made concerning constraint release processes. In addition, these blends were also tested against a coarse-grained slip-link model, the "Cluster Fixed Slip-link Model (CFSM)" of Schieber and coworkers. The CFSM with only two molecular-weight and chain-architecture-independent parameters was able to give excellent agreement with all experimental data for the blends. Finally, the applicability of slip-link models as a direct means to repair constraint-release in tube models was discussed.

CHAPTER 1

Introduction

1.1. Motivation

In the past two decades, development in constitutive rheology modeling and molecular simulations has made it feasible for rheology to be used as an accurate and quantitative tool to link molecular structure to its flow properties in commercial polymeric systems. Rheology is considered to be one of the most sensitive indicators of a molecule's structure viz. its size, molecular weight, molecular weight distribution and branching. Molecular structure and subsequently rheology, in turn dictate a macromolecule's processing times and conditions during practical industrial applications such as extrusion, injection molding, blow film molding, fiber spinning etc. Under the various processing conditions, polymers exhibit complex response to the applied stress or strain, spanning from the linear viscoelastic regime where the stress varies linearly with deformation and the departure of the molecules from their equilibrium state is negligible to the non-linear viscoelastic regime where the deformation is large or rapid enough to stretch the molecules and shift them from their equilibrium position. Thus the ability of constitutive models to predict polymer flow and rheology accurately and robustly would greatly improve the performance of melt processing and aid to advancements in rational computational design of industrial polymer processing.

Our goal is develop constitutive equations of entangled polymers that can accurately relate the stress in the material with its deformation history. To accomplish this, the starting point was the development of the so-called *tube model* by Doi and Edwards[1] which arises from the notion that entanglements or topological constraints between the polymer chains create a tube-like region that confines the polymer to a quasi 1-D motion[2], the idea of *reptation* or snake-like motion of the chain within the tube developed by de Gennes[3] which led to further development and refinement in the constitutive framework in the subsequent papers by Doi and Edwards[4-7]. Within the linear viscoelastic phenomena, the tube model theory was further improved by

inclusion of the following additional relaxation mechanisms. a) Primitive path fluctuations[8] which allow the ends of the molecule to escape the tube faster than allowed by reptation. b) Constraint release relaxations, in which a "test" chain can relax because surrounding chains, which create the confinement of the test chain to the tube, at some point cease to act as confinements, due to their own motions. Particularly for the case of a mixture of long and short chains, the rapid movement of the short chains quickly dissolves the tube confining each long chain, thus allowing it to relax substantially faster than if it remained confined in the original tube[9]. c) Dynamic dilution or tube dilation introduced by Marrucci[10] where constraint release leads to a time-dependent enlargement of the tube diameter and consequent shortening of its path, thus not only speeding relaxation at intermediate times, but also reducing the terminal relaxation time of the polymer. The implementation of these meachanisms to predict linear viscoelasticity of simple monodisperse linear polymers[11], star polymers[12], mixtures of star with linear polymers[13], nearly monodisperse "H" polymers[14,15], and nearly monodisperse comb polymers[16,17] has opened the door for developing general tube theories and algorithms for polymers of commercial interest that are polydisperse in molecular weight and in number and type of long-chain branching. General theories for such polymers were introduced first by Larson and coworkers called the "Hierarchical" model[18-20], the "BoB" (Branch-on-Branch) model by Das, McLeish, Read, and coworkers[21], and by van Ruymbeke *et al.*[22]. These tube theory based models are now publically available, and have been fairly successful in predicting the linear rheology of complex mixtures of branched and linear polymers.

Furthermore, the basic tube theory was refined to incorporate nonlinear rheological effects during fast flows and large deformations by adding nonlinear molecular mechanisms like, a) large orientation of tube segments and the chains that are contained within the tube, b) chain stretch and retraction of those chains within the tube[23,24], and c) convective constraint release (CCR) caused by flow-induced displacement of chains relative to each other which causes loss of entanglements[25-28]. The resulting tube model with all the added ingredients has been quite successful in the non-linear viscoelastic regime but is continually challenged by new experimental evidences. For example, recent experiments in extensional rheology of linear monodisperse polystyrene melts by Nielsen *et al.*[29] and Huang *et al.*[30] show that their steady extensional viscosity η_E dependence on extension rate $\dot{\varepsilon}$ is significantly different from those for

entangled polystyrene solutions by Sridhar and coworkers[31,32], even if they have the same number of entanglements Z per chain.

1.2. Current problems with the tube models

The failures of current tube models, whose sources have been difficult to trace, include the following:

1.2.1. Failed rheological predictions in both linear and non-linear viscoelasticity

While the predictions of the tube theory agree in many cases with measured rheological properties, there are numerous cases where the predictions fail badly. The most embarrassing of these are for blends of a monodisperse star polymer with a monodisperse linear polymer. This is the simplest possible mixture that contains a branched species for which the tube theory fails[20].

In non-linear viscoelasticity, the tube model fails to predict the observed quantitative difference in extensional steady state viscosity between linear monodisperse entangled polymeric solutions and melts. Experiments on entangled polystyrene solutions show that when the strain rate is larger than the inverse Rouse time, the steady-state extensional viscosity increases with increasing strain rate[31,32]. In contrast, experiments on entangled polystyrene melts show that the steady-state extensional viscosity decreases monotonically even when the strain rate is larger than the inverse Rouse time[29,30] and the tube model fails to differentiate between the two.

1.2.2. Uncertainties in input parameters to the tube models

The Hierarchical tube model version developed by Larson and coworkers uses two different sets of parameters values, the so-called "Park" values, from the work of Park, *et al.*[19], and the "Das" values, from Das *et al.*[21]. Perhaps the best-known difference between these parameters sets is the value of the so-called "dilution exponent," α, which controls the rate at which the tube expands its diameter as polymer chains relax[33]. Details describing the tube dilation process can be found in Milner and McLeish[12]. Two different theoretical concepts, one that focuses on entanglements as pair-wise interactions between chains and the other one treating entanglements as a collective phenomenon[34] give the two values $\alpha=1$ and $\alpha=4/3$, that are used in the Das and Park parameter sets, respectively. While these values are close to each other, because they are exponents on quantities that are inside an exponential function, the small

difference between them has a big impact on predictions. The uncertainty in these parameters is an outstanding problem in rheology that has stubbornly resisted numerous attempts at resolving it[35-37]. There are uncertainties in other parameter values as well, including uncertainty in the coefficient ν of the potential that controls the distribution of tube lengths. This has a value that is usually taken to be 3/2, but which some studies suggest might be lower than this[38,39]. It has not been possible to resolve which values of these parameters lead to best agreement with data, because the level of agreement depends on the particular data set chosen, and because there are multiple parameters whose values are uncertain. Thus, a change in α from 4/3 to 1 can for some data sets be offset by a compensating change in another constant, for example ν from 3/2 to 1. Recent work even suggests that neither of these "constants" is really constant, but that ν can decrease with increasing polymer molecular weight[39] and α can increase with time of relaxation[37].

Furthermore, there is a fair amount of variability in the three most fundamental tube model parameters viz, τ_e, the equilibration time or the Rouse time of one entanglement spacing, G_N^0, the plateau modulus and M_e, molecular weight between one entanglement spacing. For instance, comparison of these tube parameters of 1,4-polybutadienes from different sources/groups reveals that G_N^0 and M_e vary by about 70% and the value of τ_e at T=25°C varies by a factor of 5, and τ_e is used as a fitting parameter to fit the theory to specific data sets for linear or branched 1,4-polybutadienes[40].

1.2.3. Uncertainties in polymer characterization

Through anionic synthesis, it has long been possible to make model linear polymers of nearly uniform molecular weight. However, when long-chain branched polymers are synthesized, at least two steps are required in the synthesis, even for the simplest star-branched polymer with one branch point, and more than two steps are required for more complex polymers, such as "H" polymers which have two branch points. This requires creating "living" polymer arms in one step that are then linked together or attached to other polymers in a second reaction step. These linkage reactions can produce defects, such as arms that fail to link, or extra arms that link when they should not. Thus, a three-arm star may contain two-arm and four-arm

byproducts as well as possibly unlinked free arms. Impurities can be partially removed by precipitation in non-solvent, but this rarely gives a clean separation, especially when the polymers are not greatly different in molecular weight, as is usually the case in synthesis of specialty anionic polymers. In principle, the presence of the impurities can be detected by size-exclusion chromatography (SEC). However, defective structures and impurities whose molecular weights differ by less than a factor of two or three from that of the main product usually are not resolved by SEC as separate peaks, but only appear as a modest widening of the main peak. Thus, although relatively narrow SEC peaks are often taken as evidence of "nearly monodisperse" samples, and the rheology of these samples are then used to test rheological theories, the samples may actually contain significant amounts of impurities. We have learned that these samples can contain previously undetected impurities due to the recent development of Temperature Gradient Interaction Chromatography (TGIC), which vastly improves chromatographic separation efficiency, and exposes the previously unresolved peaks[41,42].

1.2.4. Uncertainties in accuracy of the tube models

Finally, there are reasons to doubt that current versions of the tube model are really completely up to the task of predicting the rheology of complex branched polymers, which have polydispersity in both molecular weight and in branching. The tube model is a coarse-grained mean-field model that resolves dynamics only at the scale of the distance between entanglements (typically several nanometers or more). While we hope the tube model will be accurate for the long-time relaxation processes important for polymer rheology, there is the possibility that the model may simply be insufficiently accurate for reliable quantitative predictions of complex branched polymers. Given the uncertainties discussed above, we cannot be sure either way. Resolving decisively the accuracy of the tube model will require assessing a range of polymer melts, characterizing their impurities, accounting for their effect on rheology, and pinning down the best parameters of the tube model. And it will require carrying out simulations with finer-scale models, such as molecular dynamics simulations or "slip-link" models[43-45] that simulate dynamics at or below the scale of the entanglement spacing.

Slip-link simulations[43-48] are coarse-grained stochastic simulations for resolving long-time behavior which have emerged as alternatives to tube models. These are coarse-grained molecular simulations involving ensembles of chains that are represented explicitly on a

computer. In such models, the "tube" which confines the chain *globally* along its length is replaced by "slip-links" that permit chain sliding, but impose *local* constraints on the path along which the sliding takes place. Reptation and local Rouse motions along chains are typically allowed in slip link models. Constraint release arises through disappearance and appearance of slip-links imposed when chain ends pass through a slip link or migrate far enough from a previous slip link to create a fresh slip link. A major advantage of slip-link models is that, in doing away with the tube, no accounting need be made of "tube dilation," or constraint release events, but instead these processes arise naturally from the constrained motion of the chains and the appearance and disappearance of slip links.

1.3. Objectives and outline

This thesis attempts to answer some of the inadequacies and problems mainly within the tube-based constitutive modeling framework and introduces slip-link simulations when the tube model approach fails. We will use a multi-pronged approach of that tube based constitutive model theory, coarse-grained slip-link simulations, use of the most advanced polymeric synthetic and characterization techniques which will help shed light on some of the inadequacies discussed above. This work uses new rheological data on star/linear polymers which will help us determine if the tube model is "up to the task" of correctly modeling complex branched polymer melts. We believe that this combined experimental, theoretical, and computational effort, will provides enough "firepower" to resolve some of the most troubling remaining problems in entangled polymer rheology.

The thesis is organized as follows:

In Chapter 2 we review tube theory based constitutive modeling of polymer melts and solutions under non-linear shear and extensional flows. Here, we focus on changes in rheological behavior as the concentration increases from un-entangled dilute, to entangled, to dense melt. The rheological changes are captured by constitutive equations, prototypes of which are the "FENE-P" model for un-entangled solutions and the "DEMG" model for entangled solutions and melts. We also discuss the practical implications of viscosity and concentration differences between un-entangled and entangled systems in shear and extension, on their applicability in

commercial processing like fiber drawing and understanding instabilities like edge-fractures, normal stress differences.

Chapter 3 focuses on the development of one such constitutive model for the nonlinear rheology of entangled melts and solutions. It discusses the development of a simple constitutive model based on Kuhn segment alignment that predicts the observed monotonic extension thinning in steady state viscosity η_E even at extension rates above the inverse Rouse time $\left(\dot{\varepsilon} > \tau_R^{-1}\right)$ for entangled polystyrene melts[29], while preserving the extension thickening typically seen in entangled solutions[31] for $\dot{\varepsilon} > \tau_R^{-1}$. We test two mechanisms by which Kuhn segment alignment affect rheology within the tube model. First is the effect of Kuhn segment alignment on tube diameter increase inferred from ideas of Doi and Edwards[1] and Sussman and Schweizer[49], which fails and the second is the idea of reduction in segmental friction due to Kuhn alignment, as described in recent work of Yaoita *et al.*[50] which is successful. The modified tube model is then compared against the available experimental data on steady-state extensional flows for both entangled solutions and melts to check for consistency.

Switching gears to problems in linear viscoelasticity, Chapter 4 aims at reducing the observed variability and offers strict variability limits for the three basic tube model parameters, τ_e, G_N^0, and M_e, by comparing the high frequency linear viscoelastic G' and G" mastercurves for linear, star, H, and comb 1,4-polybutadienes from the literature. We fit this high frequency transition data to the Rouse model after subtracting out the effects of glassy modes using the Kohlrausch-Williams-Watts (KWW) expression and extract out an accurate value for the equilibration time τ_e which is needed as an input parameter in the tube models. We also compare the WLF shift factors of 1,4-polybutadienes with differing 1,2-vinyl content available in literature in an attempt to fix variability limits to the values of plateau modulus, G_N^0 and thus the entanglement molecular weight, M_e since they are related by the formula, $G_N^0 = \frac{4}{5}\frac{\rho RT}{M_e}$.

In Chapter 5, we analyze, in detail, the failure of the available tube models to accurately describe the linear viscoelasticity of binary blends of 1,4-PBd star and linear polymer melts. Carefully synthesized and accurately characterized star polymer is used in this study. Finally, the

blends are tested against a coarse-grained slip-link model, called the "Cluster Fixed Slip-link Model (CFSM)" of Schieber and coworkers[51]. The CFSM is found to give excellent agreement with all the experimental data. Finally, the success of slip-link models is used to gain an improved understanding of constraint release effects within the tube model framework. Conclusions and future outlook on the work are given in Chapter 6.

1.4. References

1. Doi, M., Edwards, S. F. *The theory of polymer dynamics*, 2nd ed.; Clarendon: Oxford (1988)
2. Edwards, S. F., "The statistical mechanics of polymerized material," *Proc. Phys. Soc.* 92, 9 (1967)
3. de Gennes, P. G., "Reptation of a polymer chain in the presence of fixed obstacles," *J. Chem. Phys*. *55*, 572 (1971)
4. Doi, M., Edwards, S. F., "Dynamics of concentrated polymer systems, part 1 - Brownian motion in the equilibrium state," *J. Chem. Soc., Faraday Trans. 2: Mol. and Chem. Phys.* 74, 1789 (1978)
5. Doi, M., Edwards, S. F., "Dynamics of concentrated polymer systems, part 2 - molecular motion under flow," *J. Chem. Soc., Faraday Trans. 2: Mol. and Chem. Phys.* 74, 1802 (1978)
6. Doi, M., Edwards, S. F., "Dynamics of concentrated polymer systems, part 3 - the constitutive equation," *J. Chem. Soc., Faraday Trans. 2: Mol. and Chem. Phys.* 74, 1818 (1978)
7. Doi, M., Edwards, S. F., "Dynamics of concentrated polymer systems, part 4 - rheological properties," *J. Chem. Soc., Faraday Trans. 2: Mol. and Chem. Phys.* 38, DE4 (1979)
8. Milner, S. T., McLeish, T. C. B., "Reptation and contour-length fluctuations in melts of linear polymers," *Phys. Rev. Lett.* 81, 725 (1998)
9. Viovy, J. L., Rubinstein, M., Colby, R. H., "Constraint release in polymer melts: Tube reorganization versus tube dilation," *Macromolecules* 24, 3587 (1991)
10. Marrucci, G., "Relaxation by reptation and tube enlargement - a model for polydisperse polymers," *J. Polym. Sci., Polym. Phys. Ed.* 23, 159 (1985)
11. Milner, S. T., McLeish, T. C. B., "Reptation and contour-length fluctuations in melts of linear polymers," *Phys. Rev. Lett.* 81, 725 (1998)
12. Milner, S. T., McLeish, T. C. B., "Parameter-free theory for stress relaxation in star polymer melts," *Macromolecules* 30, 2159 (1997)
13. Milner, S. T., McLeish, T. C. B., Young, R. N., Hakiki, A., Johnson, J. M., "Dynamic dilution, constraint-release, and star-linear blends," *Macromolecules* 31, 9345 (1998)
14. McLeish, T. C. B., Allgaier, J., Bick, D. K., Bishko, G., Biswas, P., Blackwell, R., Blottiere, B., Clarke, N., Gibbs, B., Groves, D. J., Hakiki, A., Heenan, R. K., Johnson, J. M., Kant, R., Read, D. J., Young, R. N., "Dynamics of entangled H-polymers: Theory, rheology, and neutron-scattering," *Macromolecules* 32, 6734 (1999)
15. Daniels, D.R., McLeish, T. C. B., Kant, R., Crosby, B. J., Young, R. N., Pryke, A., Allgaier, J., Groves, D. J., Hawkins, R. J., "Linear rheology of diluted linear, star and model long chain branched polymer melts," *Rheol. Acta.* 40, 403 (2001)
16. Daniels, D. R., McLeish, T. C. B., Crosby, B. J., Young, R. N., Fernyhough, C. M., "Molecular rheology of comb polymer melts. 1. Linear viscoelastic response," *Macromolecules* 34, 7025 (2001)
17. Inkson, N. J., Graham, R. S., McLeish, T. C. B., Groves, D. J., Fernyhough, C. M., "Viscoelasticity of monodisperse comb polymer melts," *Macromolecules* 39, 4217 (2006)
18. Larson, R. G., "Combinational rheology of branched polymer melts," Macromolecules 34, 4556 (2001)

19. Park, S. J., Shanbhag, S., Larson, R. G., "A hierarchical algorithm for predicting the linear viscoelastic properties of polymer melts with long-chain branching," *Rheol. Acta* 44, 319 (2005)
20. Wang, Z., Chen, X., Larson, R. G., "Comparing tube models for predicting the linear rheology of branched polymer melts," *J. Rheol.* 54, 223 (2010)
21. Das, C., Inkson, N. J., Read, D. J., Kelmanson, M. A., McLeish, T. C. B., "Computational linear rheology of generally branch-on-branch polymers," *J. Rheol.* 50, 207 (2006)
22. van Ruymbeke, E., Bailly, C., Keunings, R., Vlassopoulos, D., "A general methodology to predict the linear rheology of branched polymers," Macromolecules, 39, 18, 6248 (2006)
23. Marrucci, G., Grizzuti, N., "Fast flows of concentrated polymers: Predictions of the tube model of chain stretching," *Gazz. Chim. Ital.* 118, 179 (1988)
24. Pearson, D. S., Herbolzheimer, E., Grizzuti, N., Marrucci, G., "Transient behavior of entangled polymers at high shear rates", *J. Polym. Sci.: Part B: Polym. Phys.* 29, 1589 (1991)
25. Marrucci, G., "Dynamics of entanglements: A nonlinear model consistent with the Cox-Merz rule," *J. Non-Newt. Fluid Mech.* 62, 279 (1996)
26. Mead, D.W., Larson, R. G., Doi, M., "A molecular theory for fast flows of entangled polymers," *Macromolecules* 31, 7895 (1998)
27. Ianniruberto, G., Marrucci, G., "A simple constitutive equation for entangled polymers with chain stretch," *J. Rheol.* 45, 1305 (2001)
28. Marrucci, G., Ianniruberto, G., "Flow-induced orientation and stretching of entangled polymers," *Proc. Trans. R. Soc. Lond. A* 361, 677 (2003)
29. Nielsen, J. K., Rasmussen, H. K., Hassager, O., McKinley, G. H., "Elongational viscosity of monodisperse and bidisperse polystyrene melts," *J. Rheol.* 50, 453 (2006)
30. Huang, Q., Mednova, O., Rasmussen, H. K., Alvarez, N. J., Skov, A. L., Almdal, K., Hassager, O., "Concentrated polymer solutions are different from melts: Role of entanglement molecular weight," *Macromolecules* 46, 5026 (2013a)
31. Bhattacharjee, P. K., Oberhauser, J. P., McKinley, G. H., Leal, L. G., Sridhar, T., "Extensional rheometry of entangled solutions," *Macromolecules* 35, 10131 (2002)
32. Ye, X., Larson, R. G., Pattamaprom, C., Sridhar, T., "Extensional properties of monodisperse and bidisperse polystyrene solutions" *J. Rheol.* 47, 2, 443 (2003)
33. Colby, R. H., Rubinstein, M., "Two-parameter scaling for polymers in solvents," *Macromolecules* 23, 2753 (1990)
34. Milner., S., "Predicting the tube diameter in melts and solutions," *Macromolecules* 38, 4929 (2005
35. Tao, H., Huang, C., Lodge, T. P., "Correlation length and entanglement spacing in concentrated hydrogenated polybutadiene solutions," *Macromolecules* 32, 1212 (1999)
36. Park, S. J., Larson, R. G., "Dilution exponent in the dynamic dilution theory for polymer melts," *J. Rheol.* 47, 1999 (2003)
37. van Ruymbeke, E., Masubuchi, Y., Watanabe, H., "Effective value of the dynamic dilution exponent in bidisperse linear polymers: from 1 to 4/3," 45, 4, 2085 (2012)
38. Shanbhag, S., Larson, R.G., "Chain retraction potential in a fixed entanglement network," *Phys. Rev. Lett*. 94, 076001 (2005)

39. Khaliullin, R. N., Schieber, J. D., "Analytic expressions for the statistics of the primitive - path length in entangled polymers," *Phys. Rev. Lett.* 100, 188303 (2008)
40. Park, S. J., Desai, P. S., Chen, X., Larson, R. G., "Universal relaxation behavior of entangled 1,4-polybutadiene melts in the transition frequency region," *Macromolecules* 48, 4122 (2015)
41. Chang, T., "Polymer characterization by interaction chromatography," *J. Polym. Sci., Part B: Polym. Phys.* 43, 1591 (2005)
42. Rahman, M. S., Aggarwal, R., Larson, R. G., Dealy, J. M., Mays, J., "Synthesis and Dilute Solution Properties of Well-Defined H-Shaped Polybutadienes," *Macromolecules* 41, 8225 (2008)
43. Masubuchi, Y., "Simulating the flow of entangled polymers," *Annu. Rev. Chem. Bio. Eng.* 5, 11 (2014)
44. Schieber, J. D., Andreev, M., "Entangled polymer dynamics in equilibrium and flow modeled through slip links," *Annu. Rev. Chem. Bio. Eng.* 5, 367 (2014)
45. Jensen, M. K., Khaliullin, R., Schieber, J. D., "Self-consistent modeling of entangled network strands and linear dangling structures in a single strand mean-field slip-link model," *Rheol. Acta* 51, 21 (2012)
46. Schieber, J. D., "Fluctuations in entanglements of polymer liquids," *J. Chem. Phys.* 118, 5162 (2003)
47. Likhtman, A. E., "Single-chain slip-link model of entangled polymers: Simultaneous description of neutron spin−echo, rheology, and diffusion," *Macromolecules* 38, 14 (2005)
48. Pilyugina, E., Andreev, M., Schieber, J. D., "Dielectric relaxation as an independent examination of relaxation mechanisms in entangled polymers using the discrete slip-link model," *Macromolecules* 45, 5728 (2012)
49. Sussman, D. M., Schweizer, K. S., "Microscopic theory of quiescent and deformed topologically entangled rod solutions: General formulation and relaxation after nonlinear step strain," *Macromolecules* 45, 3270 (2012a)
50. Yaoita, T., Isaki, T., Masubuchi, Y., Watanabe, H., Ianniruberto, G., Marrucci, G., "Primitive chain network simulation of elongational flows of entangled linear chains: Stretch/orientation-induced reduction of monomeric friction," *Macromolecules* 45, 2773 (2012)
51. Andreev, M., Feng, H., Yang, L., Schieber, J. D., "Universality and speedup in equilibrium and nonlinear rheology predictions of the fixed slip-link model," *J. Rheol.* 58, 723 (2014)

CHAPTER 2

Constitutive modeling of polymer melts and solutions in non-linear shear and extensional flows

2.1. Abstract

This chapter reviews the constitutive modeling of solutions and melts of linear polymers, focusing on changes in rheological behavior in shear and extensional flow as concentration increases from un-entangled dilute, to entangled, and finally, to a dense melt. The rheological changes are captured by constitutive equations, prototypes of which are the "FENE-P" model for un-entangled solutions and the "DEMG" model for entangled solutions and melts. From these, and supporting experimental data, for dilute solutions, the extensional viscosity increases with strain rate from the low-strain-rate to the high-strain-rate asymptote, but in the densely entangled state, the high-strain-rate viscosity is lower than the low-shear-rate value, especially when orientation-dependent friction is accounted for. The next chapter, chapter 3 discusses in depth, the development of one such constitutive model that can accurately describe the flow of densely entangled linear polymer melt under extension by including orientation-dependent functional forms for segmental friction. In shearing flow, shear thinning increases drastically as the entanglement density increases, which can eventually lead to a shear-banding inhomogeneity. Recent improvements in constitutive modeling are paving the way for robust and accurate numerical simulations of polymer fluid mechanics and industrial processing of polymers. (**Part of the text and figures in this chapter are reprinted with permission from Larson, R. G. and P. S. Desai, *Annu. Rev. Fluid Mech.,* 47, 47–65 (2015), R. G. Larson is the lead author of this publication)**

2.2. Introduction

While the most studied nonlinearities in fluid mechanics are inertial, governed by the Reynolds number $\mathrm{Re} \equiv \rho v D / \eta$ (where ρ is the fluid density, v the characteristic fluid velocity, D the characteristic length scale of the flow, and η the viscosity), polymeric fluids often have high viscosities (η > 10 Pa s), so that inertial effects can be neglected. However, since the viscosity η of a polymeric fluid can be approximated by a product of its modulus G and its *longest relaxation time* τ, a small value of Re often implies a large value of the dimensionless *Weissenberg number* $Wi \equiv \tau\dot{\gamma} = \eta v / DG$ which characterizes the strength of viscoelastic effects in the flows[1,2]. The Weissenberg number is a measure of nonlinearities due to polymer flow-induced deformation. Here G is the *modulus* of the fluid, $\tau \sim \eta / G$ approximates the longest relaxation time of the fluid, and $\dot{\gamma} \sim v / D$ is a characteristic strain rate. The product of Re and Wi is $\mathrm{Re} \cdot Wi = \rho v^2 / G$. Since melts and concentrated solutions of polymers typically have moduli G of order 10^3 to 10^6 Pa and density of around 10^3 kg/m^3, we find that $\mathrm{Re}Wi \sim 10^{-3} \cdot v^2 \; to \; 1 \cdot v^2$, where v is in m/s. This implies that if Re becomes very small, Re < 10^{-5} (due to high fluid viscosity or thin gap), the Weissenberg number Wi will frequently be larger than unity, unless the flow velocity is small (v < 0.1 m/s). The above considerations imply that Stokes flows are relatively rare in industry or in nature – fast, macroscopic flows that avoid inertial nonlinearities will often contain viscoelastic ones.

Several of the best-known viscoelastic nonlinear flow phenomena are illustrated in Figure 2.1. While nonlinear flow phenomena arising from inertial effects are often well understood quantitatively, viscoelastic nonlinearities, such as those depicted in Figure 2.1, are often understood only semi-quantitatively, if that. The main reasons for this relate to the constitutive equations for polymeric fluids, namely: 1) their lack of accuracy, 2) their lack of generality, and 3) the difficulty of solving flow problems, especially when using the most accurate of these constitutive equations[3,4]. For inertial nonlinearities in Newtonian fluids, the constitutive equation is of course the well-known Navier-Stokes equation, which applies with great accuracy to many common fluids. Quantitative predictions can therefore often be made for inertial nonlinear phenomena, including instabilities. Despite the lack of quantitative predictions for viscoelastic flows, qualitative and even semi-quantitative predictions of many phenomena, including those

depicted in Figure 2.1, have been attained[5-7]. Further improvements will require more accurate constitutive equations that retain enough simplicity to allow numerical solution of complex flows such as these.

The most significant nonlinear phenomena in polymeric liquids include[1,8]: 1) shear thinning, 2) normal stress differences in shear, 3) extensional thickening, and 4) nonlinear memory of deformation history. Phenomena that are caused by shear thinning can include: nonlinear relationships between flow rate and stress or pressure drop, shear banding, and wall slip[9,10]. Normal stress differences produce: rod climbing (see Figure 2.1a), edge fracture in torsional shearing flow (Figure 2.1b), and elastic instabilities[11] (Figure 2.1c). High extensional viscosity can produce: stable fiber or film formation, tubeless siphon flow (Figure 2.1d), and turbulent drag reduction. Finally, nonlinear fluid memory produces: large elastic recoil, extrudate swelling (Figure2.1e), and fluid bouncing[12] (Figure 2.1f). All of these are nonlinear viscoelastic phenomena that emerge at flow rates high enough to greatly deform polymer molecules.

Many flow phenomena distinctive to polymeric fluids have already been explained at least qualitatively. However, quantitative predictions remain very challenging, hampering computational design of industrial polymer processing. Thus, simulations of polymer processing applications such as film blowing or fiber spinning are typically much less precise than those that used in the computational design of drag and lift on aircraft or automobiles. To bring practical prediction of polymeric flows closer to the accuracy possible for simple Newtonian fluids, constitutive equations are needed that possess the right combination of accuracy, versatility, and computational tractability. This chapter reviews the development of constitutive equations for polymeric fluids, discussing relevant polymer physics as needed.

Figure 2.2 illustrates the relevant properties of the polymers. In the absence of flow, long flexible polymers take on coil configurations, whether in solution or the melt. The simplest description of these coils is that of a random walk, with random walk step size b_K and total number of random walk steps N_K. The step size b_K is several times the backbone bond length for ordinary synthetic polymers, and so is around 1 nm or so[13]. For stiff biological polymers, like double-stranded DNA, b_K can be 100 nm or so, or even higher. The root mean square distance

separating the ends of the polymer molecule is then $R = \langle R^2 \rangle_0^{1/2} = N_K^{1/2} b_K$, while the fully extended length, or contour length of the polymer, is $L = N_K b_K$. The maximum "stretch" of the molecule is defined by L divided by R; that is $\lambda_{\max} \equiv L / \sqrt{\langle R^2 \rangle_0} = \sqrt{N_K}$. For long flexible synthetic polymers, N_K can be in the range of 100 to 10,000 or so, since each Kuhn step corresponds to a molecular weight of 100 to 1000 Daltons, and the polymer molecular weight typically ranges from 10,000 to a few million Daltons. Polymer coils in solution are usually not defined precisely by random walks, even on large distance scales, since polymers can swell or shrink depending on the polymer-solvent physical interactions, such as van der Waals interactions[14,15]. This shrinking or swelling is accounted for by introducing an exponent ν in the expression $\langle R \rangle_0^2 \sim N_K^{2\nu} b_K$, or for some purposes it can be subsumed into the parameter $\lambda_{\max}$.

In addition to chain length and flexibility, polymer concentration plays an important role in rheology. In general, long polymer chains "*entangle"* with each other unless their concentration is low. The degree of entanglement varies from sparse to dense in entangled solutions or solvent-free melts, depending on polymer length L, stiffness b_K, and concentration c (in mass per unit volume). While the notion of an "entanglement" is still not completely defined or agreed upon, the effects of entanglements on rheology are profound and well understood at a phenomenological level[14]. We will discuss entanglement effects in more detail later, in Section 2.3.

The need to specify polymer solution properties sets polymeric fluids apart from Newtonian fluids, for which only viscosity and density are needed to define the properties relevant to flow. For polymeric fluids, in addition to density and viscosity, at a bare minimum the polymer *stretch relaxation time* τ_s is also needed, and for strong flows, one also needs the *polymer extensibility* $\lambda_{\max}$ defined above. The above two parameters τ_s and $\lambda_{\max}$ barely suffice for dilute solutions; for more concentrated solutions or melts, at least one additional relaxation time is needed, namely the polymer *orientation or "disengagement time"* τ_d. The ratio τ_d / τ_s of the orientational relaxation time to the stretch relaxation time depends on the degree of intermolecular entanglement of the polymer molecules. For dilute solutions, these two relaxation

times become nearly equal to each other apart from a factor of two: $\tau \equiv \tau_s/2 = \tau_d$. Thus, in addition to a Reynolds number and a Weissenberg number, $\lambda_{\max}$ and τ_d/τ_s (for entangled polymers) are additional dimensionless groups affecting flow behavior, and these are controlled by polymer molecular length, stiffness, and concentration. In truth, it is likely that even these additional dimensionless groups are inadequate to define the fluid's rheology in enough detail to allow accurate predictions of polymer flow.

Even after the fluid properties are defined, one confronts the reality that a constitutive equation that can describe one polymeric fluid might be inadequate for another. This is a complication largely absent for Newtonian fluids, for which the empirical hypothesis of Newton – that local fluid stress is proportional to the instantaneous rate of fluid deformation – suffices to specify the constitutive equation. For polymeric fluids, however, there is a need to distinguish fluids based on their level of molecular entanglement, which strongly influences the rheology. The focus here will be on linear polymers of relatively high molecular weight, which can become densely entangled and whose behavior differs most dramatically from that of ordinary Newtonian fluids. The four basic phenomena – shear thinning, normal stress difference, extension thickening, and memory-change noticeably as polymer concentration and entanglement density increases, as discussed in what follows.

We will focus our attention on two basic types of flow, namely extensional and shear flow, depicted in Figure 2.3. Extensional flow possesses no vorticity, while in shearing flow the rate of rotation of a fluid element equals the rate of straining. Polymer molecules are persistently stretched in an extensional flow, while in a shear flow, the rotation of fluid elements leads to alternating periods of stretching and compression of polymer molecules, as depicted in Figure 2.3b. In the most common extensional flow, called *uniaxial extension*, the fluid is stretched along one axis (axis "1" in Figure 2.3a) and shrinks equally along the other two directions, ultimately resulting in drawing of the fluid into an elongated fiber. Constitutive equations might perform well in shear but not in extension, or vice versa, and if an equation performs well in both types of flow, at steady state and during transients, it has a good chance at performing reasonably well in other deformations (which can be considered combinations of shear and extension). In this study, we concentrate on nearly monodisperse *linear* polymers that lack long-chain branching, and contain only pure, chemically homogeneous polymer and solvent, without solid or other

immiscible fluid additives. We will, however, discuss in a limited way the effects of polydispersity and long-chain branching where appropriate, since they are so important in many of the most common commercial polymers.

2.3. Theoretical framework: The FENE-P and tube models

As alluded to above, the most basic distinction among polymeric fluids is their state of *entanglement*. Solutions of polymers that are said to be *dilute* are dominated by the dynamics of individual chains within the surrounding (Newtonian) solvent, with negligible chain-chain interactions. For long polymers with molecular weights exceeding a few hundred thousand Daltons, the polymer volume fraction can be no higher than around 1% for it to remain dilute. Polymeric fluids of greatest importance in applications usually involve polymer molecular weights and concentrations too large to neglect entanglement effects. Nevertheless, un-entangled dilute solutions are important in several ways: 1) Some important flow phenomena, such as polymer turbulent drag reduction, occur in un-entangled dilute solutions. 2) Some aspects of dilute solution rheology carry over to entangled solutions, and these aspects are most easily understood in dilute solutions where the complications from entanglements are absent. 3) Although concentrated solutions and melts are usually strongly affected by entanglements, we will see that entanglement effects are weakened significantly at high strain rates, where even concentrated solutions exhibit behaviors that resemble those of dilute solutions. We therefore start with a simplified explanation of the rheology and constitutive modeling of dilute solutions.

2.3.1. Dilute solutions: The FENE-P model

Dilute solution rheology in the nonlinear regime is dominated by: 1) Brownian forces, 2) frictional forces proportional to the velocity of the solvent relative to the polymer, 3) elastic (or "spring") forces from the deformed polymer, 4) finite extensibility of the polymer molecules, and 5) multiple relaxation modes[16]. In addition to these, there are excluded volume interactions and hydrodynamic interactions in dilute solutions, whose importance depends on solvent-polymer interactions, and on polymer length and flexibility. The effects of these are reviewed in some detail in Larson[16]. If the fifth consideration, the multiple relaxation modes, is ignored, a serviceable constitutive equation for dilute solutions of flexible polymers, which includes the other four important influences, is the "FENE-P" model, which stands for "Finitely Extensible

Nonlinear Elastic" (FENE) model[16,17]. Here the "P" means that the "Peterlin" pre-averaging approximation is used to obtain a closed-form constitutive equation. We can write this constitutive equation in terms of the "configuration tensor" $\underline{\underline{S}} \equiv \langle \underline{R}\underline{R} \rangle / \langle R^2 \rangle_0$, where $\underline{R}$ is the end-to-end vector of the spring and $\langle R^2 \rangle_0$ is the mean-square end-to-end spring length at equilibrium (i.e., in the absence of flow). From this, we can define the relative stretch λ of the spring such that $\lambda^2 \equiv \langle R^2 \rangle / \langle R^2 \rangle_0 = S / \langle R^2 \rangle_0$, where $S \equiv trace(\underline{\underline{S}})$. The maximum stretch of the spring is specified by the parameter λ_{max}, defined earlier, which limits the extension of the spring, since the spring force diverges as the spring stretch λ approaches λ_{max}. The following, then, is one version of the FENE-P constitutive model[15]:

$$\overset{\nabla}{\underline{\underline{S}}} + \frac{1}{\tau}\left(k_s \underline{\underline{S}} - \frac{1}{3}\underline{\underline{\delta}} \right) = \underline{\underline{0}} \tag{1}$$

$$k_s = \frac{1}{3}\left(3\lambda_{max}^2 - \lambda^2\right) / \left(\lambda_{max}^2 - \lambda^2\right) \tag{2}$$

$$\underline{\underline{\sigma}}_p = 3Gk_s \underline{\underline{S}} \tag{3}$$

$$\underline{\underline{\sigma}}_s = \mu_s \left(\underline{\nabla v} + (\underline{\nabla v})^T \right) \tag{4}$$

$$\underline{\underline{\sigma}} = \underline{\underline{\sigma}}_p + \underline{\underline{\sigma}}_s \tag{5}$$

The symbol "∇" above the orientation tensor $\underline{\underline{S}}$ denotes the "upper convected derivative," defined by:

$$\overset{\nabla}{\underline{\underline{S}}} \equiv \frac{\partial}{\partial t}\underline{\underline{S}} - \underline{\underline{\kappa}} \cdot \underline{\underline{S}} - \underline{\underline{S}} \cdot \underline{\underline{\kappa}}^T \tag{6}$$

and $\underline{\underline{\kappa}} \equiv (\underline{\nabla v})^T$ is the transpose of the velocity gradient tensor. Eq. 1 describes the deformation of the polymer in flow and the relaxation of that deformation during flow and when flow ceases. The tensor $\underline{\underline{\delta}}$ in Eq. 1 is the unit tensor. The time constant governing the stress relaxation is $\tau = \tau_s / 2$, which in dilute solution scales with chain length as $\tau \propto N_K^{3\nu} \propto L^{3\nu}$; where the value of

3ν is set by the degree of polymer swelling in the solvent and is in the range 1.5 to 1.8 or so. If the polymer is not dilute, but also not concentrated enough to be entangled, then the scaling law should be roughly $\tau \propto N_K{}^2 \propto L^2$. The stress relaxation time τ is also proportional to the monomeric friction coefficient ζ, which is proportional to the solvent viscosity in dilute solution, and is strongly influenced by polymer-polymer friction in concentrated solutions or melts. This stress relaxation time constant is related to autocorrelation time, or "stretch relaxation time" τ_s by $\tau = \tau_s / 2$.

The deformation-dependent coefficient k_s accounts for the nonlinearity of the polymer force-deformation behavior and is approximated in Eq. 2 by the Cohen Padé approximation of the inverse Langevin function[18]. Other, somewhat different forms for this coefficient have been proposed[15], although the Cohen form is especially accurate for commonly used flexible polymers. The tensor $\underline{\underline{\sigma}}_p$ is the polymer contribution to the stress while $\underline{\underline{\sigma}}_s$ is the Newtonian solvent contribution.

Eq. 3 gives the polymer contribution to the stress tensor. The Newtonian solvent contribution with viscosity η_s must be added to this to give the total stress tensor $\underline{\underline{\sigma}}$, as in Eq. 5. For the solution to be dilute, the polymer contribution can be no higher than the solvent contribution; thus $\eta_{p,0} \le \eta_s$. Here $\eta_{p,0} = G\tau$ is the zero-shear polymer contribution to the viscosity. "Zero-shear" means that this is the value that prevails at low shear rate, below the rate needed for shear thinning. The polymer contribution to viscosity in dilute solution is proportional to polymer concentration c (in units of mass/volume); thus $\eta_{p,0} = [\eta]\eta_s c$, where $[\eta]$ is the *intrinsic viscosity* of the polymer and increases with polymer length raised to a power of 0.5 to 0.6. If the polymer concentration c exceeds $1/[\eta]$ (so that $c[\eta] > 1$), then the polymer is no longer dilute, and this criterion implies that lower concentrations are needed to attain diluteness as the polymer molecular weight increases.

2.3.1.1. Extensional flow

The behavior of the FENE-P model (as defined in Eqs. 1-5) in uniaxial extensional flow is rather simple, and is depicted in Figure 2.4 for dilute solutions at various values of $\lambda_{\max}$. The

polymer contribution to the uniaxial extensional viscosity $\bar{\eta}_{p,u}$ remains small until the dimensionless extensional strain rate $\dot{\varepsilon}\tau_s$ reaches a value of unity, and thereafter it rises rapidly, so that the total viscosity (including the solvent contribution) reaches a high-extension-rate plateau value of $\bar{\eta}_{p,u,\infty}+3\eta_s=3\left(G\tau\lambda_{\max}{}^2+\eta_s\right)=3\left(\eta_{p,0}\lambda_{\max}{}^2+\eta_s\right)=3\eta_{p,0}N_K+3\eta_s\approx 3\eta_{p,0}N_K$. Note that the solvent contribution is fixed at $\bar{\eta}_{s,u}=3\eta_s$ and we have neglected this contribution in the final expression above, which is reasonable if N_K is large and the polymer concentration is not vanishingly small. At low extension rate, the extensional viscosity is $3\bar{\eta}_{p,u,0}+3\eta_s=3\left(\eta_{p,0}+\eta_s\right)$. Thus, the ratio of the high-rate to the low-rate extensional viscosity is

$$\frac{\bar{\eta}_{u,\infty}}{\bar{\eta}_{u,0}}\approx\frac{\eta_{p,0}N_K}{\eta_s+\eta_{p,0}}\approx\frac{[\eta]cN_K}{1+[\eta]c} \tag{7}$$

This result implies that even for dilute solutions for which $\eta_{p,0}\le\eta_s$ (i.e., $[\eta]c<1$), the high-rate extensional viscosity of the solution, $\bar{\eta}_{p,u}$, can greatly exceed the low-rate value, if the polymer molecular weight is high and therefore N_K is large. Typically, for concentrations of 0.1% by mass of polymer with molecular weight in the millions, $\bar{\eta}_{u,\infty}/\bar{\eta}_{u,0}$ can exceed 100[16].

2.3.1.2. Shearing flow

The polymer contribution to the shear viscosity η_p and ratio $N_1/\sigma_{p,12}$ of the first normal stress difference (N_1) to the polymer contribution to the shear stress ($\sigma_{p,12}$) predicted by the FENE-P model for dilute solutions are plotted in Figure 2.5. The first normal stress difference in shearing flow is defined as $N_1\equiv\sigma_{11}-\sigma_{22}$ with direction "1" being the flow direction and "2" the gradient direction (see Figure 2.3b). The second normal stress difference $N_2\equiv\sigma_{22}-\sigma_{33}$ is predicted to be zero for the FENE-P model. Note in Figure 2.5 that the shear viscosity η_p is predicted to remain roughly constant with increasing shear rate, up to a Weissenberg number $Wi_s=\dot{\gamma}\tau_s$ comparable to the polymer extensibility $\lambda_{\max}$, and then decreases with a power-law exponent of -2/3 at high shear rate. Eventually, the total shear viscosity (polymer + solvent

contributions) reaches a high-shear-rate asymptote of η_s solvent viscosity (not shown in Figure 2.5 because the solvent stress was subtracted off). The cause of shear thinning (i.e., decrease of viscosity with increasing shear rate) is the finite extensibility of the molecule, which is represented by the "FENE" spring law given in Eq. 2. This behavior reflects a polymer shear stress $\sigma_{p,12}(\dot{\gamma})$ that rises initially linearly with shear rate $\dot{\gamma}$, before bending over to a power law of $\sigma_{p,12}(\dot{\gamma}) \propto \dot{\gamma}^{1/3}$ at high strain rates, after which it is eventually eclipsed by the solvent contribution to the shear stress. The first normal stress difference, on the other hand, initially rises quadratically with shear rate $N_1(\dot{\gamma}) \propto \dot{\gamma}^2$. Then, at a shear rate comparable to the rate at which shear thinning commences, $N_1(\dot{\gamma})$ bends over and eventually follows the scaling $N_1(\dot{\gamma}) \propto \dot{\gamma}^{2/3}$ at high $\dot{\gamma}$, according to the FENE-P model. The ratio of first normal stress difference to shear stress rises linearly at first, and eventually bends over, due to finite extensibility, as shown in Figure 2.5 (insert). Since there is no solvent contribution to the first normal stress difference, the ratio N_1/σ_{12} will eventually decrease at high shear rate, once the solvent contribution is added to the polymer contribution $\sigma_{p,12}$. The parameter controlling the maximum extension of the spring, and therefore the degree of shear thinning, is $\lambda_{\max} \equiv L/\sqrt{\langle R^2 \rangle_0} = \sqrt{N_K}$. Excluded volume (EV) and hydrodynamic interaction (HI), when accounted for, can also produce shear thinning[8].

Thus, the larger the number of Kuhn steps $N_K = L/b_K$ in the chain – i.e., the larger the molecular length L relative to the Kuhn length b_K – the higher the Weissenberg number at which strong shear thinning is predicted to occur. Likewise, the stress ratio $N_1/\sigma_{p,12}$ reaches a higher value before bending over as the chains become longer, as shown in Figure 2.5 (inset). The phenomena driven by normal stress differences – rod climbing, edge fracture, and elastic instabilities – therefore should become more prominent in dilute solution as the molecular weight of the polymer increases. However, we note that the best agreement with the above predictions is found with very viscous oligomeric solvents. For low-viscosity, small-molecule solvents, anomalous behavior has been reported in which the chain stretches only very modestly, even at high Weissenberg number[16,19-21].

2.3.2. Concentrated solutions and melts: The tube model

When the polymer concentration exceeds $1/[\eta]$ by a factor of 10 or so, which for high molecular weight polymers is typically at a concentration of 0.01 gm/cm^3 or so, entanglements among polymer molecules begin to affect their dynamics and rheology. Once entanglements dominate the dynamics, the Brownian motion of a polymer molecule over a range of distances from a few nanometers to a few 10's of nanometers is directed primarily along the coarse-grained contour of the polymer molecule itself. This occurs because large motions transverse to this direction are blocked by "entanglements" with other chains, which confines a chain to a "tube-like" region; see Figure 2.2. The precise nature of these entanglements between chains is still not resolved[22] , but their rheological consequences have been well studied. To date, the only model of entanglement interactions that yields a full, tractable, constitutive equation is the "tube" model, where the "tube" is depicted in Figure 2.2. The tube model describes the coarse-grained one-dimensional motion of chains along their tubes, where the tubes, like the polymers in them, are random walks. The tube has *Z* random-walk steps or segments at equilibrium in the absence of flow, where for flexible polymers *Z* is less than N_K by about an order of magnitude in the melt, and more than this in solutions. *Z* is thought of as the "number of entanglements" per chain, and is proportional to polymer chain length L, and also dependent on polymer concentration. We can define the number of Kuhn steps per tube segment as $N_K / Z \equiv N_{t,K}$, where $N_{t,K}$ is the number of Kuhn segments per tube segment, which is independent of polymer length and for polystyrene in the melt has a value of around 17. While the most complete theories for polymer motion along the tube are complex[14,15,23], the key idea is that there are two basic types of polymer relaxation within the tube: 1) relaxation of polymer *stretch*, which occurs along the tube and is governed by a relatively fast time constant τ_s, and 2) relaxation of polymer *orientation*, which can only occur on a longer time scale τ_d as the polymer escapes the tube. Escape occurs by a sliding motion or "*reptation*" of the chain along the tube. Reptation is much slower than relaxation of polymer stretch, if the tube contains many segments *Z*. The rheological predictions of this tube model, which captures both reptation and stretch relaxation, are given in relatively simple form by a two-mode version of the Doi-Edwards-Marrucci-Grizzuti (DEMG) model[24], given by[2,25]:

$$\overset{\nabla}{\underline{\underline{S}}}_t + 2\underline{\underline{\kappa}} : \underline{\underline{S}}_t \underline{\underline{S}}_t + \frac{1}{\tau_d}\left(\underline{\underline{S}}_t - \frac{1}{3}\underline{\underline{\delta}}\right) = 0 \tag{8}$$

$$\dot{\lambda}_t = \lambda_t \underline{\underline{\kappa}} : \underline{\underline{S}}_t - \frac{k_{s,t}\left(\lambda_t - 1\right)}{\tau_s} \tag{9}$$

$$k_{s,t} = \frac{\left(3\lambda_{t,\max}^2 - \lambda_t^{\,2}\right)\Big/\left(\lambda_{t,\max}^2 - \lambda_t^{\,2}\right)}{\left(3\lambda_{t,\max}^2 - 1\right)\Big/\left(\lambda_{t,\max}^2 - 1\right)} \tag{10}$$

$$\underline{\underline{S}} = \lambda_t^{\,2}\underline{\underline{S}}_t \tag{11}$$

$$\underline{\underline{\sigma}} = 3G_N k_{s,t}\underline{\underline{S}} \tag{12}$$

In Eq. (8), $\underline{\underline{S}}_t$ is the tube "orientation tensor" that describes the average orientation of tube segments. Its relaxation is controlled by reptation, whose rate is set by the disengagement time τ_d. Eq. 9 describes "tube stretch," in which λ_t is the stretch of the polymer along the *tube* relative to its length along the tube at equilibrium or in the absence of flow. (This differs from λ used earlier, which is the stretch of the polymer end-to-end vector, not the stretch along the tube.) When there is no chain stretch, $\lambda_t = 1$. The first term on the right side of the stretch equation (Eq. 9), $\lambda_t \underline{\underline{\kappa}} : \underline{\underline{S}}_t$, describes the stretching of the chain along the tube, while the last term describes stretch relaxation along the tube. Eq. 12 gives the stress. The coefficient $k_{s,t}$ defined in Eq. 10 accounts for the nonlinearity of the spring and is approximated here by a similar form as used in Eq. 2 for dilute solutions. Here, however, $\lambda_{t,\max}$ is the maximum stretch ratio of the tube. In addition, the spring law in Eq. 10 differs from that for dilute solutions in Eq. 2 in that Eq. 10 is normalized so that $k_{s,t}$ is unity when the tube stretch λ_t is unity. This normalization only has a minor effect if $\lambda_{t,\max}$ is much larger than unity. (In principle, a similar normalization could be used for Eq. 2.) Note that above the entanglement threshold, any solvent contribution to the stress tensor is negligible. This simple version of the tube model treats each tube segment as equivalent, which is a rough approximation, but one that captures the key features of the more complete "DEMG" model[24].

In Eq. 8, the magnitude of $\underline{\underline{S}}_{tube}$ is limited by $\underline{\underline{S}}_t : \underline{\underline{S}}_t \le 1$, where the limit $\underline{\underline{S}}_t : \underline{\underline{S}}_t = 1$ is reached when all tube segments are aligned along the same axis, and $\underline{\underline{S}}_t = \frac{1}{3}\underline{\underline{\delta}}$ when the tube segments are randomly oriented at equilibrium. Here $\underline{\underline{\delta}}$ is again the unit tensor.

The above equation set (Eqs. 8-12) for entangled polymers differs from the FENE-P model for dilute solutions (Eqs. 1-5), in that the former decomposes the conformation tensor $\underline{\underline{S}}$ into a product of the tube orientation tensor $\underline{\underline{S}}_t$ and the square of the tube stretch λ_t. The orientation tensor $\underline{\underline{S}}_t$ relaxes on the time scale τ_d of disengagement from the tube, while the tube stretch λ_t relaxes on a time scale τ_s which for densely entangled polymers is much smaller than the disengagement time; i.e., $\tau_s = \tau_d$. As a result, there are for entangled polymers two Weissenberg numbers, namely $\mathrm{Wi}_d = \tau_d \dot{\gamma}$ and $\mathrm{Wi}_s = \tau_s \dot{\gamma}$, with $\mathrm{Wi}_d \gg \mathrm{Wi}_s$ for densely entangled polymers. (These definitions are for shearing flows with shear rate $\dot{\gamma}$, but corresponding definitions are used for extensional flows with extension rate $\dot{\varepsilon}$.) The presence of entanglements is manifest in that τ_d exceeds τ_s by roughly a factor of $Z^{1.4}$, which becomes large for long polymers in the melt or in concentrated solutions. The time constant τ_s is roughly the relaxation time that the polymer would have if there were no entanglements, and τ_d is an additional relaxation time that emerges as a result of the entanglement interactions. The non-integral power-law exponent of 1.4 would be a simple exponent of unity, if relaxation only occurred by reptation, but there is additional relaxation owing to "breathing modes" of the chain in the tube, that can be empirically accounted for by using the modified exponent 1.4; see Doi and Edwards[14] and Likhtman and McLeish[26] for details. The stretch relaxation time follows the proportionality $\tau_s \propto {N_K}^2 \propto Z^2$, and the disengagement times scales roughly as $\tau_d \propto Z^{3.4}$.

The so-called "plateau" modulus G_N in Eq. 12 is proportional to the total number of polymer chains per unit volume, ν, the number of entanglements per chain Z, and $k_B T$; i.e., $G_N \approx \nu Z k_B T$. For the case of a dense melt, with no solvent, the number of chains per unit volume ν must decrease inversely with the length of the chain, since the density of the melt is nearly

independent of chain length. Hence, for a melt, the product νZ is independent of polymer molecular weight, and so the modulus G_N is independent of molecular weight, for a polymer of a given monomer type. However, for a polymer solution, if the polymer concentration *c* is increased, then G_N increases rapidly because both *Z* and ν increase with *c*. The zero shear viscosity is proportional to the product of the longest relaxation time $\tau_d \propto Z^{1.4}\tau_s$ and the modulus $G_N \approx \nu Z k_B T$, giving $\eta_0 \sim G_N \tau_d \sim \nu Z^{2.4}\tau_s k_B$. The dependence of *Z* on polymer concentration depends on solvent quality, as is discussed elsewhere[27]. For our purposes, it suffices to note that at fixed polymer molecular weight, *Z* is roughly proportional to polymer concentration to the first, or a bit higher power, around 4/3[27]. That is, $Z \approx Z_0 \phi^{\alpha}$, where Z_0 is the number of tube segments in a melt, and *Z* is the number of tube segments in a solution of polymer of the same molecular weight but with polymer volume fraction ϕ and exponent α = 1 to 4/3. This gives a rather rapid rise in zero shear viscosity with polymer concentration (to the third power or higher) even when the stretch time τ_s remains insensitive to polymer concentration. Normally, once the polymer concentration becomes high enough, the monomeric friction coefficient ζ increases as polymer chains experience increasing chain-chain, rather than chain-solvent, friction, and the viscosity of the solution can become very high indeed[28].

Now, if the flow is fast enough to either destroy entanglements, or render their effect negligible, we expect the behavior of even a densely entangled polymeric fluid to begin to resemble that of an un-entangled fluid, and to be described, to some degree, by Eqs. 1-5 for un-entangled polymers. This connection to the theory for un-entangled rheology can be made clearer by noting that the plateau modulus G_N that appears in Eq. 12 is related to the modulus G in Eq. 3 for un-entangled polymers by a factor of *Z*. And the maximum extension ratio of the tube $\lambda_{t,\max}$ is less than the maximum extension ratio $\lambda_{\max}$ of the end-to-end vector by a factor of $Z^{1/2}$. Thus,

$$\begin{aligned} &G_N \approx ZG = Z\nu k_B T \ ; \\ &\lambda_{t,\max} = \lambda_{\max} / Z^{1/2} = \sqrt{N_{t,K}} = \sqrt{N_{t,K,m}}\,\phi^{-\alpha/2} \end{aligned} \tag{13}$$

where $N_{t,K,m}$ is the number of Kuhn steps in a tube segment in the melt state. These relationships have consequences to be discussed shortly.

2.3.2.1. Extensional flow

The effect of the additional time scale τ_d in entangled polymers and absent from un-entangled ones is evident in the behavior of the steady-state extensional viscosity versus extension rate, depicted in Figure 2.4 for $\lambda_{t,\max}$ = 10 and 3. At low extension rates, the extensional viscosity is a constant, given roughly by $\bar{\eta}_{u,0} \approx 3G_N\tau_d \approx 3Z^{1.4}G_N\tau_s \propto Z^{3.4}$, where we have used the proportionality $\tau_s \propto Z^2$ mentioned earlier. Thus, the zero shear viscosity of an entangled polymer rises rapidly with *Z* or molecular weight, as the 3.4 power, as mentioned above. Once the tube orientational Weissenberg number $\mathrm{Wi}_d = \dot{\varepsilon}\tau_d$ exceeds unity, the tube segments become highly oriented, and the tube orientation tensor $\underline{\underline{S}}_t$ begins to saturate. If the chain stretch Weissenberg number $\mathrm{Wi}_s = \dot{\varepsilon}\tau_s$ is still small (< ½) so that the tube stretch λ_t remains close to unity, the saturation of $\underline{\underline{S}}_t$ causes the extensional stress $\sigma_{11} - \sigma_{22}$ to rise less than linearly with increasing shear rate. Hence, the viscosity $\bar{\eta}_u \equiv (\sigma_{11} - \sigma_{22})/\dot{\varepsilon}$ decreases, and extension thinning sets in, as depicted in Figure 2.4.

At still higher extension rate, when $\mathrm{Wi}_s = \dot{\varepsilon}\tau_s$ exceeds unity, the extensional viscosity rapidly rises to a high-strain rate plateau, given by $\bar{\eta}_{u,\infty} = 3G_N\tau_s\lambda_{t,\max}^2$. Using Eq. 13, we find that this plateau equals $\bar{\eta}_{p,u} = 3G\tau_s\lambda_{\max}^2$ which matches that of the FENE-P model, given in Section 2.3.1. Thus, at extension rates high enough that the stretch Weissenberg number Wi_s exceeds unity, the DEMG theory at steady state reduces to the FENE-P model. This might be expected, because at high strain rates, at steady state, the polymer molecules are nearly fully aligned and stretched out, and entanglements become irrelevant to their rheology. Notice that the high-extension-rate viscosity $\bar{\eta}_{u,\infty}$ is proportional to $G_N\tau_s\lambda_{t,\max}^2$, which, for fixed concentration c or volume fraction ϕ, is proportional to $\tau_s \propto Z^2$, since G_N and $\lambda_{t,\max}$ are independent of *Z* (i.e., independent of molecular weight). Thus, the viscosity at low extension rate increases more

rapidly (as $Z^{3.4}$) with polymer molecular weight than it does at high extensions rates (as Z^2), and for highly entangled polymers, especially melts, the highest viscosity is achieved at the lowest strain rates; see Figure 2.4. This contrasts strongly with the extensional viscosity of dilute solutions of long polymers, also depicted in Figure 2.4, where the low-strain-rate viscosity is dominated by the solvent and so is nearly independent of polymer length, while the high-strain-rate viscosity increases linearly with polymer molecular weight at fixed *c*. However, for highly entangled polymers, if molecular weight is held fixed at a large value, the low-strain rate extensional viscosity rises dramatically with concentration *c*, since $\bar{\eta}_{u,0} \propto \nu k_B T \tau_s Z^{2.4}$, while the high-strain rate extensional viscosity rises more modestly as $\bar{\eta}_{u,\infty} \propto \nu k_B T \tau_s \lambda_{\max}^2$. Both expressions depend directly on number concentration ν linearly, but the low-strain-rate expression also contains a strong dependence on *Z*, and both depend in the same way on τ_s, which can increase with concentration through the dependence of τ_s on the monomeric friction coefficient ζ. Thus, we find for entangled solutions that:

$$\frac{\bar{\eta}_{u,\infty}}{\bar{\eta}_{u,0}} \approx \frac{\lambda_{\max}{}^2}{Z^{2.4}} = \frac{\lambda_{t,\max}}{Z^{1.4}} = \frac{\sqrt{N_{t,K}}}{(N_K / N_{t,K})^{1.4}} = \frac{N_{t,K}{}^{1.9}}{N_K{}^{1.4}} = \frac{N_{t,K,m}^{1.9}\phi^{-1.9\alpha}}{N_K{}^{1.4}} \tag{14}$$

Note that $\lambda_{t,\max}$ is the maximum extensibility of the tube, which is independent of polymer molecular weight at fixed concentration or in the melt, while *Z* is proportional to molecular weight. Note also that $N_{t,K,m}$ is of order 20 or so, while N_K can be in the hundred or thousands for high molecular weight polymers. Thus, Eq. 14 implies that one of the major attributes of high molecular weight polymers, namely their high extensional viscosity relative to their zero shear viscosity, is limited to solutions of low or modest concentration, and does not apply to highly concentrated solutions or melts. The ratio of the high-extension-rate to low-extension-rate viscosity decreases with molecular weight or number of Kuhn steps N_K at fixed concentration ϕ. However, both higher molecular weight and higher concentration lead to an increase in the range of extension rates over which the polymeric fluid is extension thinning. Recent experimental findings support these predictions[29-33]; see the insert to Figure 2.4, where the theory used in the insert is the DEMG theory with deformation-dependent friction[34]. Details of the friction-dependent DEMG theory are described in the next chapter 3. Dilute or low-concentration

polymer solutions show pronounced extension thickening at high extension rate, while melts show little, or even no extension thickening.

In fact, recent findings show that there is an additional factor reducing extension thickening in polymer melts, which is a decrease in friction coefficient ζ with increasing alignment of polymer chains, in the melt state[35-37]. This effect, verified by both rheological experiments and molecular dynamics simulations, reduces the ratio $\bar{\eta}_{u,\infty} / \bar{\eta}_{u,0}$ even further, as shown in Figure 2.4 (insert).

These results have practical consequences. Drawing of melts into fibers and especially films is dependent on the ability of the melt to thicken under extensional flow, and so to resist capillary breakup (a simple example of which is the breakup of a stream of water into droplets). Low, or non-existent, extensional thickening poses a challenge to such processes[38]. This can be countered in two different ways. One of the most successful ways is the addition of long side branches to polymers[39]. In extensional flow, these side branches must be dragged with the polymer backbone, thus providing a great increase in the effective friction experienced by the backbone when it is being stretched[40]. This enhances the extensional viscosity of the polymer at high strain rate, producing a maximum in viscosity as a function of strain rate that can be higher than the low-rate viscosity[40]. A second tactic is to include a dilute very-high-molecular-weight component into the molecular weight distribution[41]. This allows the melt to mimic a dilute solution, with most of the melt acting as a "solvent" for the high-molecular-weight component. And as we have seen, dilute solutions can show very strong extensional thickening. Thus, designing a melt so that its extensional flow properties mimic those of a dilute solution can improve the performance of melt processing.

2.3.2.2. Shearing flow

In shearing flow, the DEMG equation predicts strong shear thinning once the orientational Weissenberg number $\mathrm{Wi}_d = \dot{\gamma}\tau_d$ exceeds unity; see the insert of Figure 2.5. This occurs at much lower shear rate than in dilute solutions, for "iso-frictional" solutions or melts, which have the same stretch relaxation time τ_s regardless of concentration. In fact, in highly entangled solutions and melts, the thinning can be so strong that the shear stress $\sigma_{12}(\dot{\gamma})$, and not

just the shear viscosity $\eta(\dot{\gamma})$, decreases with increasing shear rate above Wi_d around unity. The predicted maximum in shear stress with increasing shear rate has long been a controversial prediction of the tube model. Experimental shear-flow measurements with polymer melts or concentrated solutions are difficult to perform because of the edge-fracture instability depicted in Figure 2.1b. Edge fracture is driven by negative value of the second normal stress difference N_2 large enough to overwhelm surface tension forces at the meniscus[42,43]. (Note: N_2 is inaccurately predicted to be zero by Eqs. 8-12). The ratio of the first normal stress N_1 difference to the shear stress σ_{12}, depicted in the insert of Figure 2.5, can be lower for entangled polymers than for dilute ones, making entangled polymers less prone to instabilities driven by N_1, such as the Taylor-Couette elastic instability depicted in Figure 2.1c, even as they are more susceptible to instabilities driven by N_2, such as the edge fracture depicted in Figure 2.1b.

When steady-state measurements of shear viscosity are successful for highly entangled polymer solutions, they invariably show a monotonic increase in shear stress with shear rate, in disagreement with the predictions of Eqs. 8-12. However, often the stress is almost constant with shear rate or rises very slowly with shear rate with a weak power law, with exponent of only around 0.1 or so[8,44]. More importantly, a *non-monotonic flow curve* – i.e., a maximum in shear stress followed by a decrease in steady-state shear stress with shear rate – is not observable even in principle, because it leads to a *constitutive instability*, in which the shearing flow breaks up into bands, one with a much higher shear rate than the other(s)[9,14,45,46]. And, indeed, evidence for such banded flow, or for slip along the wall, has been presented for a variety of shearing flows for densely entangled polymers[10,47-49]. Such behavior is most often observed, and is most severe, for densely entangled melts and solutions, with $Z \approx 40$ or more entanglements, especially when the polymer is nearly monodisperse in molecular weight[50-52]. When banding occurs for highly entangled polymers, the high-shear band often forms near the wall of the shearing device, where the shear stress is typically the highest, where it may manifest itself as an apparent slip at the wall. In flow through a capillary, this may result in a so-called "spurt" phenomenon wherein at a critical stress the polymer slips like a plug through the capillary at high rates[45,53]. Predictions of phenomena resulting from tube or other models with a non-monotonic flow curve are now

becoming available[9,54,55] and in some cases show impressive agreement with experimental results.

Some versions of the tube model, however, display only a monotonic flow curve in shear, typically as a result of inclusion of convective constraint release (CCR) into the constitutive equation[23,56,57]. CCR, which is not included in Eqs. 8-12 (but is included in the predictions for an entangled solution given in the insert to Figure 2.5) describes a disentanglement effect that occurs at shear rates above the inverse disengagement time $1/\tau_d$ [56,58,59]. As noted already, at extensional strain rates above $1/\tau_s$, entanglements become irrelevant, if indeed they survive at all. Shear flow is more complicated, because of its mixture of both deformation of polymer chains and vorticity, which eventually rotates chains away from the direction of greatest stretch, and so leads to periodic chain collapse as well as extension. This "chain stretch, tumbling, and collapse" cycle is now quite well understood in dilute solutions, in large part thanks to both novel methods of imaging individual polymer molecules in flow and due to advances in computer speed and algorithms[60-63]. In the presence of entanglements, which can interfere with chain collapse during tumbling, the physical picture is not yet clear, but, again, both experimental imaging methods and advanced simulation methods and computer speed will likely lead to breakthroughs in the near future.

2.4. Summary

An ability to predict polymer fluid mechanics accurately and robustly would constitute a major advance in rational design of manufacturing with polymeric components, affecting manufacture of textiles, automobiles, aircraft, electronic equipment, medical equipment, paints and coatings, foodstuffs, cosmetics and consumer products, oil-field fluids, and others. This ability is not yet in hand, due to the difficulty of constructing accurate, general, constitutive equations, and being able to cope with the computational difficulties posed by these equations in numerical simulations. Recent advances, reviewed briefly in this chapter, suggest, however, that the field is closing in on an ability to more reliably model the constitutive behavior of at least the simplest categories of polymeric fluids, namely those composed of linear homopolymer chains in the melt or in a simple solvent. It may seem surprising that it has taken so long to understand and accurately model these "simplest" polymers even in simple extensional and shearing flows. Part

of the difficulty is experimental – performing uniform shearing and extensional flows while accurately measuring stresses is frustrated by the resistance such "simple" polymeric fluids put up to being uniformly deformed[64]. Uniform extensional flow is notoriously difficult to impose, and elastic polymers in shearing flow are susceptible to various instabilities, leading to highly non-uniform flows, that while interesting, are practically useless for measuring stresses. In retrospect, the difficulties are perhaps not so surprising – at high Weissenberg number, the viscoelastic fluids respond to some extent as a solid would, and any attempt to impose a steady deformation on a solid will lead to a drastic, and often unstable, response.

A key to recent advances is an increasing understanding of the dependence of rheological behavior on polymer concentration – from dilute solutions, to entangled solutions, to melts. These changes with concentration lead to profound differences in rheological response that are beginning to be understood quantitatively. In extensional flow, both dilute and entangled solutions can show high-strain-rate extensional viscosities that are much higher than the viscosities at low strain rate. This leads to relatively stable filaments during fiber drawing, but can lead to extreme effects in other flows, such as instabilities and large corner vortices in contraction flows[65]. In very concentrated solutions or melts, the high-strain-rate extensional viscosity can be lower than the low-strain-rate viscosity. This can lead to unstable fiber drawing, unless counteracted by long-chain branching or a dilute very-long-chain component in the melt. In shearing flow, there are also important differences in polymer behavior depending on density of entanglement. Polymer solutions, either dilute, or modestly entangled, are not as subject as melts are to shear-banding or to the edge-fracture instability depicted in Figure 2.1b, but can be more subject to instabilities driven by the first normal stress difference, such as the elastic Taylor-Couette instability depicted in Figure 2.1c.

Fortunately, in recent years there has been rapid progress in understanding polymer behavior in flow: how to model it and incorporate it into constitutive equations. As these constitutive equations become more precise and less prone to artifacts and erroneous numerical instabilities, accurate solutions of complex polymer flow problems should become common, leading to improved understanding and technological benefits. In the following Chapter 3, we describe in detail the development of one such constitutive model that can accurately discriminate extensional rheology between linear entangled solutions and linear entangled melts.

2.5. References

1. Tanner R. I. *Engineering rheology*. New York, NY: Oxford University Press (1985)
2. Dealy, J. M., Larson, R. G., *Structure and rheology of molten polymers. From structure to flow behavior and back again*, Munich, Germany, Carl Hanser Verlag (2006)
3. Baaijens, F. P. T., "Mixed finite element methods for viscoelastic flow analysis: a review," *J. Non-Newt. Fluid Mech*. 79, 361, (1998)
4. Owen, R. G., Phillips, T. N., *Computational rheology*. London: Imperial College Press (2006)
5. Thomas, D. G., Khomami B., Sureshkumar R., "Nonlinear dynamics of viscoelastic Taylor-Couette flow: effect of elasticity on pattern selection, molecular conformation and drag," *J. Fluid Mech*. 620, 353 (2009)
6. Ganvir, V., Lele, A., Thaokar, R., Gautham, B. R., "Prediction of extrudate swell in polymer melt extrusion using an Arbitrary Lagrangian Eulerian (ALE) based finite element method," *J. Non-Newt. Fluid Mech.* 156, 21 (2009)
7. Luo, X. L., "Numerical simulation of Weissenberg phenomena - the rod-climbing of viscoelastic fluids," *Comp. Methods Appl. Mech. Eng.* 180, 393 (1999)
8. Larson, R. G., *Constitutive equations for polymer solutions and melts*. Boston, MA: Butterworths (1988)
9. Adams, J. M., Fielding, S. M., Olmsted, P. D., "The interplay between boundary conditions and flow geometries in shear banding: Hysteresis, band configurations, and surface transition," *J. Non-Newt. Fluid Mech.* 151, 101 (2008)
10. Archer, L. A., Larson, R. G., Chen, Y-L., "Direct measurements of slip in sheared polymer solutions," *J. Fluid Mech*. 301, 133 (1995)
11. Larson, R. G., Muller, S. J., Shaqfeh, E. S. G., "A purely elastic instability in Taylor-Couette flow" *J. Fluid Mech*. 218, 573 (1990)
12. Thrasher, M., Jung, S. W., Pang, Y. K., Chuu, C. P., Swinney, H. L., "Bouncing jet: A Newtonian liquid rebounding off a free surface," *Phys. Rev. E.* 76, 5, 056319 (2007)
13. Flory, P. J. *Principles of Polymer Chemistry*. Ithaca, NY, Cornell Univ. Press (1953)
14. Doi, M., Edwards, S. F., *The theory of polymer dynamics*, Oxford, UK, Clarendon Press (1986)
15. Larson, R. G., *The structure and rheology of complex fluids*. New York, NY, Oxford University Press (1999)
16. Larson, R. G., "The rheology of dilute solutions of flexible polymers: Progress and problems," *J. Rheol.* 39, 17 (2005)
17. Bird, R. B., Curtiss, C. R., Armstrong, R. C., Hassager, O., *Dynamics of polymeric liquids*, Vol. 2: *Kinetic theory*. New York, Wiley. 2nd ed. (1987)
18. Cohen, A., " A Padé approximant to the inverse Langevin function," *Rheol. Acta* 30, 270 (1991)
19. Menasveta, M. J., Hoagland, D. A., "Light-scattering from dilute poly(styrene) solutions in uniaxial elongational flow," *Macromolecules* 24, 3427 (1991)
20. Armstrong, R. C., Gupta, S. K., Basaran, O., "Conformational-changes of macromolecules in transient elongational flow," *Polym. Eng. Sci.* 20, 466 (1980)
21. Solomon, M. J., Muller, S. J., "Study of mixed solvent quality in a polystyrene-dioctyl phthalate-polystyrene system," *J. Polym. Sci. B; Polym. Phys.* 34, 181 (1996)

22. Likhtman, A. E., "Whither tube theory: From believing to measuring," *J Non-Newt. Fluid Mech.*157, 158 (2009)
23. Graham, R. S., Likhtman, A. E., Milner, S. T., McLeish, T. C. B., "Microscopic theory of linear, entangled polymer chains under rapid deformation including chain stretch and convective constraint release," *J. Rheol.* 47, 1171 (2003)
24. Marrucci, G., Grizzuti, N., "Fast flows of concentrated polymers: Predictions of the tube model of chain stretching," *Gazz. Chim. Ital.* 118, 179 (1988)
25. Pearson, D. S., Herbolzheimer, E., Grizzuti, N., Marrucci, G., "Transient-behavior of entangled polymers at high shear rate," *J. Polym. Sci. B Polym. Phys. Ed.* 29(13),1589 (1991)
26. Likhtman, A. E., McLeish, T. C. B., "Quantitative theory for linear dynamics of linear entangled polymers," *Macromolecules* 35, 6332 (2002)
27. Milner, S. T., "Predicting the tube diameter in melts and solutions," *Macromolecules* 38, 4929 (2005)
28. Ferry, J. D., *Viscoelastic properties of polymers*. New York, NY, Wiley (1980)
29. Bhattacharjee, P. K., Oberhauser, J., McKinley, G. H., Leal, L. G., Sridhar, T., "Extensional rheometry of entangled solutions," *Macromolecules* 35, 10131 (2002)
30. Acharya, M. V., Bhattacharjee, P. K., Nguyen, D. A., Sridhar, T., "Are entangled polymeric solutions different from melts?" *AIP Conf. Proc.* 1027, 391 (2008)
31. Bach, A., Almdal, K., Hassager, O., Rasmussen, H. K., "Elongational viscosity of narrow molar mass distribution polystyrene," *Macromolecules* 36, 5174 (2003)
32. Nielsen, J. K., Rasmussen, H. K., Hassager, O., McKinley, G. H., "Elongational viscosity of monodisperse and bidisperse polystyrene melts," *J. Rheol.* 50, 453 (2006)
33. Huang, Q., Mednova, O., Rasmussen, H. K., Alvarez, N. J., Skov, A. L., Almdal, K., Hassager O., "Concentrated polymer solutions are different from melts: Role of entanglement molecular weight," *Macromolecules* 46, 5026 (2013a)
34. Desai, P. S., Larson, R. G., "Constitutive model that shows extension thickening for entangled solutions and extension thinning for melts," *J. Rheol.* 58, 255 (2014)
35. Yaoita, T., Isaki, T., Masubuchi, Y., Watanabe, H., Ianniruberto, G., Marrucci, G., "Primitive chain network simulation of elongational flows of entangled linear chains: Stretch/orientation-induced reduction of monomeric friction," *Macromolecules* 45, 2773 (2012)
36. Masubuchi, Y., Yaoita, T., Matsumiya, Y., Watanabe, H., Ianniruberto, G., Marrucci, G., "Stretch/orientation induced acceleration in stress relaxation in coarse-grained molecular dynamics simulations," *J. Soc. of Rheol. Japan*, 41, 35 (2013)
37. Huang, Q., Alvarez, N. J., Matsumiya, Y., Rasmussen, H. K., Watanabe, H., Hassager, O., "Extensional rheology of entangled polystyrene solutions suggest importance of nematic interactions," *ACS Macro Lett.* 2, 741 (2013b)
38. Rodd, L. E., Scott, T. P., Cooper-White, J. J., McKinley, G. H., "Capillary break-up rheometry of low-viscosity elastic fluids," *Appl Rheol.* 15, 12 (2005)
39. McKinley, G. H., Hassager, O., "The Consid`ere condition and rapid stretching of linear and branched polymer melts," *J. Rheol.* 43, 1195 (1999)
40. McLeish, T. C. B., Larson, R. G., "Molecular constitutive equations for a class of branched polymers: The pom-pom polymers," *J. Rheol.* 42, 81 (1998)

41. Minegishi, A., Nishioka, A., Takahashi, T., Masubuchi, Y., Takimoto, J., Koyama, K., "Uniaxial elongational viscosity of polystyrene/a small amount of UHMW-PS blends," *Rheol. Acta* 40, 329 (2001)
42. Lee, C. S., Tripp, B. C., Magda, J. J., "Does N1 or N2 control the onset of edge fracture," *Rheol. Acta* 31, 306 (1992)
43. Tanner, R. I., Keentok, M., "Shear fracture in cone plate rheometry," *J. Rheol.* 27, 47 (1983)
44. Pattamaprom, C., Larson, R. G., "Constraint release effects in monodisperse and bidisperse polystyrenes in fast transient shear flows," *Macromolecules* 34, 5229 (2001)
45. Kolkka, R. W., Malkus, D. S., Hansen, M. G., Ierley, G. R., Worthing, R. A., "Spurt phenomena of the Johnson Segalman fluid and related models," *J. Non-Newt. Fluid Mech.* 29, 303 (1988)
46. Larson, R. G., "Instabilities in viscoelastic flows," *Rheol. Acta*. 31, 213 (1992)
47. Tapadia, P., Wang, S. Q., "Direct visualization of continuous simple shear in non-newtonian polymeric fluids," *Phys. Rev. Lett.* 96, 016001 (2006)
48. Boukany, P. E., Wang, S. Q., "A correlation between belocity profile and molecular weight distribution in sheared entangled polymer solutions," *J. Rheol.* 51, 217 (2007)
49. Hayes, K. A., Buckley, M. R., Cohen, I., Arher, L. A., "High resolution shear profile measurements in entangled polymers," *Phys. Rev. Lett*. 101, 218301 (2008)
50. Boukany, P. E., Wang, S. Q., "Shear banding or not in entangled DNA solutions depending on the level of entanglement," *J. Rheol.* 53, 73 (2009)
51. Fukuda, M., Osaki, K., Kurata, M., Nonlinear viscoelasticity of polystyrene solutions. 1. Strain dependent relaxation modulus. *J. Polym. Sci. B Polym. Phys.* 13,1563 (1975)
52. Morrison, F. A., Larson, R. G., "A study of shear-stress relaxation anomalies in binary mixtures of monodisperse polystyrenes," *J. Polym. Sci: Polym. Phys. Ed*., 30, 943 (1992)
53. McLeish, T. C. B., Ball, R. C., "A Molecular approach to the spurt effect in polymer melt flow," *J. Polym. Sci. B Polym. Phys.* 24, 1735 (1986)
54. Adams, J. M., Olmsted, P. D., "Nonmonotonic models are not necessary to obtain shear banding phenomena in entangled polymer solutions," *Phys. Rev. Lett.* 103, 067801 (2009)
55. Adams, J. M., Fielding, S. M., Olmsted, P. D., "Transient shear banding in entangled polymers: A study using the Rolie-poly model," *J. Rheol*. 55, 1007 (2011)
56. Ianniruberto, G., Marrucci, G., "A Simple constitutive equation for entangled polymers with chain stretch," *J. Rheol.* 45, 1305 (2001)
57. Likhtman, A. E., Graham, R. S., "Simple constitutive equation for linear polymer melts derived from molecular theory: Rolie poly equation," *J. Non-Newt. Fluid Mech.* 114, 1 (2003)
58. Marrucci, G., "Dynamics of entanglements: A nonlinear model consistent with the Cox-Merz rule," *J. Non-Newt. Fluid Mech.* 62, 279 (1996)
59. Mead, D. W., Larson, R. G., Doi, M., "A molecular theory for fast flows of entangled polymers, " *Macromolecules* 31, 7895 (1998)
60. Smith, D. E., Babcock, H. P., Chu, S., "Single-polymer dynamics in steady shear flow," *Science* 283, 1724 (1999)
61. Hur, J. S., Shaqfeh, E. S. G., Larson, R. G., "Brownian dynamics simulations of single DNA molecules in shear flow," *J. Rheol.* 44, 713 (2000)

62. Doyle, P. S., Shaqfeh, E. S. G., Gast, A. P., "Dynamic simulation of freely draining flexible polymers in steady linear flows," *J. Fluid Mech*. 334, 251 (1997)
63. Dalal, I. S., Hoda, N., Larson, R. G., "Multiple regimes of deformation in shearing flow of isolated polymers," *J. Rheol*. 56, 305 (2012)
64. McKinley, G. H., Sridhar, T., "Filament-stretching rheometry of complex fluids," *Annu. Rev. Fluid Mech.* 34, 375 (2002)
65. Byars, J. A., Binnington, R. J., Boger, D. V., "Entry flow and constitutive modelling of fluid S1," *J. Non-Newt. Fluid Mech.* 72, 219 (1997)
66. Schweizer, T., Meerveld, J. V., Ottinger, H. C., "Nonlinear shear rheology of polystyrene melt with narrow molecular weight distribution: experiment and theory," *J. Rheol.* 48, 1345 (2004)

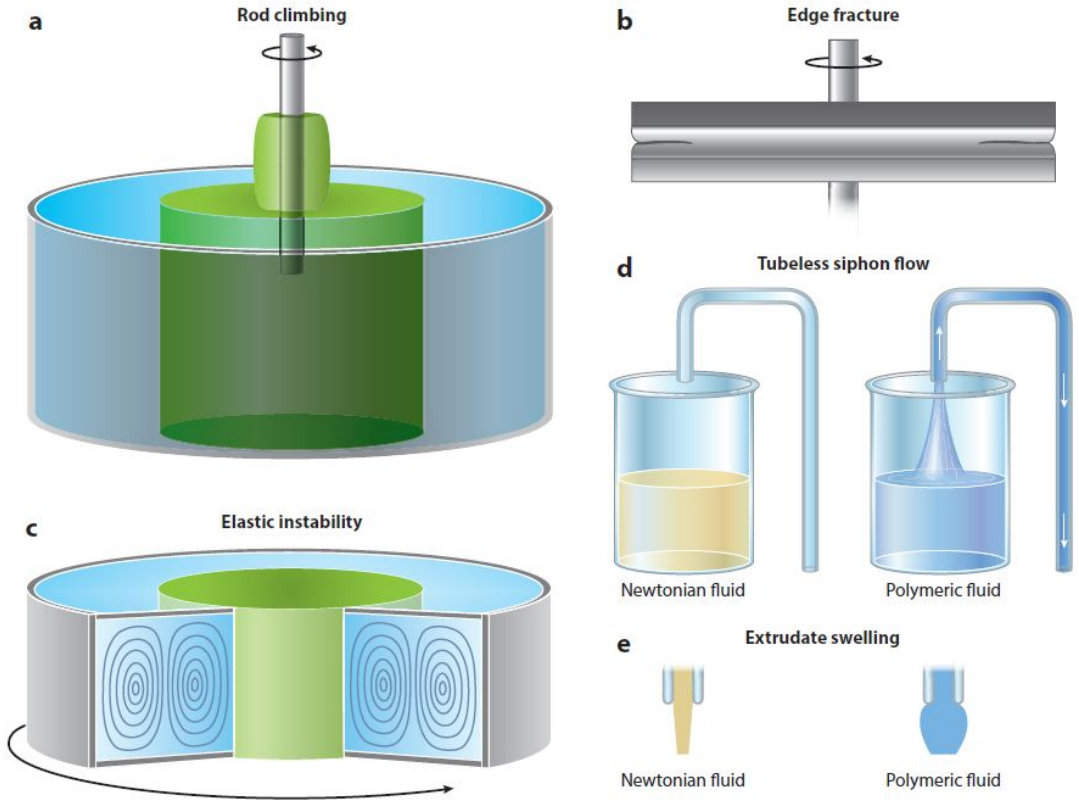

Figure 2.1. Example polymer flows: a) rod climbing; b) edge fracture; c) elastic instability in Taylor-Couette flow; d) tubeless siphon flow; e) extrudate swelling.

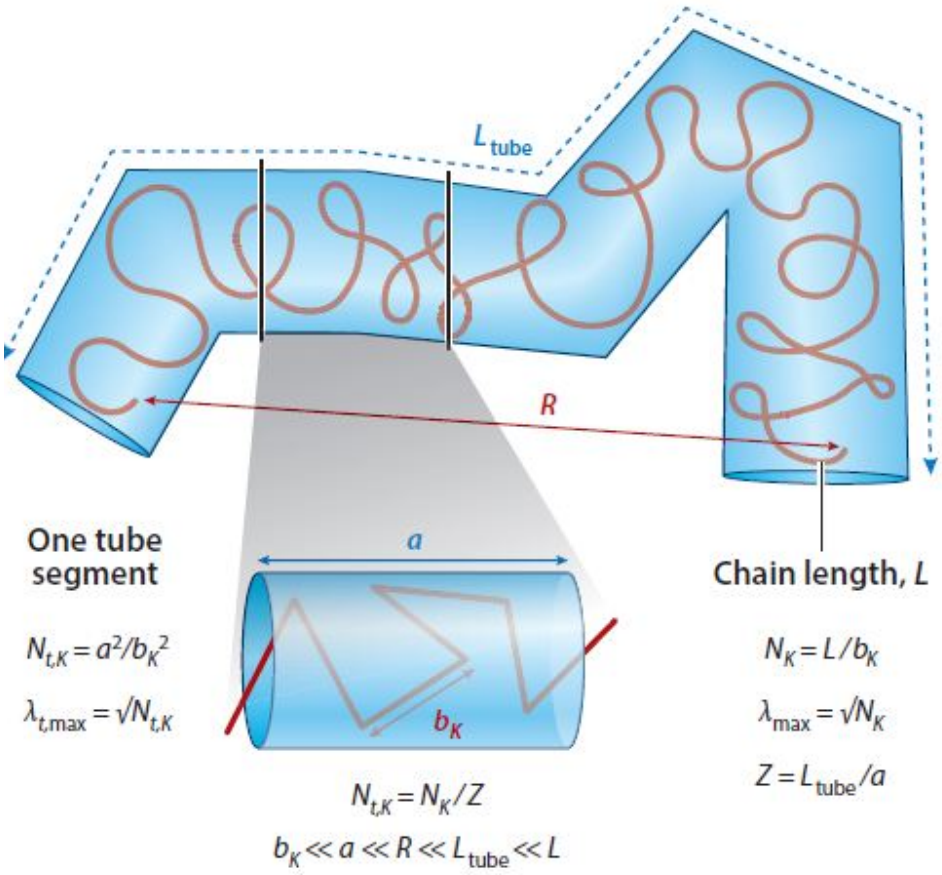

Figure 2.2. Length scales for long polymers that are entangled with other polymers, confining a given polymer to a "tube-like" region.

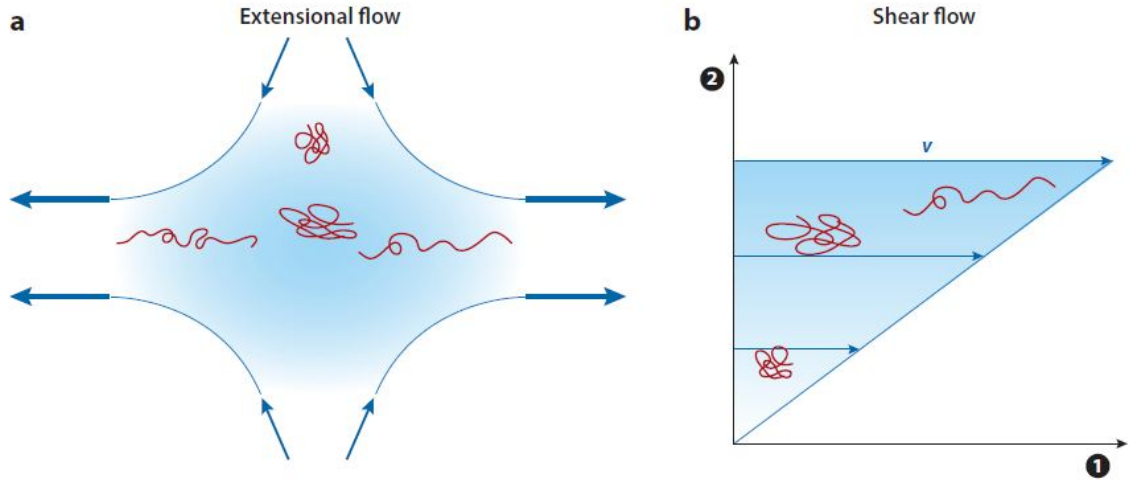

Figure 2.3. Illustration of a) extensional and b) shear flows and polymer behavior in each – showing deformation of polymers in flows; also showing directions 1 and 2 in extension and shear.

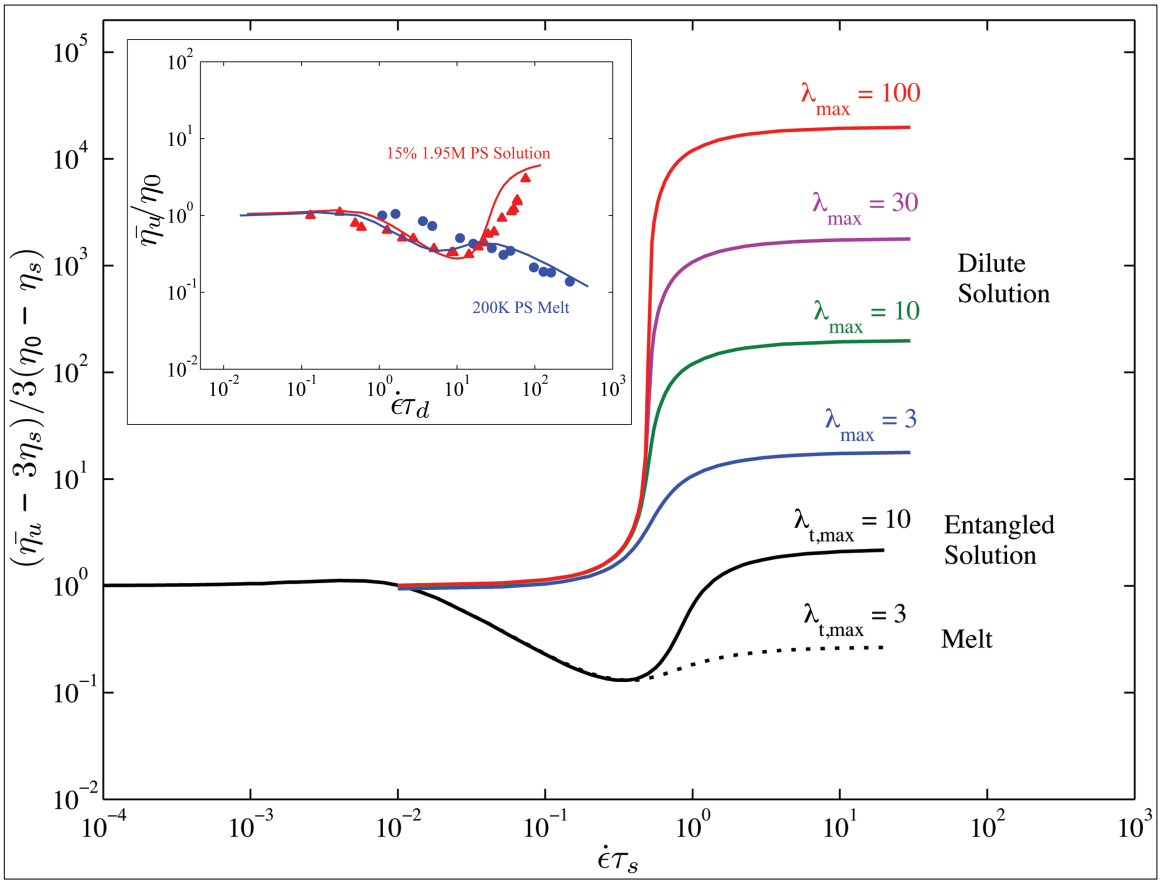

Figure 2.4. FENE-P and tube model (DEMG) predictions for the normalized polymer contribution to uniaxial extensional viscosity versus shear rate times the stretch relaxation time τ_s for various values of maximum stretch ratio λ_{max} for the FENE-P model (for dilute solutions) and maximum stretch ratio per tube segment $\lambda_{t,max}$ for the tube model (for entangled solutions and melts). For the FENE-P model, the ratio of polymer to solvent zero shear viscosity is taken as $\eta_{p,0}/\eta_s = 0.1$ while for the tube model, the ratio of reptation to stretch relaxation time τ_d/τ_s is 50. In dilute solutions, the relaxation time τ is $\tau_s/2$. The behavior for the uniaxial extension in the main figure illustrates the changes in shape of the viscosity versus strain rate curve expected upon changing polymer length (for dilute solutions) and upon changing concentration (for concentrated solutions and melts) in an "iso-viscosity solvent," where the frictional environment is insensitive to polymer concentration. The inset shows comparisons to experimental data for an entangled solution and a melt of polystyrene plotted against extension rate multiplied by the reptation time, rather than the stretch relaxation time used in the main figure. The predictions are from the tube model (DEMG), but with orientation-induced reduction in friction for the melt. The data for the solution are taken from Acharya *et al.*[30] and from melt Nielsen *et al.*[32]

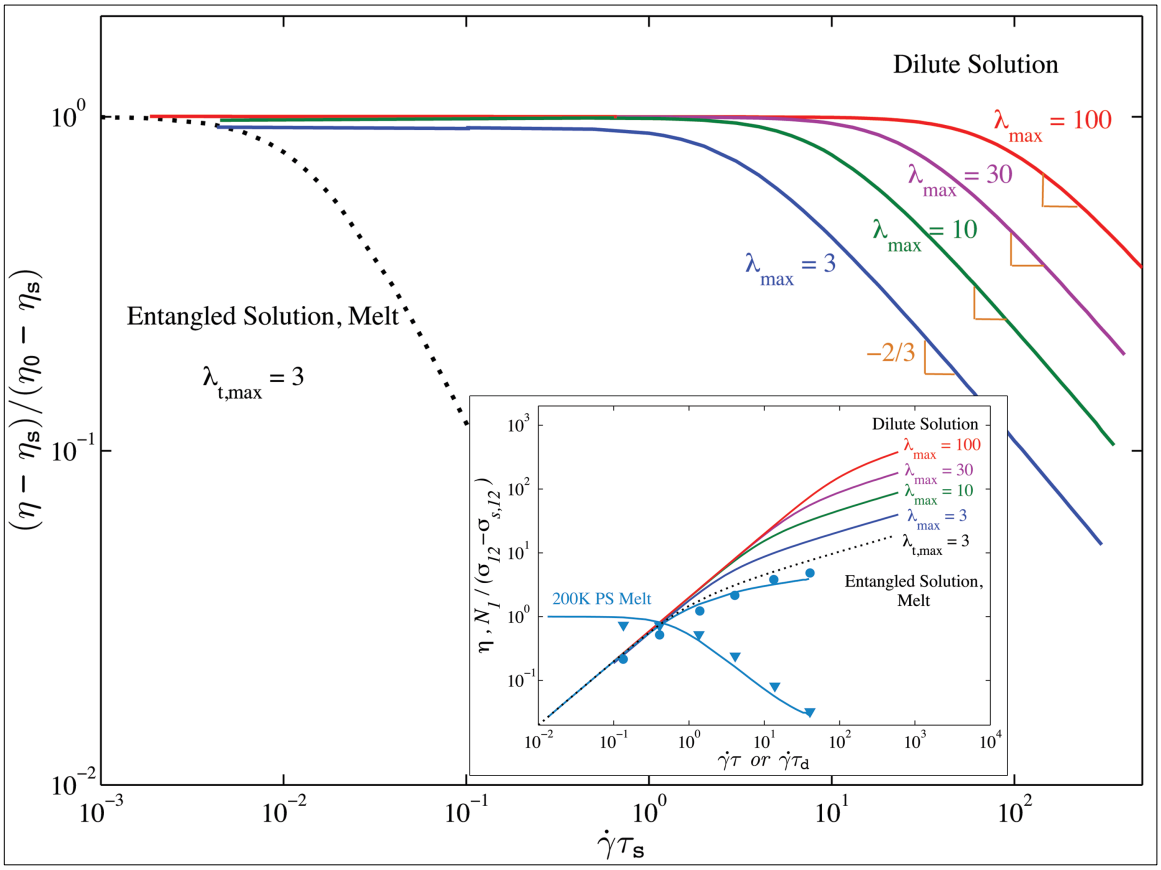

Figure 2.5. FENE-P and tube model (DEMG) predictions for the normalized polymer contribution to steady-state shear viscosity $\eta_p = \eta - \eta_s$ with insert showing the ratio $N_1/\sigma_{p,12}$ of first normal stress difference (N_1) to polymer shear stress $\left(\sigma_{p,12} = \sigma_{12} - \sigma_{s,12}\right)$ for the values of $\lambda_{\max}$ given for the FENE-P model. In the inset, the abscissa is shear rate times the longest stress relaxation time, which is $\tau = \tau_s/2$ for dilute solutions and is τ_d for melts and concentrated solutions. For the tube model, the results are insensitive to the value of $\lambda_{t,\max}$. In the inset, the tube model used for the predictions given by the blue lines is the "MLD" model, which is the "toy" DEMG model with convective constraint release and with orientation-induced reduction in friction (Desai and Larson[34]). Other details are the same as in the caption to Figure 2.4. The data are taken from Schweizer *et al.*[66]

CHAPTER 3

Constitutive model that shows extension thickening for entangled solutions and extension thinning for melts

3.1. Abstract

In this chapter we present a simple constitutive model based on Kuhn segment alignment that predicts the observed monotonic extension thinning in steady state viscosity η_E even at extension rates above the inverse Rouse time $\left(\dot{\varepsilon} > \tau_R^{-1}\right)$ for entangled polystyrene melts[1], while preserving the extension thickening typically seen in entangled solutions[2] for $\dot{\varepsilon} > \tau_R^{-1}$ .We tested two mechanisms by which Kuhn segment alignment can affect terminal relaxation time τ_d and rheology within a modified Doi-Edwards-Marrucci-Grizzuti (DEMG) model, which is a simplified tube model. The first mechanism is an increase in the tube diameter, as is inferred from ideas of Doi and Edwards[3] and Sussman and Schweizer[4], while the second mechanism is a decrease in segmental friction, as described in recent work of Yaoita *et al.*[5] . We find that the DEMG model, modified to allow tube diameter enlargement and reduction of entanglements, when done self-consistently, fails to predict extension thinning for entangled melts. The DEMG model modified by the second mechanism, to allow Kuhn segment alignment effects on local friction, correctly predicts extension thinning for entangled melts, while retaining thickening in entangled solutions with high solvent volume fractions. (**Text and figures in this chapter are reprinted from the manuscript - Desai, P. S. and R. G. Larson, *Journal of Rheology,* 58, 255 (2014)**)

3.2. Introduction

Understanding and modeling entangled polymer dynamics and rheology under fast flows has been an ongoing effort for the past four decades since the concept of an entangled test polymer chain surrounded by its mean field tube was introduced by de Gennes[6], Doi and Edwards[3,7]. Despite the successful analytical models that give an accurate description of equilibrium entangled polymer dynamics for linear viscoelasticity, molecular understanding of non-equilibrium fast flows has not yet been fully developed, even for the simplest case of nearly monodisperse linear (un-branched) polymers. Thus far, tube-based theories for nonlinear fast flows have only been partially successful. Three important nonlinear molecular mechanisms that have been included in the tube model are 1) orientation of tube segments, 2) chain stretch or retraction of the chains within the tube[8,9] and 3) flow-induced constraint release, or convective constraint release (CCR)[10-13]. The tube model, with these ingredients, predicts that concentrated polymer solutions behave roughly the same as entangled polymer melts, if they have the same number of entanglements per molecule and if stress, and strain rate, and/or time are made dimensionless using the plateau modulus and reptation time, respectively.

Although measurements of steady-state extensional viscosity for entangled polymeric melts are rare due to sample rupture, the extensional viscosities η_E found by Bach *et al.*[1] for monodisperse polystyrene melts of molecular weights 200,000g/mol and 390,000g/mol show dependencies on extension rate $\dot{\varepsilon}$ that are significantly different from those found for entangled polystyrene solutions by Sridhar and coworkers[2,14]. The results of Bach *et al.*[1] for melts show a monotonic decrease in η_E even at $\dot{\varepsilon} > \tau_R^{-1}$, where τ_R is the Rouse relaxation time, while for entangled solutions, the decrease in η_E only continues until $\dot{\varepsilon} \approx \tau_R^{-1}$, and an upturn in η_E occurs at extension rates higher than this. In addition, the extension-thinning region in both melts and solutions shows an extension-rate scaling of around $\eta_E \sim \dot{\varepsilon}^{-0.5}$ rather than the steeper decrease of $\eta_E \sim \dot{\varepsilon}^{-1}$ predicted by the tube model.

To help explain this unexpected extension thinning beyond the inverse Rouse time for melts and the power law, Marrucci and Ianniruberto[15] introduced the concept of "interchain tube

pressure" which predicts the observed exponent of -0.5 for melts, but introduces a new time constant τ_a, which lacks a clear molecular basis. It is unclear why τ_a obtained by fitting the experimental data of Bach *et al.*[1] is greater than the terminal relaxation time τ_d, for their 200K PS melt, while it is less than τ_d for the higher molecular weight melt (390K PS). Recently, Yaoita *et al.*[5] put forward the hypothesis that polymer stretch and orientation produce a decrease in the local friction coefficient ζ for chains in melts under fast extensional flows, which might explain the observed monotonic extension thinning in melts. They confirmed it by carefully analyzing stress relaxation data for PS melts in the nonlinear regime. This work was further supplemented by Kremer-Grest bead-spring MD simulations done by Masubuchi *et al.*[16] of stress relaxation following uniaxial extension for non-entangled PS chains. They observed accelerated relaxation at short times relative to what would be expected for constant friction, suggesting that alignment-induced friction reduction could occur even in un-entangled melts. Non-equilibrium MD studies on fast shear flows of PS oligomeric chains performed by Ianniruberto *et al.*[17] also suggest that monomeric friction decreases in fast shearing flows.

A second mechanism that might explain the observed differences in the extensional rheology of melts and solutions is alignment-induced tube widening. Sussman and Schweizer[4] recently developed a microscopic theory for the transverse tube confinement potential of entangled rod solutions, which they argue is relevant for flexible polymers as well and have extended it to study flexible entangled polymer melts in their recent PRL, Sussman and Schweizer[18]. A similar concept of rod-alignment-induced tube enlargement can be found in the work of Doi and Edwards[3]for rod-like polymers. One might expect greater segmental alignment in melts than in solutions, because in the former there are fewer Kuhn steps per entanglement than in the latter, and this might be a basis for the difference in their behaviors in extensional flows.

In this chapter, we test these two mechanisms by incorporating them within a basic tube model framework, namely the Doi-Edwards-Marrucci-Grizzuti (DEMG) model, which gives differential equations for the tube orientation tensor $\underline{\underline{S}}_{tube}$ and tube stretch λ, as well as an equation for the stress tensor. First we consider the effect of polymer Kuhn segment alignment on tube diameter and the effect of this, in turn, on the terminal relaxation time τ_d and plateau

modulus G_N, and through these, on the extensional rheology of melts and solutions. (The "Kuhn segment" referred to here is that of the chain itself, not that of the tube). The specific forms for the dependence of tube diameter on Kuhn segment alignment from the Doi-Edwards theory for rod-like polymers[3] and from the recent work by Sussman and Schweizer[4]. Both functional forms predict tube dilation, acceleration of rotational relaxation time and breakdown of the entanglement network for sufficiently large deformations. Note that, in a very recent study, Qin and Milner[19] have predicted a modest *shrinkage* of the tube diameter with chain alignment and stretching, based on the "packing length" and the "tension blob". Their predictions should only be relevant to rather modest chain alignment, since the "blob" picture they invoke requires that the polymer be essentially unaligned at small length scales, within a "tension blob." Our theory, on the other hand, accounts for changes in tube diameter when alignment of individual Kuhn steps becomes large, and "tension blobs" no longer exist. In this high stretch regime, evidence for a stress-induced increase in tube diameter and reduction in entanglement has also been suggested by Kushwaha and Shaqfeh[20] based on slip-link simulations under planar extension.

Our second approach is based on recent simulation results by Yaoita *et al.*[5] Masubuchi *et al.*[16] and Ianniruberto *et al.*[17] that suggest alignment of Kuhn segments causes reduction in local friction coefficient ζ in fast flows. This segmental friction decrease postulated by Yaoita *et al.*[5] should speed up both the Rouse time τ_R as well as the reptation time τ_d. We develop two specific functional forms for orientation dependent friction, $\zeta(F_{so})$ where F_{so} is the stretch/orientation parameter as coined by Yaoita *et al.*[5] .The functional forms chosen are the Doi-Edwards and Sussman-Schweizer orientational forms mentioned above, and each leads to the same orientation dependence of the reptation time τ_d as is derived from the tube-enlargement mechanism for that functional form. We choose these functional forms both to allow clear comparisons between predictions of the second mechanism (frictional changes) and those from the first mechanism (tube enlargement), and because these functional forms are similar to the effect of alignment on friction derived empirically from rheology data by Yaoita *et al*.[5]. These functional forms are then included in the one-mode version of the Doi-Edwards-Marrucci-Grizzuti (DEMG) tube model and are tested for the effect of Kuhn segment alignment on local friction, ζ and through this, on the predicted extensional rheology.

In addition, we consider the effect of convective constraint release (CCR), using the Mead-Larson-Doi formulation, which is the DEMG model with CCR. While CCR has not been regarded as essential for describing extensional flow data, we introduce it to consider its effect on extensional rheology, along with the effects of orientation-dependent friction. In addition, we briefly discuss the predictions of these models on shear flow, since our goal is to obtain a constitutive model that makes reasonable predictions for melts and solutions in general flows, including extensional and shear flows.

The chapter is organized as follows. Section 3.3 is divided into three sub-sections. We first introduce the basic DEMG model in Section 3.3.1. Section 3.3.2 presents theory and details of what we call the "self-consistent" constitutive model for tube dilation based on ideas of Doi and Edwards[3] and Sussman and Schweizer[4] that considers the effect of Kuhn segment alignment on the tube diameter and also considers the feedback that tube alignment has on the Kuhn segment alignment. Section 3.3.3 outlines a constitutive model that incorporates the effect of Kuhn-segment orientation on friction, motivated by ideas of Yaoita *et al.*[5]. Section 3.4 applies these two versions of the model to steady uniaxial extensional flow. The available experimental data in the literature for entangled melts and solutions are compared to the model in Section 3.5. A brief summary is given in Section 3.6.

3.3. Theory

3.3.1. Basic DEMG model

Our theory is based on the "toy," or one-mode, version of the DEMG model developed by Pearson *et al.*[21]. We simplify further by using a differential approximation to the orientation tensor $\underline{\underline{S}}_{tube}$ instead of its history integral equation for ease of numerical computation[22,23]. The DEMG model parameters are the plateau modulus G_N, the reptation time τ_d, the longest Rouse time τ_R, and maximum stretch ratio $\lambda_{\max}$. The toy DEMG constitutive model is given by the following set of equations:

$$\overset{\nabla}{\underline{\underline{S}}}_{tube} + 2\underline{\underline{\kappa}} : \underline{\underline{S}}_{tube}\underline{\underline{S}}_{tube} + \frac{1}{\tau_d}\left(\underline{\underline{S}}_{tube} - \frac{1}{3}\underline{\underline{\delta}}\right) = 0 \tag{1}$$

$$\dot{\lambda} = \lambda \underline{\underline{\kappa}} : \underline{\underline{S}}_{tube} - \frac{k_s\left(\lambda - 1\right)}{\tau_R} \tag{2}$$

$$\underline{\underline{\sigma}} = 3G_N k_s \lambda^2 \underline{\underline{S}}_{tube} \tag{3}$$

$$k_s = \frac{\left(3\lambda_{\max}^2 - \lambda^2\right)/\left(\lambda_{\max}^2 - \lambda^2\right)}{\left(3\lambda_{\max}^2 - 1\right)/\left(\lambda_{\max}^2 - 1\right)} \tag{4}$$

In Eq. (1), $\underline{\underline{S}}_{tube}$ is the orientation tensor that describes the average orientation of tube segments in three-dimensional space. The symbol ∇ above the orientation tensor $\underline{\underline{S}}_{tube}$ is its "upper convected derivative" and $\underline{\underline{\kappa}} = \left(\nabla v\right)^T$ is the transpose of the velocity gradient tensor. Equation (2) is the chain stretch rate equation. Here λ is the average tube (or chain) stretch, which is the length of primitive path relative to equilibrium. When there is no chain stretch, $\lambda = 1$. The first term on the right side of the stretch equation, $\lambda \underline{\underline{\kappa}} : \underline{\underline{S}}_{tube}$ describes the affine stretching of the primitive path while the last term describes chain retraction and hence shrinkage of the primitive path during flow. Equation (3) is the stress equation. The coefficient k_s accounts for the nonlinearity of the spring and is approximated by using the Padé approximation of the inverse Langevin function[24] given by Eq. (4). Here $\lambda_{\max}$ is the maximum stretch ratio of the chain, given by $\lambda_{\max} = L \Big/ \sqrt{\left\langle R^2 \right\rangle_0}$, where L is the fully stretched length of the tube segment and $\left\langle R^2 \right\rangle_0$ is the mean-square equilibrium end-to-end length of the tube segment in the absence of flow.

3.3.2. Self-consistent model for tube diameter enlargement based on rod orientation

In the Doi-Edwards model for semi-dilute solutions of rods, a given rod is confined by the surrounding rods to a tube-like region, analogous to the tube for flexible polymers. The rods are free to move along their length, while motion perpendicular to the rod is restricted due to surrounding polymer rods. In the non-linear regimes and under fast flow rate, the effective tube diameter increases as the orientations of surrounding rods become more nearly parallel to the

tube. Fast flow, for example fast extension, thus causes the tube diameter to increase as rods become more and more oriented and aligned toward the flow direction. We now apply this basic idea to flexible chains, whose entanglement density should in principle also be reduced as the chains become highly aligned. This reduction in entanglement density caused by orientation leads to tube dilation.

The entanglement effect in rod-like polymers is captured using the tube model where the dominant interaction is due to topological constraints, since the rods cannot cross each other. Doi and Edwards[3] gave a form for the effect of the rod alignment on the tube diameter a;

$$a = a_0 \left(1 - S^2\right)^{-1} = a_0 \left(1 - \underline{\underline{S}}_{rod} : \underline{\underline{S}}_{rod}\right)^{-1} \tag{5}$$

here $\underline{\underline{S}}_{rod} \equiv \langle \underline{u}\underline{u} \rangle$ is the rod alignment tensor which describes the average orientation of a rod segment in three-dimensional space and S is the scalar order parameter where $S^2 = \underline{\underline{S}}_{rod} : \underline{\underline{S}}_{rod}$ (Here we find it convenient to omit the subtraction of an isotropic tensor $\underline{\underline{\delta}}/3$ in our definition of $\underline{\underline{S}}_{rod}$, which accounts for our omission of a factor of 3/2 from Eq. (5)). Doi and Edwards used Eq. (5) to obtain the dependence of the average rotary diffusivity $\overline{D}_r$, and rotational relaxation time, on rod alignment through the tensor $\underline{\underline{S}}_{rod}$.

Our interest is in applying similar ideas to flexible polymers. Following a similar objective, Sussman and Schweizer[4] recently derived an orientation-induced enlargement of a "localization length" that can be identified with the tube diameter. Sussman and Schweizer's form shows a somewhat different dependence on the order parameter than that of Eq. (5), namely

$$a = a_0 \left(1 - S\right)^{-1/2} = a_0 \left(1 - \left(\underline{\underline{S}}_{rod} : \underline{\underline{S}}_{rod}\right)^{1/2}\right)^{-1/2} \tag{6}$$

Although equations (5) and (6) were developed for rod-like polymers, the hope is that similar formulas apply to flexible polymers. In what follows, we will use both the Doi-Edwards (DE) and Sussman-Schweizer (SS) expressions for the tube diameter. For flexible polymers, the number of entanglements per chain scales with the tube diameter as a^{-2}, and the reptation time of the unoriented polymer is given by $\tau_{d0} = 3Z\tau_R$, where τ_R is the Rouse time and τ_{d0} is the

reptation time in the absence of contour-length fluctuations (for details, see standard references such as Doi and Edwards (1986)). Here $Z = M/M_e$ is the number of entanglements per chain in the absence of deformation, with M_e being the entanglement spacing. The effect of deformation dependent tube diameter on the reptation time is therefore given by

$$\tau_{d0} = 3Z\left(\frac{a_0}{a}\right)^2 \tau_R \tag{7}$$

where a_0 is the tube diameter in the absence of deformation. Similarly, the plateau modulus also scales roughly inversely with the square of the tube diameter. As a first guess, let us assume that the tube diameter a for flexible polymers depends on the orientation of the Kuhn segments of the polymer chain in a similar way that a depends on rod orientation in stiff polymers.

Then, from Eq. (5) and Eq. (7),

$$\tau_d = \tau_{d0}(1-S^2)^2 = \tau_{d0}\left(1-\left(\underline{\underline{S}}_{rod} : \underline{\underline{S}}_{rod}\right)\right)^2 \tag{8}$$

Alternatively, using the Sussman-Schweizer expression, Eq. (6), with Eq. (7),

$$\tau_d = \tau_{d0}(1-S) = \tau_{d0}\left(1-\left(\underline{\underline{S}}_{rod} : \underline{\underline{S}}_{rod}\right)^{1/2}\right) \tag{9}$$

Now consider a freely jointed chain made up of N_k rigid links each of length b_k and connected to each other at flexible joints. Its contour length is $L = N_k b_k$, and its orientation is given as,

$$\underline{\underline{S}}_{Kuhn} = \underline{\underline{S}}_{rod} = \langle \underline{u}\underline{u} \rangle \tag{10}$$

Where $\underline{u}$ is the orientation vector of a single link in a chain and $\langle\ \rangle$ denotes an average overall conformations of the chain. It is important to note here that we assume $\underline{\underline{S}}_{rod}$ to be same as $\underline{\underline{S}}_{Kuhn}$, where the latter is the orientational order parameter of the Kuhn steps in the chain.

Solving for $\underline{\underline{S}}_{rod} : \underline{\underline{S}}_{rod}$,

$$\underline{\underline{S}}_{rod} : \underline{\underline{S}}_{rod} = \langle \underline{u}\underline{u} \rangle : \langle \underline{u}\underline{u} \rangle \tag{11}$$

Kuhn and Grün[25] and Fuller[26] showed that for a chain strand that is constrained to have an end-to-end vector $\underline{R}$, for modest departures from equilibrium (i.e., modest chain deformation), here $\underline{\underline{\delta}}$ being a unit tensor,

$$\langle \underline{u}\underline{u} \rangle = \frac{1}{3}\underline{\underline{\delta}} - \frac{1}{5}\frac{1}{L^2}\langle R^2 \rangle_0 \underline{\underline{\delta}} + \frac{3}{5}\frac{1}{L^2}\langle \underline{R}\underline{R} \rangle \tag{12}$$

For a highly oriented chain, however, we must approach the limit

$$\langle \underline{u}\underline{u} \rangle \approx \frac{1}{L^2}\langle \underline{R}\underline{R} \rangle \tag{13}$$

In principle one should develop an expression for $\langle \underline{u}\underline{u} \rangle$ that interpolates between these two limits, but it suits our purposes here to simply use Eq. (13) for all chain orientations, since it is at least qualitatively correct even for small chain orientations.

The Doi-Edwards-Marrucci-Grizzuti (DEMG) theory[21,23], with the independent alignment approximation (IAA), allows us to obtain the stress tensor from the average orientation and stretch of a single tube segment. If $\underline{R}$ is the end-to-end vector of the tube segment after it has been stretched and oriented by the flow, then, within the DEMG theory with IAA, we can relate the moment tensor $\langle \underline{R}\underline{R} \rangle$ to the average orientation of tube segments $\underline{\underline{S}}_{tube}$ and the average tube (or chain) stretch λ as,

$$\langle \underline{R}\underline{R} \rangle = \langle R^2 \rangle_0 \lambda^2 \underline{\underline{S}}_{tube} \tag{14}$$

Solving for $\langle \underline{u}\underline{u} \rangle : \langle \underline{u}\underline{u} \rangle$ and using Eqs. (13) and (14),

$$\langle \underline{u}\underline{u} \rangle : \langle \underline{u}\underline{u} \rangle = \frac{1}{L^4}\langle \underline{R}\underline{R} \rangle : \langle \underline{R}\underline{R} \rangle = \frac{\langle R^2 \rangle_0^2}{L^4}\lambda^4 \underline{\underline{S}}_{tube} : \underline{\underline{S}}_{tube} = \frac{\lambda^4}{\lambda_{\max}^4}\underline{\underline{S}}_{tube} : \underline{\underline{S}}_{tube} \tag{15}$$

Here $\lambda_{\max}$ is the maximum stretch ratio of the chain as defined earlier.

From Eqns. (8), (11) and (15), we estimate the relationship between the effective tube relaxation time, τ_d and the tube orientation tensor, $\underline{\underline{S}}_{tube}$ based on the Doi-Edwards relationship for the tube diameter is,

$$\tau_d = \tau_d^f \left(1 - \frac{\lambda^4}{\lambda_{\max}^4} \left(\underline{\underline{S}}_{tube} : \underline{\underline{S}}_{tube} \right) \right)^2 \tag{16}$$

An analogous expression applies for the plateau modulus,

$$G_N = G_N^f \left(\frac{a_0}{a} \right)^2 = G_N^f \left(1 - \frac{\lambda^4}{\lambda_{\max}^4} \left(\underline{\underline{S}}_{tube} : \underline{\underline{S}}_{tube} \right) \right)^2 \tag{17}$$

By using Eqns. (9), (11) and (15), we obtain the Sussman-Schweizer (SS) expression that relates final relaxation time, τ_d to the orientation tensor, $\underline{\underline{S}}_{tube}$,

$$\tau_d = \tau_d^f \left(1 - \frac{\lambda^2}{\lambda_{\max}^2} \left(\underline{\underline{S}}_{tube} : \underline{\underline{S}}_{tube} \right)^{1/2} \right) \tag{18}$$

Correspondingly,

$$G_N = G_N^f \left(1 - \frac{\lambda^2}{\lambda_{\max}^2} \left(\underline{\underline{S}}_{tube} : \underline{\underline{S}}_{tube} \right)^{1/2} \right) \tag{19}$$

The above expressions suggest that the tube diameter increases as the chains becomes aligned in the direction of stretch, which causes the reptation time to decrease with increasing Kuhn segment alignment, which is reflected in the increasing values of both λ and $\underline{\underline{S}}_{tube} : \underline{\underline{S}}_{tube}$. Notice that we use the primitive path fluctuation corrected values for reptation time and plateau modulus viz. τ_d^f and G_N^f instead of pure reptation time τ_d^0 and uncorrected plateau modulus G_N^0 since the DEMG model does not explicitly account for early time contour length fluctuations. This correction is easily calculated from formulas given by Likhtman and McLeish[27].

Remarkably, if we use the Sussman-Schweizer expression for the tube diameter, the above expressions for the reptation time and plateau modulus yield very good predictions for the extensional viscosity for both polystyrene solutions and melts. However, we do not present these results, because the model, as developed thus far, *is not self-consistent*. In the basic DEMG framework, the stretch ratio λ and maximum stretch ratio $\lambda_{\max}$ are defined based on the average number of chain segments (or "Kuhn segments") between consecutive entanglements and that is why $\lambda_{\max}$ is smaller for entangled melts than for entangled solutions. Furthermore $\lambda_{\max}$ depends only on the number of Kuhn segments and is a constant as long as the tube diameter remains unchanged. However, our theory described above is based on the idea that chain alignment at the Kuhn level induced by fast flows decreases the topological constraints to lateral motion thus increasing the tube diameter a. This dependence of the tube diameter on the order parameter of Kuhn segments of the chain is given by Eqns. (5) (DE form) or (6) (SS form). Consequently, as the tube diameter a increases with tube alignment, $\lambda_{\max}$ is no longer a constant (as a helpful referee of our manuscript pointed out) and should also consistently increase by a factor α as a function of the tube order parameter as given below, in terms of the DE tube diameter,

$$\alpha = \frac{\lambda_{\max}}{\lambda_{\max 0}} = \frac{a}{a_0} = \left(1 - S^2\right)^{-1} \tag{20}$$

where $\lambda_{\max 0}$ is the maximum stretch in the absence of tube dilation and S is just the rod scalar order parameter first mentioned in Eqns. (5) and (6) . Similarly, in terms of the SS tube diameter,

$$\alpha = \frac{\lambda_{\max}}{\lambda_{\max 0}} = \frac{a}{a_0} = \left(1 - S\right)^{-1/2} \tag{21}$$

This change should also be consistently reflected in Eqns. (16) and (18), which relate the effective tube relaxation time, τ_d to the tube orientation tensor, $\underline{\underline{S}}_{tube}$. The "self-consistent" DE expression for terminal relaxation as a function of the tube order parameter is given by,

$$\tau_d = \tau_d^f \left(1 - \frac{\lambda^4}{\lambda_{\max 0}^4 \alpha} \left(\underline{\underline{S}}_{tube} : \underline{\underline{S}}_{tube} \right) \right)^2 \tag{22}$$

The corresponding "self-consistent" SS expression is,

$$\tau_d = \tau_d^f \left(1 - \frac{\lambda^2}{\lambda_{\max 0}^2 \alpha} \left(\underline{\underline{S}}_{tube} : \underline{\underline{S}}_{tube} \right)^{1/2} \right) \tag{23}$$

To complete the equation set, we need to revise Eq. (2), the equation for the dynamics of tube stretch, to account for the changing value of $\lambda_{\max}$ as the tube diameter grows. The dynamics of tube stretch involves details of how tube segments merge together as the tube enlarges. During start-up of extensional flow fast enough to stretch out the chain, there will first be alignment of tube segments, while preserving the back folds in the tube contour. The chain within each tube segment becomes nearly fully extended at modest strains in a melt, since $\lambda_{\max}$ is small. Depending on the number of entanglements in the chain, one or more additional Hencky strain units are required to remove the backfolds and straighten out the tube. If Kuhn segment alignment causes the tube to widen, then the back folded segments will merge, so that there is more chain contour in the same length of enlarged tube. And this causes chain stretch to decrease. A cartoon of this process is shown in Figure 3.1. The relationship of this process to "convective constraint release" (CCR) is not entirely clear to us, but the simplest representations of CCR have involved changes in reptation time, but not in $\lambda_{\max}$ or in the plateau modulus, which are implied by the tube enlargement considered here. While capturing the details of the "tube enlargement process" will require a model that goes beyond a simple extension of the "two-mode" DEMG model presented here, we can, at least, ensure that the model behaves properly at high strains and high strain rates, where the difference between entangled melts and entangled solutions is most obvious. At asymptotically high extensional strains and rates, where the entire polymer molecule, and not just the individual tube segments, becomes nearly fully aligned, the stress is determined by tension in the chain, and the tube becomes irrelevant. This limit is approximately described by the "FENE-P" constitutive model, whose stress is given by[28]

,

$$\underline{\underline{\sigma}} = 3GH_c \left\langle \underline{R}\underline{R} \right\rangle \Big/ \left\langle R^2 \right\rangle_0 \tag{24}$$

where G is the modulus, given by $k_B T$ times the number of molecules per unit volume, $\left\langle R^2 \right\rangle_0$ is the mean-square end-to-end vector of the chain at equilibrium, and H_c is the pre-averaged

spring constant for the whole chain. H_c depends on the average stretch, which we take to be given by the Cohen Padé approximation,

$$H_c = \frac{\left(3\lambda_{c,\max}^2 - \lambda_c^2\right)/\left(\lambda_{c,\max}^2 - \lambda_c^2\right)}{\left(3\lambda_{c,\max}^2 - 1\right)/\left(\lambda_{c,\max}^2 - 1\right)} \tag{25}$$

We used this form for the nonlinearity of the spring in the DEMG model in Eq. (4), with λ being the ratio of the length L of the stretched tube segment to its equilibrium length a, and $\lambda_{\max}$ being the maximum value of this ratio. In Eq. (25), λ_c and $\lambda_{c,\max}$ are the stretch and maximum stretch *of the chain as a whole*. Hence, λ_c is the ratio of the stretched length L_c of the entire chain to its equilibrium coil end-to-end distance $aZ^{1/2}$ where Z is the number of entanglements in the chain. Thus, in the fully stretched state, the stretch of the whole chain L_c is given by ZL, so that $\lambda_c = Z^{1/2}\lambda$ and $\lambda_{c.\max} = Z^{1/2}\lambda_{\max}$. For a large $\lambda_{\max}$, the factor of Z nearly cancels out in Eq. (25), and H_c becomes nearly equal to k_s, in Eq. (4), as long as the tube stretch equation, Eq. (2), remains otherwise the same, *with the same value of the frictional Rouse time* τ_R. Also, the modulus G in Eq. (24) is related to G_N by $G = G_N/Z$. Once chains become fully aligned in extensional flow, the FENE-P stress along the x (or flow axis) then becomes

$$\sigma_{xx} \;=\; 3GH_c\left(\frac{\langle R_x R_x\rangle}{\langle R^2\rangle_0}\right) \rightarrow\; 3Gk_s\lambda_{c,\max}^2 = 3\left(\frac{G_N}{Z}\right)k_s\left(\lambda_{\max}^2 Z\right) \;=\; 3G_N k_s\lambda_{\max}^2 \tag{26}$$

The stress in the DEMG theory, given by Eq. (3), $\underline{\underline{\sigma}} = 3G_N k_s \lambda^2 \underline{\underline{S}}_{tube}$, for nearly fully stretched chains, reduces to

$$\sigma_{xx} = 3G_N k_s \lambda_{\max}^2 \tag{27}$$

This is the same as is given by the FENE-P theory, as expected, since entanglements are irrelevant in the fully stretched state. Thus, in the fully stretched state, the stress predicted by the DEMG theory reduces to that of fully stretched un-entangled chains, given by the FENE-P theory. The larger value of the maximum stretch $\lambda_{c,\max} \approx Z^{1/2}\lambda_{\max}$ of the un-entangled chains

relative to the entangled ones, is compensated by the smaller modulus $G = G_N / Z$. The dynamics of the change in maximum stretch and modulus are affected by the way in which tube segments merge during tube enlargement, but the stress in the asymptotic high-stretch limit should revert to that of the FENE-P, and hence of the DEMG theory.

Thus, without developing a detailed model, we know already that orientation-induced tube enlargement will not account for the high-strain-rate differences between melts and solutions, since melts and solutions will both be described by the ordinary DEMG theory at high extensions. We can illustrate this more concretely by incorporating a simple form for the tube stretch equation that accounts for tube enlargement. We start with a generalized expression for the length L of a tube segment, incorporating affine stretch, and relaxation back to unstretched length,

$$\frac{d\left(L/a_0\right)}{dt} = \left(\frac{L}{a_0}\right)\underline{\underline{\kappa}} : \underline{\underline{S}}_{tube} - \frac{k_s}{\tau_R}\left(\frac{L}{a_0} - \frac{a}{a_0}\right) \tag{28}$$

Next we allow that the length of the stretched tube segment is the product of the instantaneous tube diameter a and the stretch ratio λ. That is,

$$L = a\lambda\,,\ L/a_0 = \left(a/a_0\right)\lambda = \alpha\lambda \tag{29}$$

The above two equations yield,

$$\frac{d\left(\alpha\lambda\right)}{dt} = \alpha\lambda\underline{\underline{\kappa}} : \underline{\underline{S}}_{tube} - \frac{k_s}{\tau_R}\alpha\left(\lambda - 1\right)$$

and hence

$$\frac{d\lambda}{dt} = -\frac{\lambda}{\alpha}\frac{d\alpha}{dt} + \lambda\underline{\underline{\kappa}} : \underline{\underline{S}}_{tube} - \frac{k_s}{\tau_R}\left(\lambda - 1\right) \tag{30}$$

In this way, the merger of tube segments caused by loss of entanglements causes the tube diameter a to increase, as given by Eqs. (5) or (6), and this causes the stretch ratio λ to decrease, as shown by the first term on the right side of Eq. (30) above. Note that as the chain becomes fully stretched, λ becomes inversely proportional to the tube diameter a, and hence

the product of λ^2 and the plateau modulus G_N (which is proportional a^{-2}) becomes independent of tube diameter a, and we thus recover the FENE-P stress at high extension, as we should.

The following set of equations constitute, what we call, the "self-consistent" DEMG-R(DE) model with "R" designating the physics borrowed from the tube theory for rods. And "DE" designates the use of the expression for tube diameter from the Doi-Edwards theory.

$$\overset{\nabla}{\underline{\underline{S}}}_{tube} + 2\underline{\underline{\kappa}} : \underline{\underline{S}}_{tube}\underline{\underline{S}}_{tube} + \frac{1}{\tau_d}\left(\underline{\underline{S}}_{tube} - \frac{1}{3}\underline{\underline{\delta}}\right) = 0 \tag{31}$$

$$\alpha = \frac{\lambda_{\max}}{\lambda_{\max 0}} = \frac{a}{a_0} = \left(1 - S^2\right)^{-1} \tag{32}$$

$$\tau_d = \tau_d^f \left(1 - \frac{\lambda^4}{\lambda_{\max 0}^4 \alpha}\left(\underline{\underline{S}}_{tube} : \underline{\underline{S}}_{tube}\right)\right)^2 \tag{33}$$

$$G_N = G_N^f \left(1 - \frac{\lambda^4}{\lambda_{\max 0}^4 \alpha}\left(\underline{\underline{S}}_{tube} : \underline{\underline{S}}_{tube}\right)\right)^2 \tag{34}$$

$$\frac{d\lambda}{dt} = -\frac{\lambda}{\alpha}\frac{d\alpha}{dt} + \lambda \underline{\underline{\kappa}} : \underline{\underline{S}}_{tube} - \frac{k_s}{\tau_R}(\lambda - 1) \tag{35}$$

$$\underline{\underline{\sigma}} = 3G_N k_s \lambda^2 \underline{\underline{S}}_{tube} \tag{36}$$

$$k_s = \frac{\left(3\lambda_{\max 0}^2 \alpha^2 - \lambda^2\right)/\left(\lambda_{\max 0}^2 \alpha^2 - \lambda^2\right)}{\left(3\lambda_{\max 0}^2 \alpha^2 - 1\right)/\left(\lambda_{\max 0}^2 \alpha^2 - 1\right)} \tag{37}$$

We can write similar set of equations for the "self-consistent" DEMG-R(SS) model where "SS" designates the use of Sussman-Schweizer expression for the tube diameter. In either case, the stress at large deformations reverts to that of the DEMG theory, as we will see shortly, and hence fails to distinguish between melts and solutions.

3.3.3. Friction model based on rod orientation/stretch

It is well documented that in nematic liquid crystals there is friction reduction along the alignment direction as the rod-like molecules become highly oriented[3,22]. However, molecular theories for fast flows of polymeric liquids where strong alignment occurs even at the level of the Kuhn segment generally still assume that the local friction, ζ of each polymeric Kuhn step remains that at the equilibrium value, ζ_{eq}. Recently, however, Yaoita *et al.*[5] suggested that the monomeric friction, ζ between a polymer chain and the surrounding molecules is affected by chain orientation and proposed that the local friction coefficient, ζ is dependent on a stretch/orientation parameter, $F_{so} = \tilde{\lambda}^2 \overline{S}$. Here $\tilde{\lambda} = \lambda / \lambda_{\max}$ represents the stretch ratio normalized by its fully stretched limit and $\overline{S}\left(= \phi_p S_p\right)$ is the average orientational anisotropy of both polymer and any solvent present with ϕ_p the polymer volume fraction. We note here that for melts, for which ϕ_p = 1, $F_{so} = \frac{\lambda^2}{\lambda_{\max}^2}\left(\underline{\underline{S}}_{tube} : \underline{\underline{S}}_{tube}\right)^{1/2}$, which is identical to the measure of Kuhn segment alignment used above in our theories of alignment-induced tube enlargement. Yaoita *et al.*[5] obtained the dependence of ζ on F_{so} by analyzing stress decay data following cessation of extensional flow for both melts and solutions. The empirical equation for the friction reduction ratio, $\zeta(F_{so})/\zeta(0)$, determined in this way shows a decrease with increasing F_{so}(> 0.15). This function, when included in 3-D Primitive Chain Network (PCN)-FENE slip link simulations, correctly mimics the monotonic thinning of steady-state $\eta_E(\dot{\varepsilon})$ data for polystyrene (PS) melts.

Drawing from this work, we seek to test the effect of Kuhn segment alignment on local friction, ζ when incorporated within the Doi-Edwards-Marrucci-Grizzuti (DEMG) model. The local friction decrease reduces both the terminal reptation relaxation time and the Rouse time according to

$$\tau_d = \tau_d^0 \zeta(F_{so}) \tag{38}$$

$$\tau_R = \tau_R^0 \zeta(F_{so}) \tag{39}$$

To compare the effects of frictional reduction to those of tube enlargement, and taking advantage of the fact that Kuhn segment alignment is measured with the same scalar factor in both

approaches, we propose forms for the dependent of friction coefficient on Kuhn segment alignment that for melts give the same dependence of reptation time of Kuhn segment alignment that we used in the earlier sections. Thus, we propose:

$$\zeta(F_{so}) = \left(1 - \phi_p \frac{\lambda^4}{\lambda_{\max}^4} \left(\underline{\underline{S}}_{tube} : \underline{\underline{S}}_{tube} \right) \right)^2 \tag{40}$$

$$\zeta(F_{so}) = \left(1 - \phi_p \frac{\lambda^2}{\lambda_{\max}^2} \left(\underline{\underline{S}}_{tube} : \underline{\underline{S}}_{tube} \right)^{1/2} \right) \tag{41}$$

Eq. (40) is motivated by the Doi-Edwards theory for Kuhn step alignment and loss of entanglements while, Eq. (41) is motivated by the Sussman-Schweizer treatment of the topologically entangled rodlike polymer solutions. We note that these forms are qualitatively similar to the dependence of ζ on F_{so} inferred from experimental data by Yaoita *et al.*[5] and from molecular dynamics simulations of Ianniruberto *et al.*[17]. While these forms give us the same dependence of reptation time on alignment as given by the DEMG-R equations, the latter tube-enlargement theories contained *no dependence of Rouse time on Kuhn segment alignment*, but do contain a dependence of modulus on alignment, which is lacking in the friction-based theories. And, of course, friction-based theories do not need a "feedback" mechanism to make them self-consistent, as is required for the tube-enlargement theories. More generally, our various models can be used to explore the consequences of alignment-induced changes to the reptation time, the Rouse time, and the modulus.

Equations (1)-(4), from the DEMG theory, along with Eqns. (38), (39) and (40) are referred to here as the DEMG-F(DE) model while Equations (38), (39) and (41) along with Equations (1)-(4) is called the DEMG-F(SS) model, "F" standing for friction reduction resulting from chain orientation and stretch.

We note here that recent work by Huang *et al.*[29] suggests that the friction depends not only on stretch and orientation of tube segments, but also on the solvent, since they observed that identical polymers at the same concentration in different solvents show different viscosities at high strain rate. Thus, the simple expressions given in Eqs. (40) and (41) are evidently not adequate for all cases, and the nature of the solvent will have to be taken into account in the

expression for the orientation-dependent friction. Nevertheless, we show below that the above expressions are adequate for at least the cases considered here.

3.4. Application to steady state uniaxial extensional flow

We now explore the predictions of the DEMG model that has been modified to include flow-induced tube enlargement in Section 3.3.2 and to include orientation dependent decrease in local friction coefficient ζ in Section 3.3.3, for steady state viscosity functions under steady uniaxial extension for a set of monodisperse polystyrene solutions and melt samples. The constitutive equations given in Section 3.4 are solved numerically using an explicit time stepping scheme until steady state values for the orientation tensor $\underline{\underline{S}}_{tube}$, the reptation time τ_d, the modulus G_N, the stretch ratio λ, the stress tensor $\underline{\underline{\sigma}}$, and extensional viscosity $\bar{\eta}$ are reached. The time step size for all cases is kept small enough (Δt = 10^{-6} sec) to ensure good convergence.

For uniaxial extension, the transpose of velocity gradient tensor is given by,

$$\underline{\underline{\kappa}} = (\nabla v)^T = \begin{pmatrix} \dot{\varepsilon} & 0 & 0 \\ 0 & -\dot{\varepsilon}/2 & 0 \\ 0 & 0 & -\dot{\varepsilon}/2 \end{pmatrix} \tag{42}$$

where $\dot{\varepsilon}$ is the extension rate.

The tube orientation tensor is given by,

$$\underline{\underline{S}}_{tube} = \begin{pmatrix} S_{11} & 0 & 0 \\ 0 & S_{22} & 0 \\ 0 & 0 & S_{33} \end{pmatrix} \tag{43}$$

For uniaxial extension, $S_{22} = S_{33}$. Therefore, the rate of affine stretching of the mesh of entanglements is given by,

$$\underline{\underline{\kappa}} : \underline{\underline{S}}_{tube} = \begin{pmatrix} \dot{\varepsilon} & 0 & 0 \\ 0 & -\dot{\varepsilon}/2 & 0 \\ 0 & 0 & -\dot{\varepsilon}/2 \end{pmatrix} : \begin{pmatrix} S_{11} & 0 & 0 \\ 0 & S_{22} & 0 \\ 0 & 0 & S_{33} \end{pmatrix} = \dot{\varepsilon}\left(S_{11} - S_{22}\right) \tag{44}$$

The extensional viscosity is given as,

$$\bar{\eta} = \frac{\sigma_{11} - \sigma_{22}}{\dot{\varepsilon}} \quad \text{where} \quad \underline{\underline{\sigma}} = 3G_N k_s \lambda^2 \underline{\underline{S}}_{tube} \tag{45}$$

3.5. Results and discussion

3.5.1. Determination of the model parameters

The key parameters for the DEMG-R model are the plateau modulus G_N^0, the uncorrected reptation time τ_{d0}, the longest Rouse time τ_R, the average number of entanglements per chain *Z* and the maximum stretch ratio $\lambda_{\max}$, which is the ratio of maximum to equilibrium tube segment length. The parameters used in the model for all the solutions and melt samples studied here are taken from Acharya *et al.*[30], except for melts 100K PS, 285K PS, 545K PS, 145K PS, 200K PS-Shear, and solutions 7% 8.42M PS-Shear and 10% 2M PS-Shear. Acharya *et al.*[30] obtained τ_{d0} and τ_R by fitting the predictions of Milner-McLeish model[31] to the linear viscoelastic data, whereas Z and G_N^0 are obtained from established literature correlations. We followed this same procedure to obtain parameters for the melts 100K PS, 145K PS, 200K PS-Shear and solution 10% 2M PS-Shear. Parameters for melts 285K PS and 545K PS are taken from Huang *et al.*[32],and those for the 7% 8.42M PS solution are taken from Pattamaprom and Larson[33]. The value of τ_d^f was taken as half the reptation time given in Pattamaprom and Larson[33], where the factor of 1/2 is introduced because they used a double reptation formulation of the MLD theory, which we do not use, and double reptation reduces the terminal reptation time by a factor of two, as discussed in Pattamaprom and Larson[33]. The τ_{d0} value reported in our table was calculated from our reported τ_d^f by back-calculating using the fluctuation correction. Table 3.1 summarizes parameters of the entangled polymeric solutions and melts studied here. Note that inclusion of the new physics has introduced no additional parameters into the tube model.

There have been reports that in step shear experiments the time constant governing retraction of the chain in the tube is longer than the Rouse time, as estimated from the traditional

tube theory[34-36] . However, in start-up of extension, to date, the extension rate at which an upturn is observed is more or less consistent with the value of the Rouse time, as estimated using standard formulas[2]. If the time constant governing retraction were much larger than the Rouse time assumed here, then the upturn in extensional viscosity observed in solutions would occur at much lower extension rates than is observed experimentally. So, at this point, we apply the normal expressions for the Rouse time as estimated by Acharya *et al.*[30].

3.5.2. Quantitative comparison with data for polymer melts

Figure 3.2 compares predictions of the DEMG (dot-dashed lines) with the "self-consistent" DEMG-R(DE) model (dashed lines) and the "self-consistent" DEMG-R(SS) model (solid lines) for steady state viscosity $\eta_E(\dot{\varepsilon})$ data for five different polystyrene (PS) melts, viz.100K PS, 200K PS, 285K PS, 390K PS and 545K PS. The DEMG version of the tube model, which includes chain stretch (but does not include convective constraint release or CCR), exhibits a sharp upturn in viscosity as the extension rate reaches a value on the order of the inverse Rouse time, indicating the onset of chain stretch. This prediction deviates from the melt data, as has been previously documented[1,15] . The "self-consistent" DEMG-R(XX) model, where "XX" stands for either "DE" or "SS", also follows the original DEMG model predictions and shows an upturn in steady viscosity for melts. The reason was explained earlier: at asymptotically high stretch, the entanglements no longer matter, and the stress must approach that given by the FENE-P model, just as does the stress in the DEMG model. So, flow induced changes in entanglement structure can have no effect on the asymptotic behavior and the DEMG model must be correct in this limit.

Figure 3.3 shows predictions for the friction based DEMG-F(DE) (dashed lines) and DEMG-F(SS) (solid lines) models with the standard DEMG (dot-dashed lines) for steady state viscosity $\eta_E(\dot{\varepsilon})$ data of polystyrene (PS) melts. In the intermediate flow regime, where $\tau_d^{-1} < \dot{\varepsilon} < \tau_R^{-1}$, both the DEMG-F(DE) and the DEMG-F(SS) models show a monotonic decrease in η_E. On reaching fast flows, where $\dot{\varepsilon} \approx \tau_R^{-1}$, there is a slight upturn in η_E which is cut-off by the reduction in monomeric friction due to Kuhn segment alignment and thinning of the viscosity resumes at high rates. Thus both of the friction-based models agree fairly well with the

experimental data. Moreover, the predictions are not very sensitive to the form used for the dependence of friction on F_{so}, implying that these predictions are robust ones. The friction-based models succeed where the tube-enlargement models fail because in the highly aligned limit where entanglements no longer matter, for a given strain rate, the friction-based models reduce the Rouse relaxation time, and hence reduce the drag on the chains and therefore the extensional viscosity, while the tube-enlargement models only contain changes in the tube diameter and not the friction, and hence are impotent to affect the stress.

Figure 3.4 shows friction based DEMG-F(DE) model predictions for the melt 200K PS, for the diagonal entries, S_{11} and S_{22} of the orientation tensor $\underline{\underline{S}}_{tube}$, the stretch ratio λ, and the tube relaxation time τ_d and Rouse time τ_R as functions of extension rate $\dot{\varepsilon}$. S_{11} increases from 1/3 to 1 as the Kuhn steps become oriented in the direction of flow. Consequently, S_{22} falls from a value 1/3 to a small value close to zero. The stretch ratio λ increases and then saturates at $\lambda_{\max}$. In the fast-flow regime for which the extension rate is around the inverse Rouse time $\dot{\varepsilon} \approx \tau_R^{-1}$, the reptation time falls, indicating the onset of local friction reduction, which accelerates both the terminal relaxation time as well as Rouse time.

In Figure 3.5 we plot the normalized stress decay data $\sigma_E(t)/\sigma_E(1)$, for melt 145K PS at 120°C immediately after cessation of elongational flow. For all the mentioned extension rates, the flow was stopped when a Hencky strain of ε = 3 was reached and stress was allowed to relax. Solid lines show predictions of the friction based DEMG-F(DE) model. The agreement is not so good; however, this can be attributed to the absence of fast Rouse relaxation modes in our two-mode "toy" theory, which contains only the longest Rouse relaxation time and the reptation time. While the DEMG-F(DE) model with just two relaxation times (cannot capture time-dependent phenomena at short times, we do observe a speed-up in the normalized stress decay $\sigma_E(t)/\sigma_E(1)$ with increasing extension rates. This suggests acceleration of relaxation due to reduction in monomeric friction caused by high alignment at short times immediately after flow cessation. The model also includes acceleration of relaxation due to FENE springs, which is why it shows faster relaxation even at relatively short times in the regime of chain-stretch relaxation. However, in the stress relaxation data, the two effects are combined.

3.5.3. Quantitative comparison with data for polymer solutions

Figure 3.6 compares predictions of the basic DEMG (dot-dashed lines) with the DEMG-F(DE) model (dashed lines) and the DEMG-F(SS) model (solid lines) for steady state viscosity $\eta_E(\dot{\varepsilon})$ data of six different polymer solutions viz. 10% 1.95M PS, 15% 1.95M PS, 20% 1.95M PS, 10% 3.9M PS, 15% 3.9M PS and 17% 3.9M PS. As expected, the predictions of the friction based DEMG-F(DE) and DEMG-F(SS) models for solutions are insensitive to the orientation-induced friction reduction that we found to be important in melts. This is because the orientation effect in solutions is diluted by the presence of a solvent. Thus, the maximum stretch ratio $\lambda_{\max}$ is larger for solutions than for melts (which causes the term $\lambda^2/\lambda_{\max}^2$ to be smaller in solutions than in melts at a similar Weissenberg number). The result is that for solutions, both the DEMG-F(DE) and DEMG-F(SS) models give results almost identical to those for the DEMG model.

3.5.4. The effect of convective constraint release (CCR)

In the above, we left out the additional relaxation mechanism of convective constraint release (CCR), which describes a form of flow-induced disentanglement, which has been found to be important in shearing flows, but is generally less important in extensional flows. Figure 3.7(a) compares predictions in extensional flow of the basic DEMG model (dot-dashed line) to that of a model that includes CCR, namely the basic MLD model, given by a dotted line (not seen in the figure since it is superposed on the solid-crossed line) for a 10% 3.9M PS solution. For the MLD model, since CCR contributes to tube randomization and reduces the degree of alignment at higher extension rates, the upturn in η_E occurs at a greater value of $\dot{\varepsilon}$ as compared to the DEMG model. This moves the predictions of $\eta_E(\dot{\varepsilon})$ further away from the experimental data as shown for case of polymer solutions. The solid-crossed line in Figure 3.7(a) shows predictions of the MLD model modified to include effects of local friction reduction which we call the MLD-F(DE) model. These predictions are identical to the pure MLD model predictions (shown by dotted line), thus confirming that even with CCR (included here in the form of MLD equations), the predictions of the friction based MLD-F(DE) model for polymer solutions are insensitive to orientation-induced friction reduction. Figure 3.7(b) compares predictions of the pure MLD model (dotted line) to the basic DEMG model (dot-dashed line) and the friction based

MLD-F(DE) model (solid-crossed line) for a 100K PS melt. Tube randomization due to CCR coupled with the effect of monomeric friction reduction due to alignment decrease both the terminal time τ_d and the Rouse time τ_R. This causes the viscosity $\eta_E(\dot{\varepsilon})$ to decrease with a steeper slope than in the absence of CCR, thus slightly under-predicting the experimental data. This effect is shown in Figure 3.8 which compares predictions of the friction based MLD-F(DE) model (solid-crossed lines) to the friction based DEMG-F(DE) model (dashed lines) for a set of melts viz. 100K PS, 200K PS and 390K PS. The orientation-induced friction reduction thus eliminates the upturn in η_E as a function of $\dot{\varepsilon}$ in the fast flow regime ($\dot{\varepsilon} > \tau_R^{-1}$) for melts, but not for solutions in the MLD CCR model. Thus, the main conclusion of our work holds irrespective of CCR being included in the constitutive equation using the MLD expressions.

3.5.5. Shear flow predictions using the DEMG-F and MLD-F model

In this section, we explore the predictions made by the DEMG-F(DE) and MLD-F(DE) models for start up of shear and steady state shear in entangled polymer solutions and melts. This will help us quantify the effect of Kuhn orientation-induced reduction in friction in shearing flows. For shear, the velocity gradient tensor can be written as,

$$\underline{\underline{\kappa}} = \left(\nabla v\right)^T = \begin{pmatrix} 0 & \dot{\gamma} & 0 \\ 0 & 0 & 0 \\ 0 & 0 & 0 \end{pmatrix} \tag{46}$$

The tube orientation tensor is

$$\underline{\underline{S}}_{tube} = \begin{pmatrix} S_{11} & S_{12} & S_{13} \\ S_{21} & S_{22} & S_{23} \\ S_{31} & S_{32} & S_{33} \end{pmatrix} \tag{47}$$

The rate of affine stretching of the mesh of entanglements is,

$$\underline{\underline{\kappa}} : \underline{\underline{S}}_{tube} = \begin{pmatrix} 0 & \dot{\gamma} & 0 \\ 0 & 0 & 0 \\ 0 & 0 & 0 \end{pmatrix} : \begin{pmatrix} S_{11} & S_{12} & S_{13} \\ S_{21} & S_{22} & S_{23} \\ S_{31} & S_{32} & S_{33} \end{pmatrix} = \dot{\gamma} S_{12} \tag{48}$$

and the extensional viscosity is given as,

$$\bar{\eta} = \frac{\sigma_{12}}{\dot{\gamma}} \text{ where } \underline{\underline{\sigma}} = 3G_N k_s \lambda^2 \underline{\underline{S}}_{tube} \tag{49}$$

In Figure 3.9 we compare the steady state values of experimental first normal stress difference N_1 and shear viscosity η for a lightly entangled (number of entanglements, $Z = 15$) solution, 10% 2M PS (in part a), and highly entangled solution (number of entanglements, $Z = 44$), 7% 8.42M PS (in part b), with the predictions of the friction based DEMG-F(DE) model (dashed lines) and friction based MLD-F(DE) model (solid-crossed lines). We find that these predictions are identical to their respective basic DEMG model and basic MLD model predictions, indicating that the magnitude of orientation-induced local friction reduction in simple shear is negligible. Consequently, shear predictions are insensitive to the inclusion of orientation-dependent frictional effects presented here. Moreover, for lower molecular weight solution, 10% 2M PS ($Z = 15$) that we consider here, CCR does not have a strong effect on shear predictions as shown in Figure 3.9a.

However, for the densely entangled solution, 7% 8.42M PS ($Z = 44$), CCR effects are stronger and the MLD model deviates more dramatically from the DEMG model as shown in figure 9b. Note, in particular, that the MLD model predicts significantly less shear thinning in the shear viscosity at high rates than does the DEMG model. This can also be seen in the work of Pattamaprom and Larson (2001). The MLD-F(DE) predictions for the first normal stress difference N_1, however, deviate from the data more than do the DEMG-F(DE) predictions, which differs from what Pattamaprom and Larson[33] found. Pattamaprom and Larson[33] used a somewhat different formulation of the tube model (with an integral equation for the orientation tensor) and different values of the parameters, which accounts for this difference. It is beyond our purpose to explore this further here; our main point is that the ability of the DEMG model without CCR to fit shear rheology data seems to be dependent on entanglement density. While for the highly entangled solution CCR needs to be included to avoid overly severe shear thinning, for the modestly entangled solution ($Z = 15$), the DEMG (or DEMG-F) model seems to be adequate, at least for the parameter set chosen here.

Figure 3.10 compares the predictions of the DEMG-F(DE) (dashed lines) and MLD-F(DE) (solid-crossed lines) against experimental steady state values of shear stress σ_{12}, first normal stress difference N_1, and shear viscosity η for a modestly entangled polymer melt 200K (Z = 15) The addition of CCR (through the MLD-F-(DE) model) improves the predictions marginally relative to the DEMG-F(DE) predictions. Thus, in general, addition of CCR within our simple formulation of the tube model appears to improve the predictions in shearing flows, while degrading the predictions somewhat in extensional flows. Different or more accurate formulations of the CCR mechanism may well lead to somewhat different conclusions.

3.6. Summary

In this chapter, we have tested two mechanisms based on the concept of flow induced Kuhn segment alignment that might explain the observed contrast in elongational flow behavior between entangled polystyrene solutions and melts. In the first approach, we tested the effect of Kuhn orientation on the tube diameter with expressions to capture this effect adapted from the theory of Doi and Edwards[3] and Sussman and Schweizer[4] for rod-like polymers. These formulas give the dependence on Kuhn segment alignment of tube diameter, and through this on the terminal relaxation time τ_d and plateau modulus G_N, which are then incorporated into the Doi-Edwards-Marrucci-Grizzuti (DEMG) version of the tube model. When done self-consistently, this mechanism fails to capture the observed extensional viscosity thinning for melts at $\dot{\varepsilon} > \tau_R^{-1}$. This is because tube widening causes an increase in the maximum extensibility of the tube, $\lambda_{\max}$ which then allows a reduction of Kuhn segment alignment. In the limit of high strain and high strain rate, entanglement density becomes irrelevant as the stress is given by the friction of fully extended chains sliding past each other, and so any mechanism that relies on changes in entanglement structure, and has no effect on the frictional Rouse time, must fail.

The second mechanism we tested is the effect of Kuhn segment alignment on segmental friction based on the work of Yaoita *et al.*[5]. We worked on their hypothesis that friction ζ is dependent on stretch/orientation parameter, F_{so} and developed specific functional forms for $\zeta(F_{so})$. These functional forms when included in the DEMG model accelerates both the terminal reptation relaxation as well as fast Rouse relaxation processes but does not cause $\lambda_{\max}$ to change

as a function of orientation. As a consequence, melt subchains between entanglements show significant stretching and orientation, which leads the local friction to decrease in fast flows. On the other hand, for solutions with high volume fractions of solvent, because of a high value of the maximum stretch ratio $\lambda_{\max}$, chain stretching outweighs the Kuhn segment orientation effect and viscosity thickening is observed for fast flows. While the specific functional forms chosen for $\zeta(F_{so})$ work well for predicting the polystyrene solutions and melts considered here, very recent work by Huang *et al.*[29] suggest that details of the solvent, including its molecular weight, can influence the orientation dependence of the friction, and so the forms used here are not universal.

3.7. References

1. Bach, A., Almdal, K., Hassager, O., Rasmussen, H. K., "Elongational viscosity of narrow molar mass distribution polystyrene," *Macromolecules* 36, 5174 (2003)
2. Bhattacharjee, P. K., Oberhauser, J. P., McKinley, G. H., Leal, L. G., Sridhar, T., "Extensional rheometry of entangled solutions," *Macromolecules* 35, 10131 (2002)
3. Doi, M., Edwards, S. F. *The Theory of Polymer Dynamics*, Clarendon: Oxford (1986)
4. Sussman, D. M., Schweizer, K. S., "Microscopic theory of quiescent and deformed topologically entangled rod solutions: General formulation and relaxation after nonlinear step strain," *Macromolecules* 45, 3270 (2012a)
5. Yaoita, T., Isaki, T., Masubuchi, Y., Watanabe, H., Ianniruberto, G., Marrucci, G., "Primitive chain network simulation of elongational flows of entangled linear chains: Stretch/orientation-induced reduction of monomeric friction," *Macromolecules* 45, 2773 (2012)
6. de Gennes, P. G., "Reptation of a polymer chain in the presence of fixed obstacles," *J. Chem. Phys*. *55*, 572 (1971)
7. Doi, M., Edwards, S. F., "Dynamics of rod-like macromolecules in concentrated solution," *J. Chem. Soc., Faraday Trans.* 2, 74, 560 (1978)
8. Marrucci, G., Grizzuti, N., "Fast flows of concentrated polymers: Predictions of the tube model of chain stretching," *Gazz. Chim. Ital.* 118, 179 (1988)
9. Pearson, D. S., Herbolzheimer, E., Grizzuti, N., Marrucci, G., "Transient behavior of entangled polymers at high shear rates," *J. Polym. Sci.: Part B: Polym. Phys.* 29, 1589 (1991)
10. Marrucci, G., "Dynamics of entanglements: A nonlinear model consistent with the Cox-Merz rule," *J. Non-Newt. Fluid Mech.* 62, 279 (1996)
11. Mead, D. W., Larson, R. G., Doi, M., "A molecular theory for fast flows of entangled polymers," *Macromolecules* 31, 7895 (1998)
12. Ianniruberto, G., Marrucci, G., "A simple constitutive equation for entangled polymers with chain stretch," *J. Rheol.* 45, 1305 (2001)
13. Marrucci, G., Ianniruberto, G., "Flow-induced orientation and stretching of entangled polymers," *Proc. Trans. R. Soc. Lond. A* 361, 677 (2003)
14. Ye, X., Larson, R. G., Pattamaprom, C., Sridhar, T., "Extensional properties of monodisperse and bidisperse polystyrene solutions" *J. Rheol.* 47, 2, 443 (2003)
15. Marrucci, G., Ianniruberto, G., "Interchain pressure effect in extensional flows of entangled polymer melts," *Macromolecules* 37, 3934 (2004)
16. Masubuchi, Y., Yaoita, T., Matsumiya, Y., Watanabe, H., Ianniruberto, G., Marrucci, G., "Stretch/orientation induced acceleration in stress relaxation in coarse-grained molecular dynamics simulations," *J. Soc. Rheol. Japan* 41, 1, 35 (2012)
17. Ianniruberto, G., Brasiello, A., Marrucci, G., "Simulations of fast shear flows of PS oligomers confirm monomeric friction reduction in fast elongational flows of monodisperse PS melts as indicated by rheooptical data," *Macromolecules* 45, 8085 (2012)
18. Sussman, D. M., Schweizer, K. S., "Microscopic theory of entangled polymer melt dynamics: Flexible chains as primitive-path random walks and supercoarse grained needles," *Phys. Rev. Lett.* 109, 168306 (2012b)
19. Qin, J., Milner, S., "Tube diameter of oriented and stretched polymer melts," *Macromolecules* 46, 1659 (2013)

20. Kushwaha, A., Shaqfeh, E. S. G., "Slip-link simulations of entangled polymers in planar extensional flow: Disentanglement modified extensional thinning," *J. Rheol.* 55, 463 (2011)
21. Pearson, D. S., Kiss, A. D., Fetters, L. J., Doi, M., "Flow-induced birefringence of concentrated polyisoprene solutions," *J. Rheol.* 33, 517 (1989)
22. Larson, R. G., *Constitutive equations for polymer melts and solutions*, Butterworths, London (1988)
23. Dealy, J. M., Larson, R. G., *Structure and rheology of molten polymers: From structure to flow behavior and back again*, Hanser, Munich (2006)
24. Cohen, A., "A Padé approximant to the inverse langevin function," *Rheol. Acta* 30, 270 (1991)
25. Kuhn, W., Grün, F., "Beziehungen zwischen elastischen Konstanten und Dehnungsdoppelbrechung hochelastischer Stoffe," *Kolloid-Z* 101, 248 (1942)
26. Fuller, G. G., "Optical rheometry of complex fluids," Oxford (1995)
27. Likhtman, A. E., McLeish, T. C. B., "Quantitative theory for linear dynamics of linear entangled polymers," *Macromolecules* 35, 6332 (2002)
28. Larson, R. G., *The structure and rheology of complex fluids*, Oxford University Press, London (1999)
29. Huang, Q., Alvarez, N. J., Matsumiya, Y., Rasmussen, H. K., Watanabe H., Hassager, O., "Extensional rheology of entangled polystyrene solutions suggest importance of nematic interactions," *ACS Macro Lett.* 2**,** 741 (2013b)
30. Acharya, M. V., Bhattacharjee, P. K., Nguyen, D. A., Sridhar, T., "Are entangled polymeric solutions different from melts?" *AIP Conf. Proc.* 1027, 391 (2008)
31. Milner, S. T., McLeish, T. C. B., "Reptation and contour-length fluctuations in melts of linear polymers," *Phys. Rev. Lett.* 81, 3, 725 (1998)
32. Huang, Q., Mednova, O., Rasmussen, H. K., Alvarez, N. J., Skov, A. L., Almdal K., Hassager, O., "Concentrated polymer solutions are different from melts: Role of entanglement molecular weight," *Macromolecules* 46, 5026 (2013a)
33. Pattamaprom, C., Larson, R. G., "Constraint release effects in monodisperse and bidisperse polystyrenes in fast transient shearing flows," *Macromolecules* 34, 5229 (2001)
34. Inoue T., Uematsu, T., Yamashita, Y., Osaki, K., "Significance of the longest Rouse relaxation time in the stress relaxation process at large deformation of entangled polymer solutions," *Macromolecules* 35, 4718 (2002)
35. Sanchez-Reyes J., Archer, L. A., "Step shear dynamics of entangled polymer liquids," *Macromolecules* 35, 5194 (2002)
36. Wang, S. Q., Wang, Y., Cheng, S., Li, X., Zhu, X., Sun, H., "New experiments for improved theoretical description of nonlinear rheology of entangled polymers," *Macromolecules* 46, 3147 (2013)
37. Nielsen, J. K., Rasmussen, H. K., Hassager, O., McKinley, G. H., "Elongational viscosity of monodisperse and bidisperse polystyrene melts," *J. Rheol.* 50, 453 (2006)
38. Schweizer, T., Meerveld, J. V., Öttinger, H. C., "Nonlinear shear rheology of polystyrene melt with narrow molecular weight distribution-Experiment and theory," *J. Rheol.* 48, 1345 (2004)

Table 3.1. Parameters of polystyrene (PS) samples. Polymer weight percent % is given only if the sample is a solution. The abbreviation 1M refers to molecular weight of 1,000,000 and 1K refers to 1000. (For example, 100K PS is a polystyrene melt of 100,000 g/mol molecular weight.

Sample	T(°C)	G_N^0 (kPa)	G_N^f (kPa)	τ_{d0}(s)	τ_d^f (s)	τ_R (s)	Z	$\lambda_{\max}$
100K PS	130	200	55.9	621	159	23	9.0	4.2
200K PS	130	200	75.7	4,254	1,610	94.3	15.0	4.2
390K PS	130	200	101.6	25,340	12,880	288	29.3	4.2
285K PS	130	250	113	13,867	6,220	216	21.4	4.2
545K PS	130	250	145.7	95,817	54,418	779	41.0	4.2
145K PS	120	290	90.4	25,144	7,839	1,134	10.7	4.2
200K PS-S	175	200	88.6	3.5	1.33	0.065	15.0	4.2
10% 3.9M PS	21	1.71	0.88	17.8	9.22	0.2	30.5	13.1
15%3.9M PS	21	3.82	2.24	60.8	35.64	0.45	45.7	10.7
17% 3.9M PS	21	4.9	2.97	120.17	72.87	0.78	51.7	10.1
10% 1.95M PS	21	1.8	0.68	2.11	0.8	0.05	14.7	13.1
15% 1.95M PS	21	3.82	1.76	8.63	3.98	0.13	22.8	10.7
20% 1.95M PS	21	6.8	3.48	12.16	6.26	0.17	30.4	9.3
7% 8.42M PS-S	40	0.52	0.3	53.4	31.65	0.6	44.3	17.6
10% 2M PS-S	40	1.15	0.5	2.08	0.7	0.04	15.0	13.1

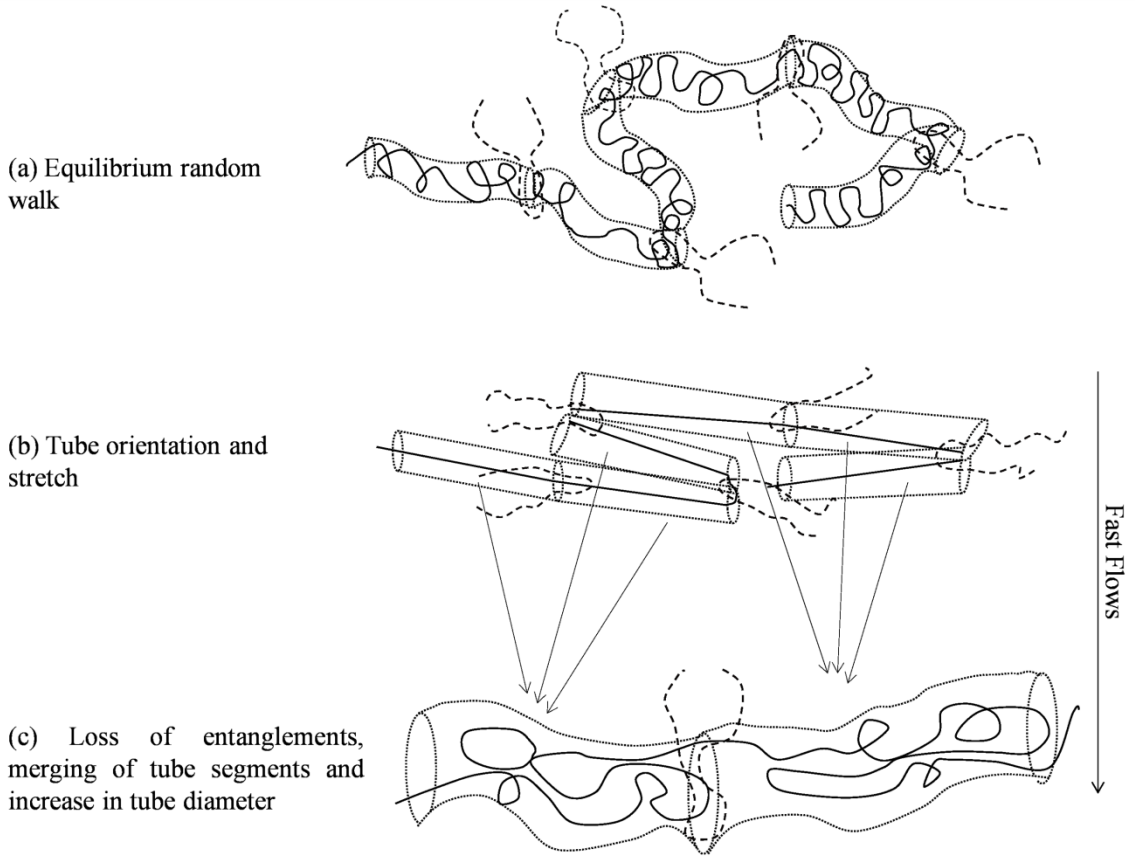

Figure 3.1. Schematic step-wise representation of tube enlargement mechanism during fast elongational flows: (a) No flow conditions; equilibrium random walk, (b) Tube orientation, backfolding and stretch due to fast flows, (c) Loss of entanglements, merging of tube segments and tube diameter enlargement.

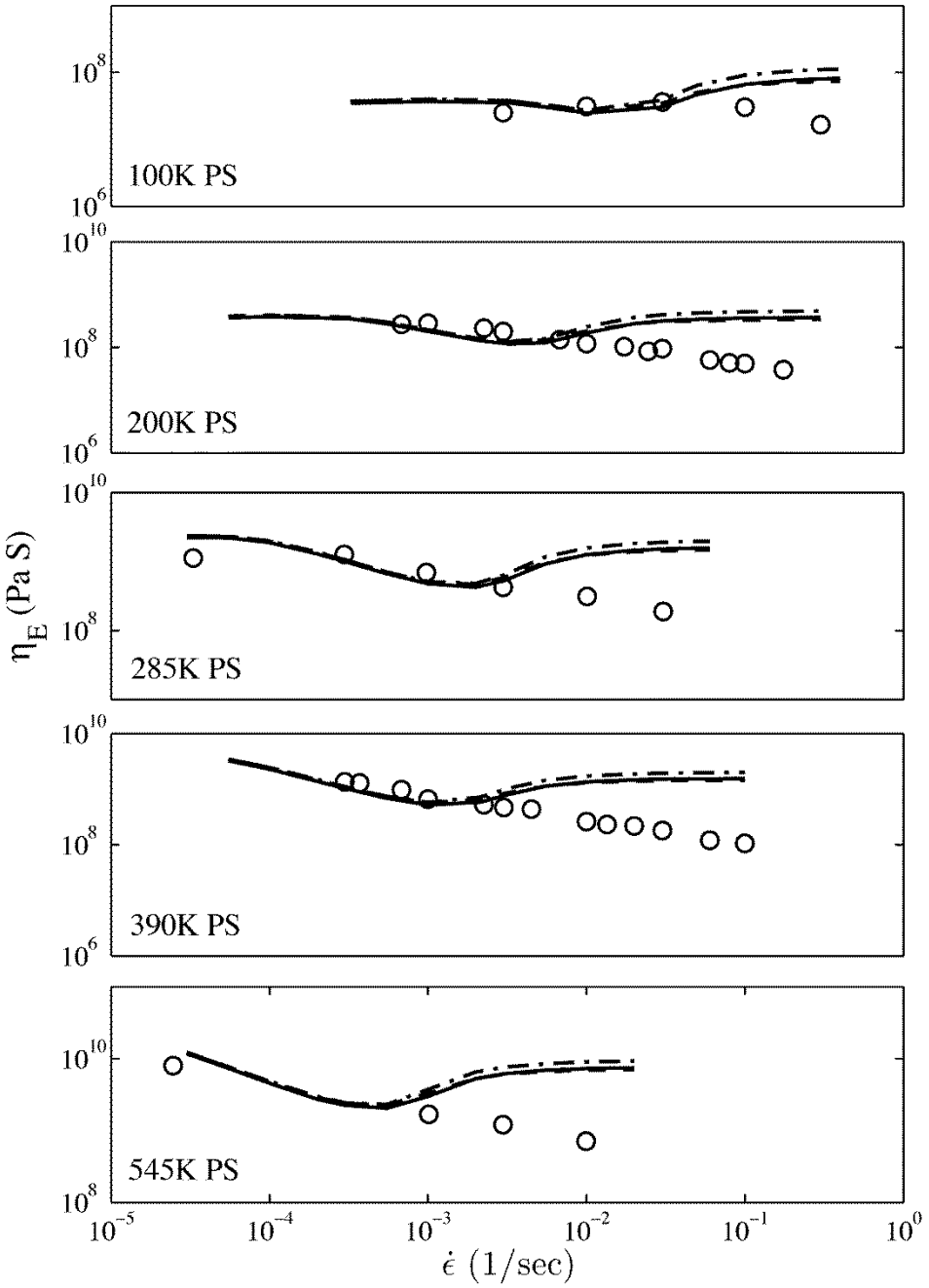

Figure 3.2. Steady state extensional viscosity η_E as a function of extension rate $\dot{\varepsilon}$ for polystyrene melts, 100K PS, 200K PS, 285K PS, 390K PS and 545K PS at 130°C. Data (open circles) for melts 100K PS, 200K PS and 390K PS are taken from Nielsen *et al.*[37] and for melts 285K PS and 545K PS are taken from Huang *et al.*[32]. DEMG model predictions are shown with dot-dashed lines, Self-Consistent DEMG-R(DE) predictions with dashed lines, and Self-Consistent DEMG-R(SS) predictions with solid lines.

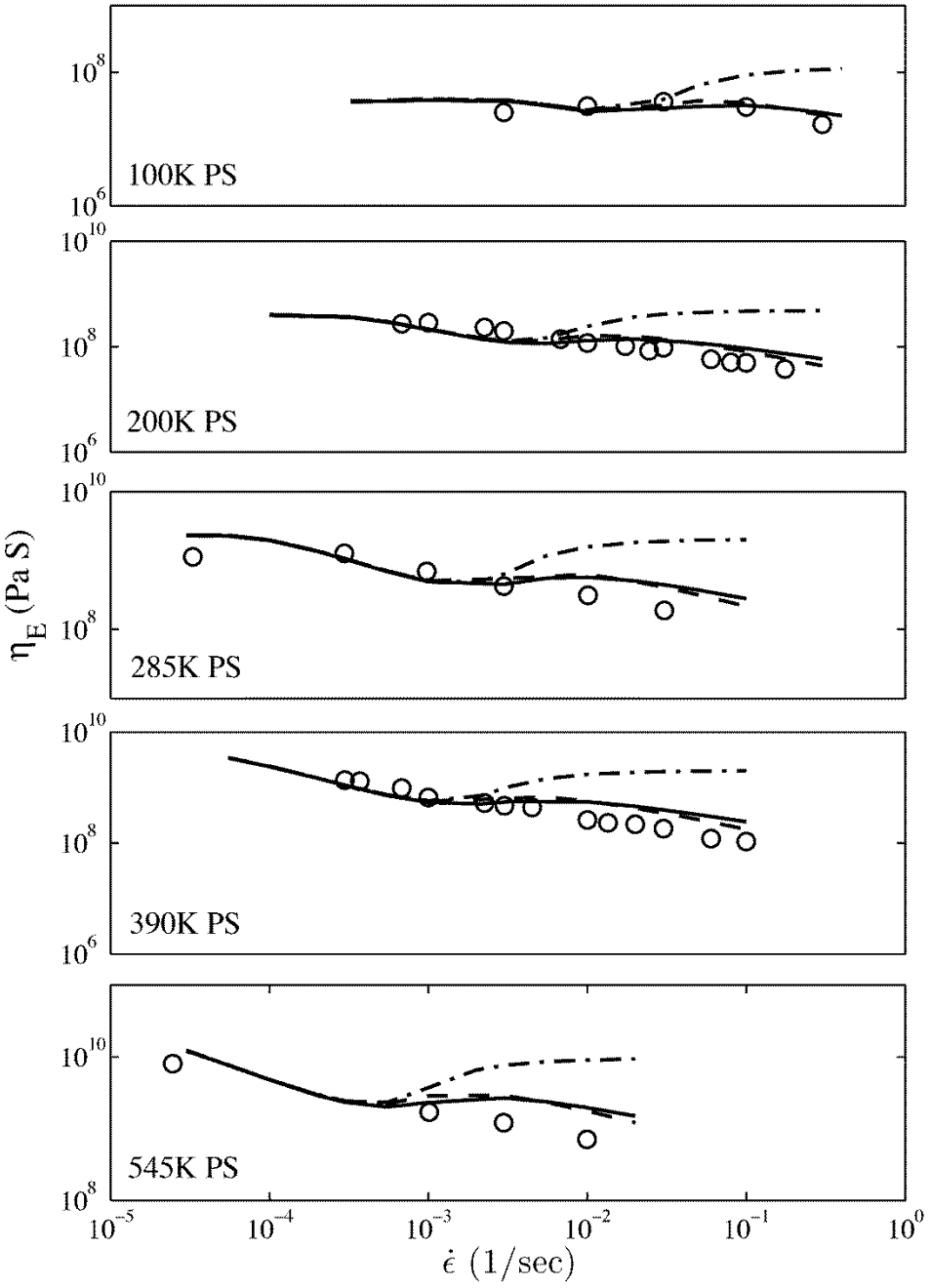

Figure 3.3. Same as Fig.3.2 except dashed lines are DEMG-F(DE) predictions, and solid lines are DEMG-F(SS) predictions. The dot-dashed lines are again the predictions of the DEMG model.

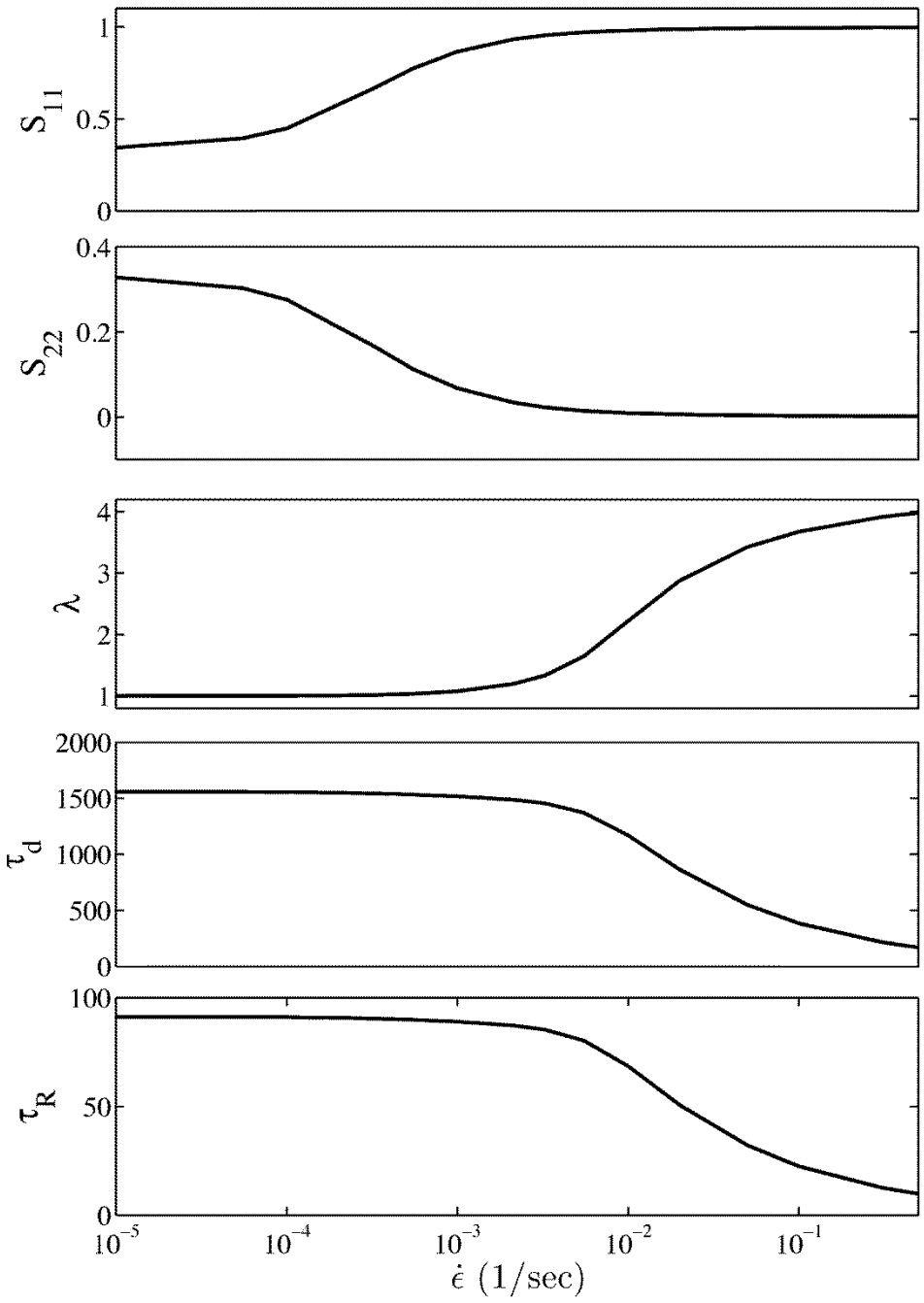

Figure 3.4. DEMG-F(SS) predictions for the diagonal entries, S_{11} and S_{22} of the orientation tensor $\underline{\underline{S}}_{tube}$, stretch ratio λ, tube relaxation time τ_d, and Rouse time τ_R as functions of extension rate $\dot{\varepsilon}$ for melt 200K PS at 130°C.

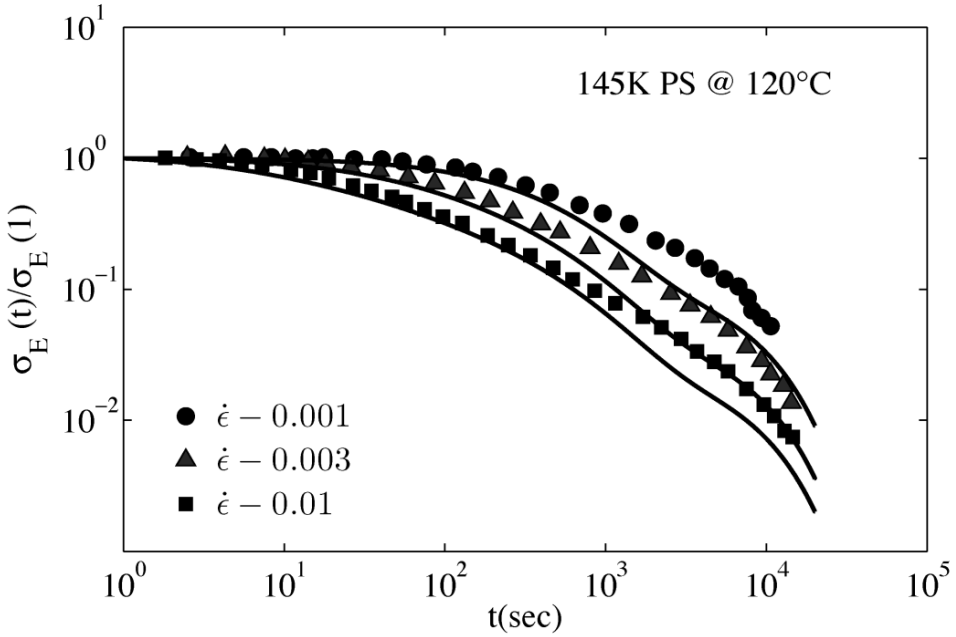

Figure 3.5. Stress relaxation data from Yaoita *et al.*[5] for melt 145K PS at 120°C after stopping the flow at a Hencky strain $\varepsilon = 3$ for all extension rates. Symbols indicate the experimental data and solid lines indicate the DEMG-F(DE) predictions for different extension rates.

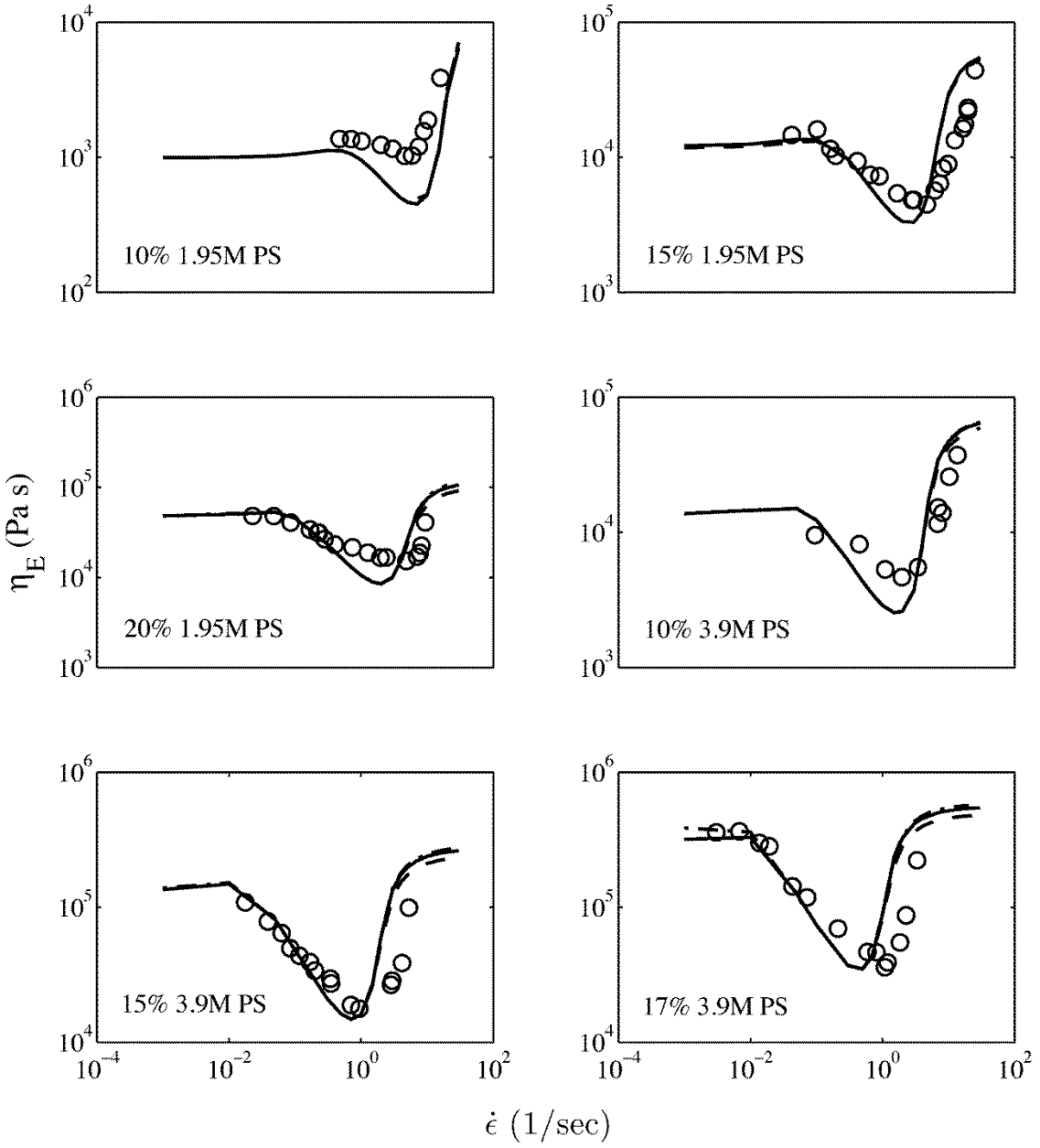

Figure 3.6. Steady state extensional viscosity η_E data as a function of extension rate $\dot{\varepsilon}$ for a set of entangled polystyrene solutions as labeled in the figures. Data (open circles) for 10% 1.95M PS, 15% 1.95M PS, 20% 1.95M PS and 17% 3.9M PS are taken from Acharya *et al.*[30] ;and for 10% 3.9M PS and 15% 3.9M PS are taken from Bhattacharjee *et al.*[2]. DEMG predictions are shown with dot-dashed lines, DEMG-F(DE) predictions with dashed lines, and DEMG-F(SS) predictions with solid lines.

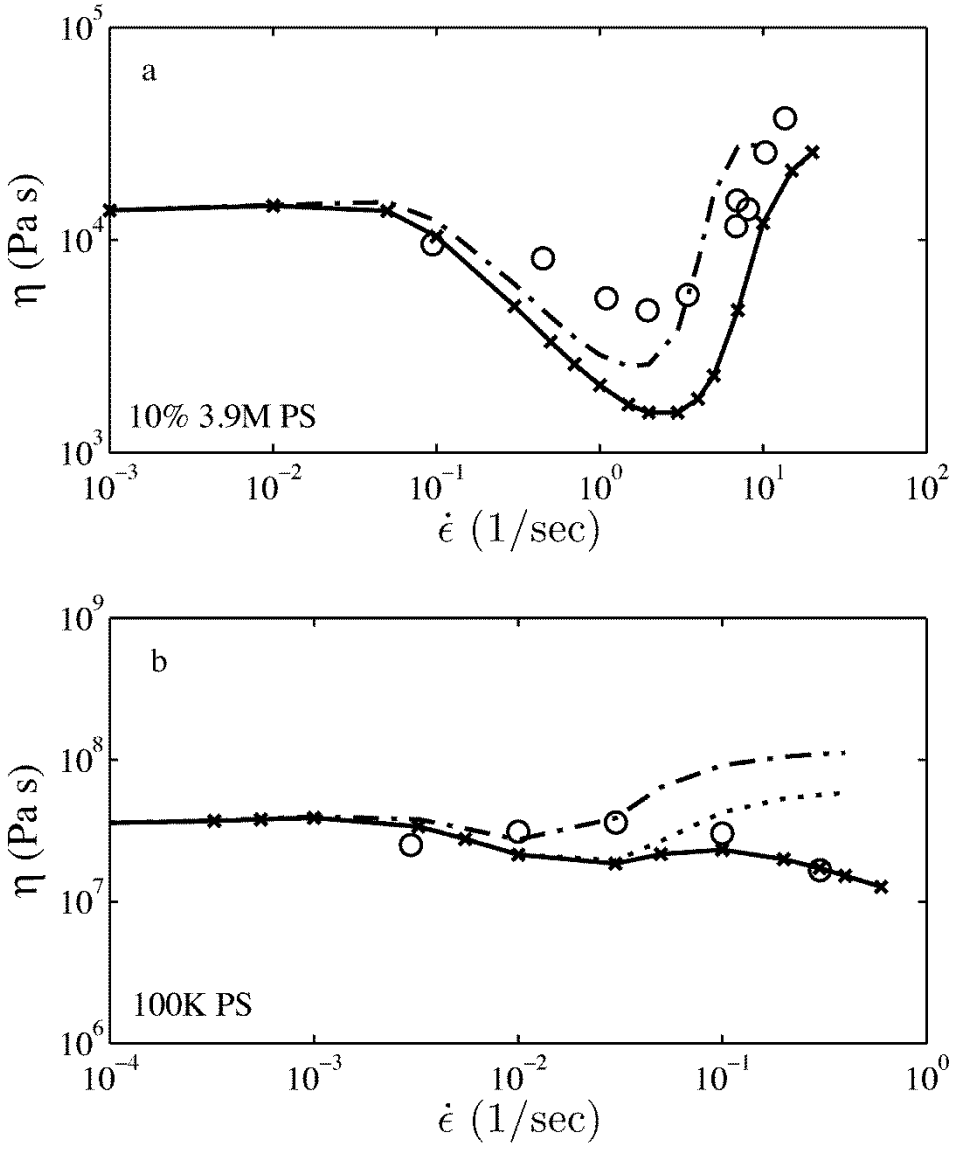

Figure 3.7. (a) Steady state extensional viscosity η_E as a function of extension rate $\dot{\varepsilon}$ for 10% 3.9M PS solution from Bhattacharjee *et al.*[2] and (b) 100K PS melt from Nielsen *et al.*[37]. Open circles are the experimental data. In both (a) and (b), the dot-dashed lines show the DEMG predictions, the dotted lines show the MLD model predictions and solid-crossed lines show the friction based MLD-F(DE) model predictions.

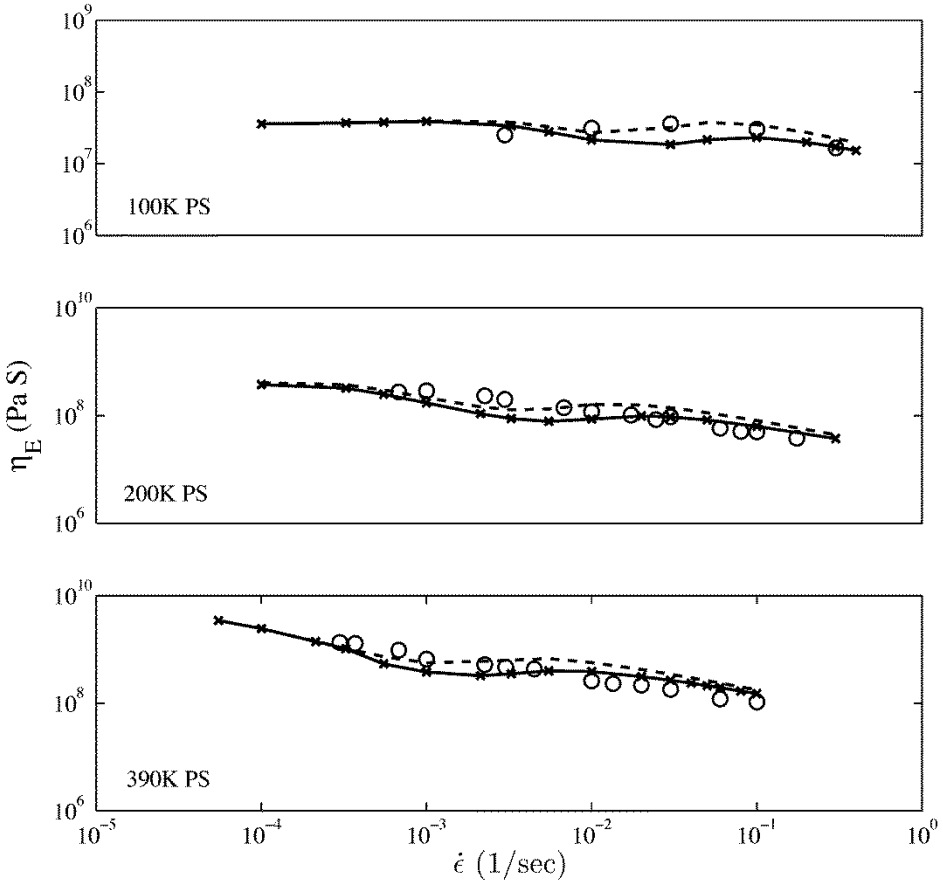

Figure 3.8. Steady state extensional viscosity η_E as a function of extension rate $\dot{\varepsilon}$ for polystyrene melts, 100K PS, 200K PS, and 390K PS at 130°C. Data (open circles) are taken from Nielsen *et al.*[37]. Dashed lines show the friction based DEMG-F(DE) model predictions while solid-crossed lines are predictions of the friction based MLD-F(DE) model.

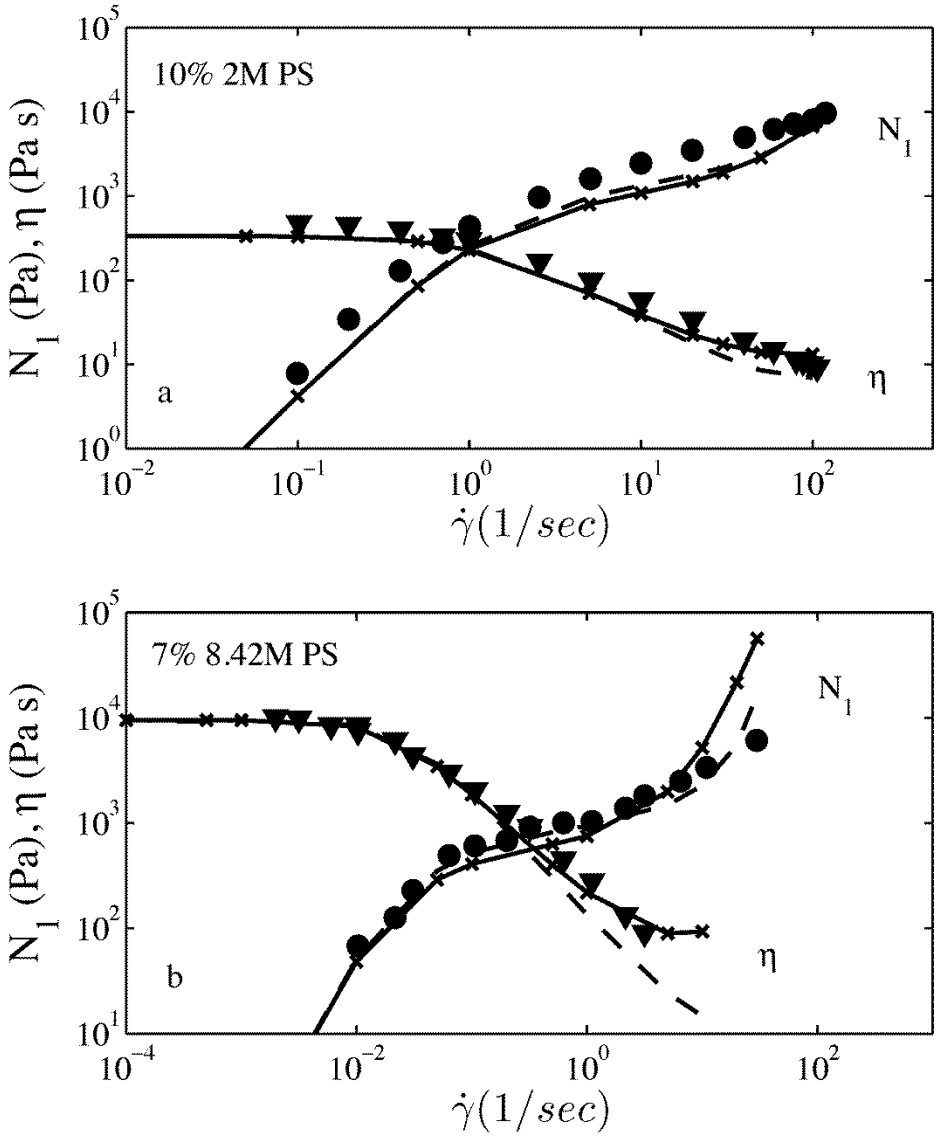

Figure 3.9. Steady-state shear viscosity η (filled circles) and first normal stress difference N_1 (filled triangles) as a function of strain rate $\dot{\gamma}$ for (a) 10% 2M PS solution from Mead *et al.*[11] and (b) for 7% 8.42M PS solution from Pattamaprom and Larson[33]. In both (a) and (b), dashed lines show the friction based DEMG-F(DE) model predictions while solid-crossed lines are predictions of the friction based MLD-F(DE) model.

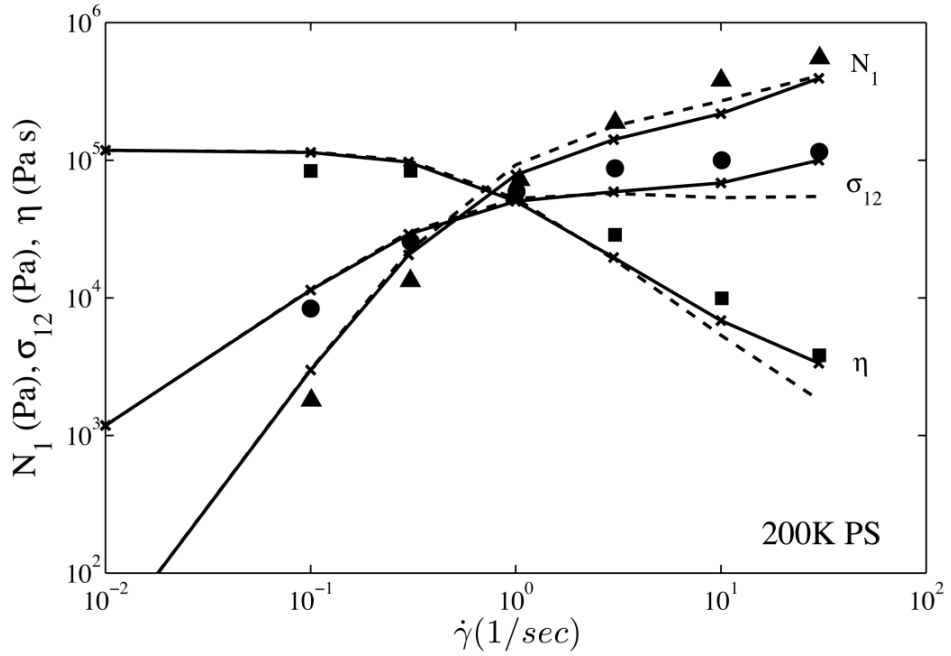

Figure 3.10. Steady-state shear viscosity η (filled squares), shear stress σ_{12} (filled circles), and first normal stress difference N_1 (filled triangles) as a function of strain rate $\dot{\gamma}$ for melt 200K PS at 175°C from Schweizer *et al.*[38]. Dashed lines show the friction based DEMG-F(DE) model predictions while solid-crossed lines are predictions of the friction based MLD-F(DE) model.

CHAPTER 4

Universal relaxation behavior of entangled 1,4-polybutadiene melts in the transition frequency region

4.1. Abstract

This chapter focuses on obtaining a universal tube model parameter set for the polymer 1,4-polybutadiene, applicable in the linear viscoelastic regime. To that end, we have compared the linear viscoelastic G' and G" mastercurves for linear, star, H, and comb architecture 1,4-polybutadienes from literature which have found to agree well in the transition frequency region, where G' and G" exceed the plateau modulus, irrespective of molecular weight and branching structures. A value of $\tau_e = (3.7 \pm 0.93) \times 10^{-7} (s)$ for the equilibration time at T=25 ^{o}C can therefore be determined from fitting Rouse predictions to the transition frequency data, after subtracting effects of glassy modes represented by the Kohlrausch-Williams-Watts (KWW) expression. Good agreement among multiple data sets was obtained in the transition region despite large variations in low-temperature shift factors, evidently due to small sample-to-sample variations in 1,2 content. These variations in 1,2 content can also cause small changes in the plateau modulus G_N^0 and the entanglement molecular weight M_e, which should have only a small effect on linear polymers, but for long-chain branched polymers it could lead to large variations in terminal relaxation time predicted by tube models. The small variations in G_N^0 can, however, be inferred from the dependence of shift factor on temperature, allowing all three tube model parameters τ_e, G_N^0, and M_e to be obtained from high frequency data for 1,4 polybutadienes, thus in principle removing these as parameters that can be adjusted to fit specific data sets for linear or branched 1,4-polybutadienes. (**Text and figures in this chapter are reprinted with permission from Park S.J., P.S. Desai, X. Chen and R.G. Larson, *Macromolecules,* 48 (12), 4122–4131 (2015), S. J. Park is the lead author of this publication**)

4.2. Introduction

Tube models have been steadily improved, leading to ever more quantitative predictions of the dynamics of entangled polymer melts. Ideal reptation theory developed by de Gennes[1] and Doi and Edwards[2] has been augmented to include various additional mechanisms such as longitudinal stress relaxation along the tube, contour-length fluctuations and constraint release[3-10]. While recently developed tube models use different approaches for theoretical predictions, they all need the same common parameters, the most important of which are the plateau modulus G_N^0, the entanglement molecular weight M_e, and the equilibration time or the Rouse reorientation time required to relax a piece of the chain just large enough to occupy a single tube segment, τ_e[8,11]. Because the plateau modulus and entanglement molecular weight are related to each other by, where ρ is the density of polymer, R is the gas constant, and T is the absolute temperature, only two of these three parameters are really independent. However, $G_N^0 = \frac{4}{5}\frac{\rho RT}{M_e}$ M_e is sometimes independently adjusted to fit theoretical predictions with experimental data in some cases[8,12,13].

Theoretical tube models are tested by comparing their predictions with experimental data. To do so, accurate and consistent experimental data are necessary, and the parameters of the tube model must be determined. Generally, tube model parameters have been determined by using experimental linear viscoelastic data, for nearly monodisperse linear (un-branched) polymers of a given chemistry[5,12,14]. The linear viscoelastic measurements are usually performed over a limited frequency (or time) range at any given temperature due to experimental limitations. Thus, the data obtained at single temperature are usually not sufficient to capture all relevant relaxation processes of entangled polymer melts and to obtain the tube model parameters.

The low frequency (or long time scale) behavior of entangled polymer melts is strongly dependent on the molecular weight and its distribution and on long chain branching[2,15]. However, the behavior at high frequencies (which we take here to be at frequencies above that of the plateau modulus) should be almost independent of the molecular structure. Therefore, in principle, the equilibration time τ_e, which is the fundamental time scale for polymer relaxations at sub-entanglement length scales, should be obtainable from high frequency data alone.

However, various values of τ_e have been used for tube model predictions for 1,4 polybutadienes[10,16], and often these values are used to adjust predictions to fit low frequency data. If τ_e could be obtained from high frequency data alone, it would be no longer be available as an adjustable parameter to fit low frequency data, and tube model predictions could then be tested more rigorously.

Liu *et al.*[17] (2006) showed that at high frequencies in the transition region between the plateau and the glassy regions, G' and G" of linear 1,4-polybutadienes of high molecular weight follow a power law in frequency with an exponent close to 0.7, which differs from the value of 0.5 predicted by the Rouse relaxation processes that are expected to be important at high frequencies[2,8]. In addition, they proposed a possible experimental definition for the equilibration time using the crossover frequency of the loss modulus with the plateau modulus in the transition frequency region.

Time temperature superposition (TTS) is typically used to increase the range of frequencies (or times) accessed in linear viscoelastic measurements of polymers[14]. The principle of TTS is that if all the relaxation processes of polymer melts have the same temperature dependency, then changing the measuring temperature will simply shift the linear viscoelastic data horizontally along the log(time) or log(frequency) axis. This shift is done using a horizontal shift factor a_T.

The Williams-Landel-Ferry (WLF) equation is often used to model the temperature-dependent shift factor, and is given as:[14]

$$\log a_T(T) = \frac{-C_1(T - T_0)}{C_2 + (T - T_0)} \qquad (1)$$

where T is the measuring temperature, T_0 is the reference temperature, and C_1 and C_2 are parameters determined by fitting the shift factors. The shift factor can, for example, be obtained as a function of temperature by measuring the zero-shear viscosity η_0 at several temperatures. In an alternative, and more common method, G' and G" curves from oscillatory experiments at various temperatures are shifted horizontally and vertically, so that they superimpose at a reference temperature to form a master curve. From this, a shift factor is obtained at each

measurement temperature[15]. While TTS often works well for some linear polymers at least in the range of rubbery relaxation, some long-branched polymers do not follow TTS[18,19]. Even when branched polymers do follow TTS, it is not always certain that they have the same WLF parameters as the linear polymers do[13,14,20,21].

1,4-polybutadienes with well characterized molecular structures have been widely used for both experimental and theoretical studies of entangled polymer dynamics[8-10,13,22-29]. In addition, 1,4-polybutadienes are among the few polymers that show consistent agreement with TTS with similar shift factors for linear and long-chain branched species. In this work we compare literature data for 1,4-polybutadienes in the transition frequency region for various molecular architectures to test their consistency and to obtain the equilibration time to be used in the tube model. Because the experimental data for linear and branched polybutadienes over a wide frequency range were obtained using TTS, the consistency of the WLF parameters will be checked for the various molecular architectures. In addition, we compare tube model predictions with experimental data using the "hierarchical model" described in Wang *et al.*[10] and the "bob" model of Das *et al.*[9] using the equilibration time obtained from the linear rheology data in the transition frequency region.

4.3. Results and discussion

4.3.1. Comparison of linear viscoelastic data of 1,4-polybutadienes

4.3.1.1. Linear polybutadienes

Figure 4.1 shows a master curve of storage and loss moduli for linear 1,4-polybutadienes having similar molecular weights in the narrow range 97,000 to 100,000 at temperature T=25^{o}C, see Table 4.1.[23-25,28]. The data having reference temperatures different from T=25^{o}C were shifted to T=25^{o}C using the WLF parameters reported in the original paper. The amount of 1,2 addition is similar in each data set, varying from 7% to no more than 10%. But the glass transition temperature for the sample of Baumgaertel *et al*.[24] is somewhat higher (-89.6^{o}C) than the others, which are between -97^{o}C and -100.1^{o}C (see Table 4.1). As shown in Figure 4.1, all data show similar terminal behavior and crossover points in the low frequency region. The data of Struglinski *et al*.[23] were reported only over a limited frequency range without the high frequency region. The storage moduli superimpose well over the whole frequency range. However, the loss

modulus of Baumgaertel *et al.*[24] differs somewhat from those of Wang *et al.*[25] and Liu *et al.*[28]. Because moduli data for 1,4-polybutadienes having molecular weight differing from 100,000 match each other well in the transition frequency region in their respective original papers, it was not certain which data showed correct relaxation behavior for 1,4-polybutadienes in the transition region considering only the difference shown in Figure 4.1 [See the Figures 1-2 of Baumgaertel *et al.*[24], Figure 3 of Wang *et al.*[25], and Figure 1 of Liu *et al.*[28]]. The data of Baumgaertel *et al.*[24] have been compared frequently in the literature with theoretical predictions[8,13,27], and therefore its deviation from the data sets of Wang *et al.*[25] and Liu *et al.*[28] is of concern. Likhtman and McLeish[8] pointed out that the data of Baumgaertel *et al.*[24] could not be accurately predicted using the values of G_N^0 and M_e constrained by tube model relationship, $G_N^0 = \frac{4}{5}\frac{\rho RT}{M_e}$, and they therefore independently adjusted the values of G_N^0 and M_e for these data.

We next compare rheological data for linear polybutadienes having different molecular weight, but the same reference temperature of T=25°C, in Figure 4.2[22,28,29]. The polybutadiene of Li *et al.*[29] is not monodisperse, but is a 9:1 mixture of 130,000 and 92,000, with average molecular weight of 95,800. While we expect differences in storage and loss moduli at low and modest frequency because of the differences in molecular weight, the data sets merge, as expected, in the transition region, although the data of Colby *et al.*[22] show a very slight discrepancy. Considering the superposition of the transition frequency data of Liu *et al.*[28] with the other linear polybutadienes shown in Figure 4.2, we must consider the data of Baumgaertel *et al.*[24] to be an outlier in that it does not follow the same relaxation behavior as the other linear polybutadienes, even at high frequencies. Because the amount of 1,2 addition of polybutadiene of Baumgaertel *et al.*[24] is similar to that of the other samples, we could not find a clear reason for this discrepancy. However, we recommend that comparisons with theory focus on the 1,4-polybutadiene data sets whose transition frequency behavior is consistent, namely the four data sets of Colby *et al.*[22], Wang *et al.*[25], Liu *et al.*[28], and Li *et al.*[29].

4.3.1.2. Branched polybutadienes

In Figure 4.3 we show the storage and loss moduli of linear and various branched polybutadienes, namely star, H, and comb polymers having narrow molecular weight

distribution[13,25,29-31,43]. The molecular characteristics are shown in Table 4.2. All data are shifted to the reference temperature of T=25°C. While their branching structures are different, and so is their rheology in the terminal and modest frequency regions, their storage and loss moduli superpose almost perfectly in the transition frequency region, and overlaps well with the one available set of data that extends into the very high frequency glassy region.

Since entangled polymer chains do not feel entanglement constraints at short times (corresponding to high frequencies above the plateau region), in principle the relaxation behavior should be the same in this regime for linear and branched structures. To our knowledge, the high frequency literature data have not previously been compared systematically for linear and various branched 1,4-polybutadienes. Recent computational algorithms based on the tube model have predicted the relaxation process of general mixtures of linear and various branched polymers over a wide frequency range including the transitional frequency region up to the beginning of the glassy relaxation region[9,10,27]. Because, as shown in Figure 4.3, the relaxation of entangled polymer melts in the transition frequency region shows almost the same behavior irrespective of molecular weight and branching structures, it should be possible to extract a universal value for the equilibration time from this frequency range that would apply to all 1,4-polybutadienes at the same temperature.

While various tube models use different approaches to deal with the stress relaxation in the terminal and plateau regions, they use the same model of longitudinal relaxation and fast Rouse motion in the transition frequency region.[8-10,31] Therefore the value of the equilibration time needed to model the transition frequency behavior should be the same in these models and should be insensitive to polymer architecture, since the high frequency behavior is almost the same irrespective of the molecular structures. Because the glassy dynamics may affect the high frequency behavior, the model of longitudinal relaxation - the fast Rouse motion developed by Doi and Edwards[2] or Likhtman and McLeish[8] cannot explain quantitatively the power-law with exponent of about 0.7 obtained experimentally at frequencies above the high-frequency crossover of G' and G" for 1,4-polybutadienes. However, they can be used to describe approximately the data at frequencies lower than the high-frequency crossover of G' and G".

Figure 4.3b shows that in the frequency range above the second G'-G" crossover, which is observed at a frequency of $\omega = 2.7\times10^{7}$(rad/sec), the slope of the loss modulus against

frequency is around 0.68 on a log-log plot, which is larger than the value of 0.5 predicted by the Rouse theory. Liu *et al.*[17] similarly showed that for linear 1,4-polybutadienes with molecular weights of 1.2M and 410K, G" followed a power-law with an exponent of 0.71. They modeled the transitional frequency behavior using an empirical equation having this power-law exponent and a monomer re-equilibration equation expressed as a single mode, giving the following expression for the loss modulus:

$$G''(\omega) = G_N^0 \left[\frac{1}{4} \frac{\omega\tau_e}{1+(\omega\tau_e)^2} + (\omega\tau_e)^{0.71} \right] \tag{2}$$

The loss modulus using the longitudinal relaxation model and the fast Rouse motion, as described by Likhtman and McLeish[8], on the other hand is given by:

$$G''(\omega) = G_N^0 \left[\frac{1}{4Z} \sum_{p=1}^{Z-1} \frac{(\omega\tau_e)(p/Z)^2}{(p/Z)^4 + (\omega\tau_e)^2} + \frac{5}{4Z} \sum_{p=Z}^{N_eZ} \frac{2(\omega\tau_e)(p/Z)^2}{4(p/Z)^4 + (\omega\tau_e)^2} \right] \tag{3}$$

where $Z = M / M_e$ and $N_e = M_e / M_0$ (M_0 = monomer molecular weight).

The Likhtman-McLeish (LM) formula shows an approximate power-law exponent of 0.5 rather than the experimentally observed 0.71, evidently because the LM formula leaves out glassy modes, which assume increasing importance as the frequency increases. However, the LM formula offers the prospect of allowing determination of the equilibration time τ_e by fitting data to Eq. 3, but only if the influence of glassy relaxation can first be removed or shown to be small over the frequency range fitted.

Various values of τ_e have been used in different tube models because they were adjusted to fit experimental data with the predictions of the particular model over frequency ranges below the transitional range. In Table 4.3 we show that the values of τ_e for linear and for branched polybutadienes vary by a factor of 5 even when compared at the same temperature. The variation in τ_e allows the same low and moderate frequency data to be fit by theories that use different values of the dilution exponent α, of the hopping frequency of branch points, and of the values of G_N^0 and M_e[10]. In principle the equilibration time could be directly determined from the

monomer friction coefficient which could be obtained from the zero-shear viscosity of un-entangled polymers[14]. However, un-entangled polymers typically show differences in glass transition temperature relative to entangled polymers[14,22]. Thus, to avoid using τ_e as a fitting parameter, it seems to be necessary to obtain the value of τ_e from transition frequency data of entangled polymers.

Liu *et al.*[17] proposed that for highly entangled polymers, the equilibration time could be determined by the frequency at which the loss modulus is equal to the value of the plateau modulus [$G''(\omega = 1/\tau_e) = G_N^0$], which matches the value of τ_e needed to fit Eq. (2) with the loss modulus in the transition frequency region. Using the data of Figure 4.3b we thereby get a value of $\tau_e = 1.8\times10^{-7}(s)$ with $G_N^0 = 1.15\times10^5(Pa)$, which is almost the same as that obtained by Liu *et al.*[17].

In Figure 4.4 we compare the prediction using Eq. (2) with that from Eq. (3) using the same parameter values at T=25°C. They are $G_N^0 = 1.15\times10^6(Pa)$, $M_e = 1543$, which is calculated from $G_N^0 = \frac{4}{5}\frac{\rho RT}{M_e}$ and $\tau_e = 1.8\times10^{-7}(s)$. If we use the value of τ_e obtained from $G''(\omega = 1/\tau_e) = G_N^0$, we fit experimental data in the transition frequency region very well using Eq. (2). However, using $\tau_e = 1.8\times10^{-7}(s)$, the prediction of Eq. (3) from the Rouse theory does not fit the experimental data well. Thus, to fit Eq. (3) to the data, the value of τ_e should be increased to $\tau_e = 3.7\times10^{-7}(s)$. This value, $\tau_e = 3.7\times10^{-7}(s)$ is identical to the so-called "Park" value in Table 4.2 of Wang *et al.*[10], and is somewhat different from the "Das" parameter also discussed in Wang *et al.*[10].

Figure 4.5 includes the predictions of the Kohlrausch-Williams-Watts (KWW) relaxation function, shown by solid red line, to describe the very fast, high frequency glassy relaxation in the master data set plotted in Figure 4.3b. The KWW contribution is given by Eq. (4);

$$F_{KWW}(t) = \exp\left[-\left(t/\tau_{KWW}\right)^{\beta}\right] \tag{4}$$

Here $F_{KWW}(t)$ is the linear relaxation glassy modulus, τ_{KWW} is the characteristic relaxation time and β defines the stretch/breadth of the exponential spectrum and is material and temperature dependent.

We use β=0.35 which is well within the typical range of 0.3-0.45 specified by Palade *et al*.[43] for entangled polybutadienes with 1,2 content between 7-11% at 25 ^{o}C. For comparison, the prediction of fast Rouse modes given by Likhtman and McLeish[8] in Eq. (3) is also reproduced in Figure 4.5 as a black solid line. As seen from the fitted curves, the glassy modes, as given by the KWW function, are active only in the region above the second G'-G" crossover frequency and hence do not affect the determination of equilibration time τ_e. Additionally, the inset shows a zoomed-in log-log plot of the data of Palade *et al*.[43] (shown as left triangles in the main plot), and a plot of the same data with the glassy modes subtracted off and the separate KWW and Rouse model predictions. The results show that the glassy modes can be neglected below a frequency of around 10^8, which is well above the second cross-over frequency. It is below this frequency that the Rouse model can be used for the determination of the value of τ_e. By fitting the Likhtman and McLeish version of the Rouse model, Eq. (3) to these data we are able to set bounds on the equilibration time, $\tau_e = (3.7 \pm 0.93) \times 10^{-7} (s)$ at 25 ^{o}C. We note that Osaki and coworkers[44] have also subtracted glassy modes from the linear viscoelastic response for polyisoprene, and found that the Rouse model fit well the resulting rubbery data in the transition region.

In Figure 4.6 we show the predictions of the hierarchical model[10] and the bob model[9] for linear, star, and H polybutadienes at T=25^{o}C. We used the same parameter values of $G_N^0 = 1.15 \times 10^6 (Pa)$, $M_e = 1543$ and $\tau_e = 3.7 \times 10^{-7} (s)$ in both models. Because the hierarchical and bob models use the same models for longitudinal relaxation and the fast Rouse motion, given by Likhtman and McLeish[8], the predictions are similar in the transition frequency region. However, the hierarchical model predictions show better agreement with experimental data than those of bob model. The model predictions are dependent on the assumptions used, such as the dilution exponent (α) and the branch-point hopping frequency coefficient (p^2) [see Das *et al*.[9] and Wang *et al*.[10] for a detailed explanation for the effects of α and p^2 on the model predictions]. Here we use "standard" values of $\alpha = 4/3$ and $p^2 = 1/12$ in the hierarchical model

and $\alpha = 1$ and $p^2 = 1/40$ in the bob model, respectively, as used in previous publications. We don't claim that one model is better than the other in general, but are using these examples only to illustrate how the value of τ_e obtained from high-frequency data can help assess the success of various tube models with fewer adjustable parameters.

4.3.2. Comparison of the WLF parameters of 1,4-polybutadienes

While there have been various sets of WLF parameters for 1,4-polybutadienes reported in the literature[13,22,24,28-31], the values cannot be compared directly because the reference temperatures are different in some cases. Since the high frequency data were generated by shifting data measured at low temperature, it is important to determine if the shift factors used in making the master curve are consistent with each other.

In Table 4.4 we therefore compare the WLF parameters and the temperature ranges over which they were determined, as reported in the literature for 1,4-polybutadienes[13,22,24,25,28-31]. Because Wang *et al.*[25] simply plotted the shift factors instead of reporting the WLF parameters, we calculated the WLF parameters using non-linear regression for their shift factors. As shown in Table 4.4, the values of the WLF parameters vary significantly at low temperature. Considering the good agreement of the moduli data in the transition frequency region for the various molecular structures it is somewhat strange that the WLF parameters show so much variation. We will discuss possible reasons for this shortly.

In Figure 4.7 we plot the shift factors calculated from the WLF equation having the same reference temperature of T=25°C[22,28-30]. Li *et al.*[29] reported different shift factors for linear and H polymers. The shift factors are of course very similar near the reference temperature, but differ increasingly with decreasing temperature, especially at the lowest temperature, at which the high frequency data are generated. The shift factors of Liu *et al.*[28] and Li *et al.*[29] for linear polymers are very similar to each other, consistent with the good agreement of their transition frequency data. Although the shifted transition frequency data of Colby *et al.*[22] are only slightly different from others as shown in Figure 4.2, the shift factor of Colby *et al.*[22] at T= -75°C is about three times higher than that of Liu *et al.*[28] and of Li *et al.*[29] for a linear polymer. While the shift factor of the star polybutadiene of Shivokhin *et al.*[30] is much higher than that of the others, the shift factor of an H polymer of Li *et al.*[29] is similar to that of the linear sample of Colby *et al.*[22].

In Figure 4.8 we plot the normalized shift factor, which is defined as the ratio of the shift factor for a given temperature to the shift factor at a temperature of T=25°C[13,22,24,25,28-31,40]. This normalization effectively changes the reference temperature to 25°C for samples for which the reference temperature differs from 25°C, as shown in Table 4.4. While all the rheological data except for these of Baumgaertel *et al.*[24] match well in the transition frequency region as shown in Figures 4.1-4.3, the normalized shift factors show significant variation, especially at low temperatures.

Carella *et al.*[40] reported the WLF parameters for polybutadienes having various 1,2 contents. While the glass transition temperature is dependent on the content of 1,2 linkage, they obtained the following general correlation of the shift factor for polybutadienes having various 1,2 contents (in their paper the negative sign in -5.78 was missing.):

$$\log a_T(T) = \frac{-5.78(T - T_g - 55)}{94.8 + (T - T_g - 55)} \tag{5}$$

In Table 4.5 we show the glass transition temperatures and the plateau moduli of polybutadienes having different 1,2 contents, as reported by Carella *et al.*[40]. Using the reference temperature of $T_0=T_g+55°C$ we calculated the shift factors at each temperature. While Carella *et al.*[40] used Eq. (5) over their experimental temperature range of 100-200°C above T_g, we extended the range to -75°C to show the effect of 1,2 content on the shift factors at low temperatures. As shown in Figure 4.8, the normalized shift factor increases with increasing contents of 1,2 linkage of polybutadienes, and this increase is dramatic at low temperatures. While the data of Colby *et al.*[22], Kapnistos *et al.*[13], and Shivokhin *et al.*[30] were reported to have the same 1,2 content of 10%, the normalized shift factors at -75°C show differences of about a factor of three.

The generation of a master curve can be done manually by checking the superposition of data onto the reference data or can be calculated by software using a two-dimensional residual minimization technique[14,21,41]. The WLF parameters are then calculated using a regression fit of Eq. (1) to the shift factors obtained at each temperature. Thus, there can be errors in determining the parameters and be possibly also due to small errors in the measured value of the 1,2 content in the polybutadienes. In addition, systematic temperature measurement errors can occur in rheometry especially at low temperatures, if there are thermal gradient in the rheometer fixtures

or insufficient time is allowed for thermal equilibration between temperature changes. This could cause differences in shift factors even when the moduli almost superpose in the transition frequency region[28]. Even if the shift-factor dependence on temperature is in error, the master curve can still be correct, given good overlap is obtained during shifting, and there is no systematic drift in the shifting relative to the true shifting needed for perfect overlap.

4.3.3. Determination of tube model parameters for 1,4-polybutadienes

The plateau modulus of an entangled polymer can be obtained by integration over the terminal loss peak[14]:

$$G_N^0 = \frac{2}{\pi}\int_{-\infty}^{\infty} G''(\omega)\, d\ln\omega \qquad (6)$$

where the upper bound on the integration obviously must be cut off before the plateau region comes to an end. Because of the incomplete resolution of the terminal region, as shown in Table 4.3, various values of the plateau modulus have been reported for 1,4-polybutadienes in literature. For nearly monodisperse linear 1,4-polybutadienes, the empirical relationship reported by Raju *et al*.[42] is also sometimes used for determining the plateau modulus:

$$G_N^0 = 3.56 G_m'' \qquad (7)$$

where G_m'' is the value of G" at the terminal loss peak.

As shown in Table 4.5, the plateau modulus for polybutadienes, which is determined using Eq. (7) by Carella *et al*.[40], is found to vary by 9.6% for 1,2 content ranging from 0.08 to 0.18, and a similar variability of the entanglement molecular weight can be inferred for this range of 1,2 content. Accordingly, for typical 1,4-polybutadienes, with 1,2 content ranging from 0.06 to 0.1, the plateau modulus may vary within a range of about 4%.

In Figure 4.9 the hierarchical model[10] predictions of loss moduli for linear[25], star[30], and H[31] 1,4-polybutadienes at 25°C are shown for values of the plateau modulus varying from 1.05(MPa) to 1.25(MPa), which is a ±10% variation from the reference value of 1.15(MPa). For each plateau modulus, the entanglement molecular weight is calculated from $G_N^0 = \frac{4}{5}\frac{\rho RT}{M_e}$.

Because the model predictions in the transition frequency region are almost independent of the value of the plateau modulus, we used the same equilibration time of $\tau_e = 3.7\times10^{-7}$(s) determined in Figure 4.4 for all model predictions. As shown in Figure 4.9, the 10% variation of the entanglement molecular weight significantly changes the model predictions, especially for the star and H polybutadienes. Thus in order to carefully compare different tube theories to experimental data, an accurate value of the plateau modulus is required especially for branched polymers.

In Figure 4.10 we show the variation of the plateau modulus with the glass transition temperature for polybutadienes with varying 1,2 content[40]. Up to the glass transition temperature of -85^{o}C, which corresponds to 30% 1,2 content, the plateau modulus is linearly dependent on the glass transition temperature. While the absolute value of the plateau modulus reported by Carella *et al*.[40] may be changed if we use a different method to determine the plateau modulus, this linear relationship does not change. Thus, if we measure the glass transition temperature of polybutadiene, we can infer the value of the plateau modulus from this correlation more accurately than from the measured 1,2 content, and from it get the entanglement molecular weight. In this way, possible errors in determining the 1,2 content can be bypassed by correlating the plateau modulus directly with the value of T_g inferred from the shift factors using Eq. (5). This means that, because the high frequency glassy behavior determines the value of T_g from Eq. (5), all three canonical parameters of the tube model, namely the G_N^0, M_e, and τ_e can be fixed within a tight range for 1,4-polybutadienes of any architecture.

4.4. Conclusions

In this chapter, linear viscoelastic data for well-characterized 1,4-polybutadienes drawn from literature were compared in the transition frequency region for linear, star, H, and comb structures. The storage and loss moduli of well entangled 1,4-polybutadiene melts in the transition frequency region superposed well irrespective of their molecular weight and its distribution and of branching structures. This suggests that the equilibration time τ_e needed in the theoretical tube models can be determined using these data, rather than being left as an adjustable parameter to be fit by matching the predictions to measurements at low or modest frequencies

The WLF shift parameters, however, show significant deviations from one data set to the next. Because the moduli show good agreement in the transition region, the discrepancy in shift factors at low temperature could be due to systematic temperature measurement errors or more likely due to small variations in 1,2 content in the polybutadienes. It is unlikely to be due to accumulation of errors in generating the master curve, because then the agreement of transition frequency data at the same reference temperature would become inexplicable.

Because recently developed tube models use the same equations for longitudinal relaxation and fast Rouse motion in the transition frequency region, the value of equilibration time can be determined to be $\tau_e = (3.7 \pm 0.93) \times 10^{-7} (s)$ at 25°C by fitting experimental data at transition frequency and then is no longer available to be tuned to fit the terminal behavior of entangled polymers. Thus, limitations and inaccuracies in available tube models might be discovered more easily, since τ_e is no longer available to be fit to cover over errors in model predictions. In addition, because the plateau modulus is linearly correlated to the glass transition temperature for polybutadienes with 1,2 content up to 30%, G_N^0 and M_e can be taken as fixed within a range for 1,4-polybutadienes having different 1,2 content, and can even be corrected for small variations in 1,2 content by using the T_g value obtained by fitting the WLF equation to the temperature-dependent shift factor. The removal of the freedom to adjust τ_e, G_N^0 and M_e to fit rheological data should be useful in revealing flaws and limitations of tube models, slip-link models and other theories of entangled polymer rheology. The next chapter, chapter 5, presents tube model predictions for pure monodisperse linear and star shaped 1,4-polybutadienes and their bidisperse blends using the universal parameter set, τ_e, G_N^0 and M_e, obtained in this chapter.

4.5. References

1. de Gennes, P. G., "Reptation of a Polymer Chain in the Presence of Fixed Obstacles," *J. Chem. Phys*. *55*, 572 (1971)
2. Doi, M., Edwards, S. F. *The theory of polymer dynamics,* Clarendon: Oxford (1986)
3. Doi, M., "Explanation for the 3.4-power law for viscosity of polymeric liquids on the basis of the tube model," *J. Polym. Sci., Polym. Phys. Ed. 21*, 667 (1983)
4. Marrucci, G., "Relaxation by reptation and tube enlargement: A model for polydisperse polymers," *J. Polym. Sci., Polym. Phys. Ed. 23*, 159 (1985)
5. Milner, S. T., McLeish, T. C. B., "Parameter-free theory for stress relaxation in star polymer melts," *Macromolecules 30*, 2159 (1997)
6. Milner, S. T., McLeish, T. C. B, "Reptation and contour-length fluctuations in melts of linear polymers," *Phys. Rev. Lett. 81*, 725 (1998)
7. Milner, S. T., McLeish, T. C. B., Young, R. N., Hakiki, A., Johnson, J. M., "Dynamic dilution, constraint-release, and star−linear blends," *Macromolecules 31*, 9345 (1998)
8. Likhtman, A. E., McLeish, T. C. B., "Quantitative theory for linear dynamics of linear entangled polymers," *Macromolecules 35*, 6332 (2002)
9. Das, C., Inkson, N. J., Read, D. J., Kelmanson, M. A., McLeish, T. C. B., "Computational linear rheology of general branch-on-branch polymers," *J. Rheol. 50*, 207 (2006)
10. Wang, Z., Chen, X., Larson, R. G., "Comparing tube models for predicting the linear rheology of branched polymer melts," *J. Rheol. 54*, 223 (2010)
11. Larson, R. G., Sridhar, T., Leal, L. G., McKinley, G. H., Likhtman, A. E., McLeish, T. C. B., "Definitions of entanglement spacing and time constants in the tube model," *J. Rheol. 47*, 809 (2003)
12. Park, S. J., Larson, R. G., "Dilution exponent in the dynamic dilution theory for polymer melts," *J. Rheol*. *47*, 199 (2003)
13. Kapnistos, M., Vlassopoulos, D., Roovers, J., Leal, L. G., "Linear rheology of architecturally complex macromolecules: Comb polymers with linear backbones," *Macromolecules 38*, 7852 (2005)
14. Ferry, J. D. *Viscoelastic properties of polymers,* 3rd ed.; Wiley: New York (1980)
15. Dealy, J. M., Larson, R. G. *Structure and rheology of molten polymers,* Hanser: Cincinnati (2006)
16. van Ruymbeke, E., Liu, C. Y., Bailly, C., "Quantitative tube model predictions for the linear viscoelasticity of linear polymers," *Rheology Reviews* 53 (2007)
17. Liu, C. Y., Keunings, R., Bailly, C., "Direct rheological evidence of monomer density reequilibration for entangled polymer melts," *Macromolecules 40*, 2946 (2007)
18. Graessley, W. W., "Effect of long branches on the temperature dependence of viscoelastic properties in polymer melts," *Macromolecules 15*, 1164 (1982)
19. Wood-Adams, P. M., Costeux, S., "Thermorheological behavior of polyethylene: Effects of microstructure and long chain branching," *Macromolecules 34*, 6281 (2001)
20. Carella, J. M., Gotro, J. T., Graessley, W. W., "Thermorheological effects of long-chain branching in entangled polymer melts," *Macromolecules 19*, 659 (1986)
21. Dealy, J. M., Plazek, D., "Time temperature superposition - a users guide," *Rheol. Bulletin 78*, 16 (2009)
22. Colby, R. H., Fetters, L. J., Graessley, W. W., "The melt viscosity-molecular weight relationship for linear polymers," *Macromolecules 20*, 2226 (1987)

23. Struglinski, M. J., Graessley, W. W., Fetters, L. J., "Effects of polydispersity on the linear viscoelastic properties of entangled polymers. 3. Experimental observations on binary mixtures of linear and star polybutadienes," *Macromolecules 21*, 783 (1988)
24. Baumgaertel, M., de Rosa, M. E., Machado, J., Masse, M., Winter, H. H., "The relaxation time spectrum of nearly monodisperse polybutadiene melts," *Rheol. Acta 31*, 75 (1992)
25. Wang, S., Wang, S., Halasa, A., Hsu, W.-L., "Relaxation dynamics in mixtures of long and short chains: Tube dilation and impeded curvilinear diffusion," *Macromolecules 36*, 5355 (2003)
26. Park, S. J., Larson, R. G., "Tube dilation and reptation in binary blends of monodisperse linear polymers," *Macromolecules 37*, 597 (2004)
27. van Ruymbeke, E., Keunings, R., Bailly, C., "Prediction of linear viscoelastic properties for polydisperse mixtures of entangled star and linear polymers: Modified tube-based model and comparison with experimental results," *J. Non-Newtonian Fluid Mech*. *128*, 7 (2005)
28. Liu, C. Y, Halasa, A. F., Keunings, R., Bailly, C., "Probe rheology: A simple method to test tube motion," *Macromolecules 39*, 7415 (2006)
29. Li, S. W., Park, H. E., Dealy, J. M., "Evaluation of molecular linear viscoelastic models for polydisperse H polybutadienes," *J. Rheol*. *55*, 1341 (2011)
30. Shivokhin, M. E., van Ruymbeke, E., Bailly, C., Kouloumasis, D., Hadjichristidis, N., Likhtman, A. E., "Understanding constraint release in star/linear polymer blends," *Macromolecules 47*, 2451 (2014)
31. van Ruymbeke, E., Lee, H., Chang, T., Nikopoulou, A., Hadjichristidis, N., Snijkers, F., Vlassopoulos, D., "Molecular rheology of branched polymers: decoding and exploring the role of architectural dispersity through a synergy of anionic synthesis, interaction chromatography, rheometry and modeling," *Soft Matter*, *10*, 4762 (2014)
32. Snijkers, F., van Ruymbeke, E., Kim, P., Lee, H., Nikopoulou, A., Chang, T., Hadjichristidis, N., Pathak, J., Vlassopoulos, D., "Architectural dispersity in model branched polymers: Analysis and rheological consequences," *Macromolecules 44*, 8631 (2011)
33. Roovers, J., Toporowski, P., "Relaxation by constraint release in combs and star-combs," *Macromolecules 20*, 2300 (1987)
34. Inkson, N. J., Graham, R. S., McLeish, T. C. B., Groves, D. J., Fernyhough, C. M., "Viscoelasticity of monodisperse comb polymer melts," *Macromolecules 39*, 4217 (2006)
35. Park, S. J., Shanbhag, S., Larson, R. G., "A hierarchical algorithm for predicting the linear viscoelastic properties of polymer melts with long-chain branching," *Rheol. Acta 44*, 319 (2005)
36. Park, S. J., Larson, R. G., "Long-chain dynamics in binary blends of monodisperse linear polymers," *J. Rheol. 50*, 21 (2006)
37. Lee, J. H., Fetters, L. J., Archer, L. A., Halasa., A. F., "Tube dynamics in binary polymer blends," *Macromolecules 38*, 3917 (2005)
38. Ahmadi, M., Bailly, C., Keunins, R., Nekoomanesh, M., Arabi, H., van Ruymbeke, E., "Time marching algorithm for predicting the linear rheology of monodisperse comb polymer melts," *Macromolecules 44*, 647 (2011)

39. Shchetnikava, V., Slot, J. J. M., van Ruymbeke, E., "A comparison of tube model predictions of the linear viscoelastic behavior of symmetric star polymer melts," *Macromolecules 47*, 3350 (2014)
40. Carella, J. M., Graessley, W. W., Fetters, L. J., "Effects of chain microstructure on the viscoelastic properties of linear polymer melts: polybutadienes and hydrogenated polybutadienes," *Macromolecules 17*, 2775 (1984)
41. Honerkamp, J., Weese, J., "A note on estimating mastercurves," *Rheol. Acta 32*, 57 (1993)
42. Raju, V. R., Menezes, E. V., Marin, G., Graessley, W. W., Fetters, L. J., "Concentration and molecular weight dependence of viscoelastic properties in linear and star polymers," *Macromolecules 14*, 1668 (1981)
43. Palade, L. I., Verney, V., Attane P., "Time-temperature superposition and linear viscoelasticity of polybutadienes," *Macromolecules 28*, 7051 (1995)
44. Okamoto, H., Inoue, T., Osaki, K., "Viscoelasticity and birefringence of polyisoprene," *J. Polym. Sci., Polym. Phys.* 33, 417 (1995)

Table 4.1. Molecular characteristics of linear 1,4-polybutadienes

Source	%1,4	%1,2	M	M_n	M_w	M_w/M_n	T_g(°C)	T_{ref}(°C)
Colby *et al*.[22]	90	10			130,000	<1.1	-99.2	25
Struglinski *et al*.[23]	93	7	100,000*				-97	25
Baumgaertel *et al*.[24]	92	8			97,000	1.07	-89.6	28
Wang *et al*.[25]	91.8	8.2		98,850	99,060	1.01	-100.1	40
Liu *et al.*[28]	> 90				98,000	1.03	-97.7	25
Li *et al*.[29]	95	5			95,800**			25
Palade *et al*.[43]	89	11		70,000	70600	1.16	-86.5	25

* Only the "molecular weight" M was reported.
** Binary mixture of 130,000 : 92,000 = 0.1 : 0.9

Table 4.2. Molecular characteristics of branched 1,4-polybutadienes

Source	Branch type	%1,4	%1,2	M_n	M_w	M_w/M_n	T_g(°C)	T_{ref}(°C)
Kapnistos *et al.*[13] *	Comb	90	10		464,000			0
Li *et al.*[29]	H	94	6	82,000		1.03		25
Shivokhin *et al.*[30]	3 arm-star	90	10		76,000	1.04		25
van Ruymbeke *et al.*[31] **	H	87-90	13-10		94,400	1.04	-91	20

* Reported by Snijkers *et al.*[32]
** Reported by Roovers and Toporowski.[33]

Table 4.3. Equilibration time τ_e used in theoretical predictions based on the tube model

Source	Structure	M_e	G_N^0 (MPa)	τ_e (s)×10^{-7}	α	T (^{o}C)
Likhtman and McLeish[8]	linear	1930	1.47	4.9	-	28
		1610	1.67	2.9	-	26
Inkson *et al*.[34]	comb	1800	1.28	2.2	4/3	27.5
Das *et al*.[9]	comb	1836	0.97	2.75	1	25
Park and Larson[12]	linear, star	2200	1.15	9.5	1	25
		1650	1.15	3.7	4/3	25
Park *et al.*[35]	linear, star, comb	1650	1.15	3.7	4/3	25
Park and Larson[36]	linear	1543	1.15	2.0	1	28
Wang *et al*.[10]	linear, star, comb	1620	1.095	3.7	4/3	25
Lee *et al.*[37]	linear, star	1800	1.42	3.0	4/3	28
Kapnistos *et al*.[13]	comb	1460	1.12	5.6 ~10.0	1	0
van Ruymbeke *et al*.[27]	linear, star	1650	1.05	7.0	1.2	28
Ahmadi *et al.*[38]	comb	1650	1.1	10.0 ~15.0	1	27.5
van Ruymbeke *et al*.[31]	H, comb	1520	1.2	2.3	1	20
Shchetnikava *et al*.[39]	star	1680	1.25	2.5	1	27

* Lines separate results from different research groups.

Table 4.4. The WLF parameters of 1,4-polybutadienes from the literature

Source	Structure	Temperature range (^{o}C)	T_{ref} (^{o}C)	C_1	C_2
Colby *et al*.[22]	linear	-91 ~ 25	25	3.48	163
Baumgaertel *et al.*[24]	linear	-77 ~ 28	28	4.17	25
Wang *et al*.[25] *	linear	-80 ~ 100	100	2.57	248
Kapnistos *et al*.[13]	comb	-90 ~ 100	0	4.9	154
Liu *et al*.[28]	linear	-80 ~ 25	25	3.76	175
Li *et al*.[29]	linear	-75 ~ 25	25	3.98	177.5
	H	-75 ~ 25	25	4.42	181.0
van Ruymbeke *et al*.[31]	H, comb	-80 ~ 100	20	4.8	180
Shivokhin *et al*.[30]	star	-75 ~ 25	25	4.66	179.3
Palade *et al*.[43] *	linear	-115~80	25	4.93	181.3

*The WLF parameters were calculated by applying nonlinear regression to the shift factors reported here.

Table 4.5. Glass transition temperature and plateau modulus of polybutadienes from Carella *et al*.[40]

1,2 content (%)	T_g (^oC)	G_N^0 (MPa)*
8	-97	1.25
18	-91	1.13
23	-88	1.09
30	-85	1.01

* Average of the plateau modulus at multiple temperatures.

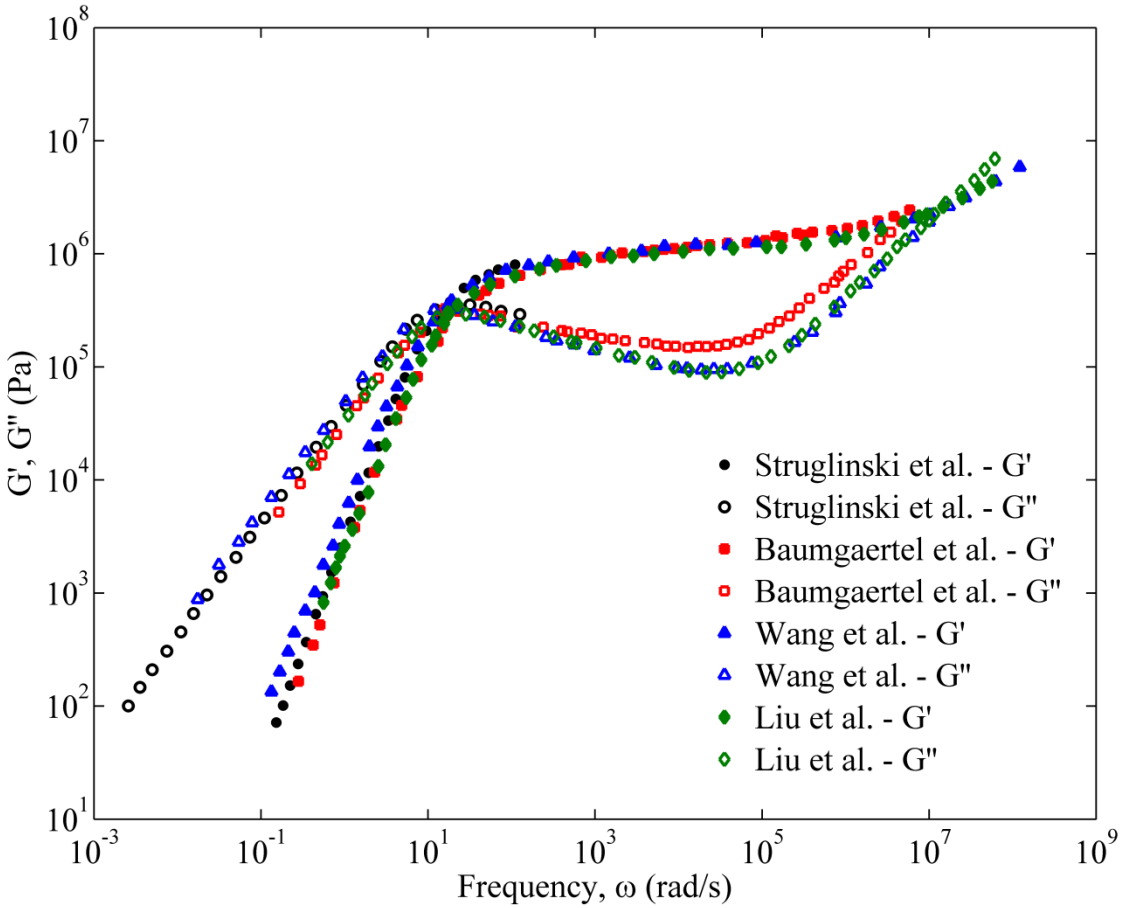

Figure 4.1. Storage and loss moduli of monodisperse linear 1,4-polybutadienes with molecular weights within the range from 97,000 to 100,000 at T=25°C. The data of Baumgaertel *et al.*[24] and Wang *et al.*[25] were shifted from T=28°C and T=40°C, respectively to T=25°C using the shift factor calculated by the WLF equation.

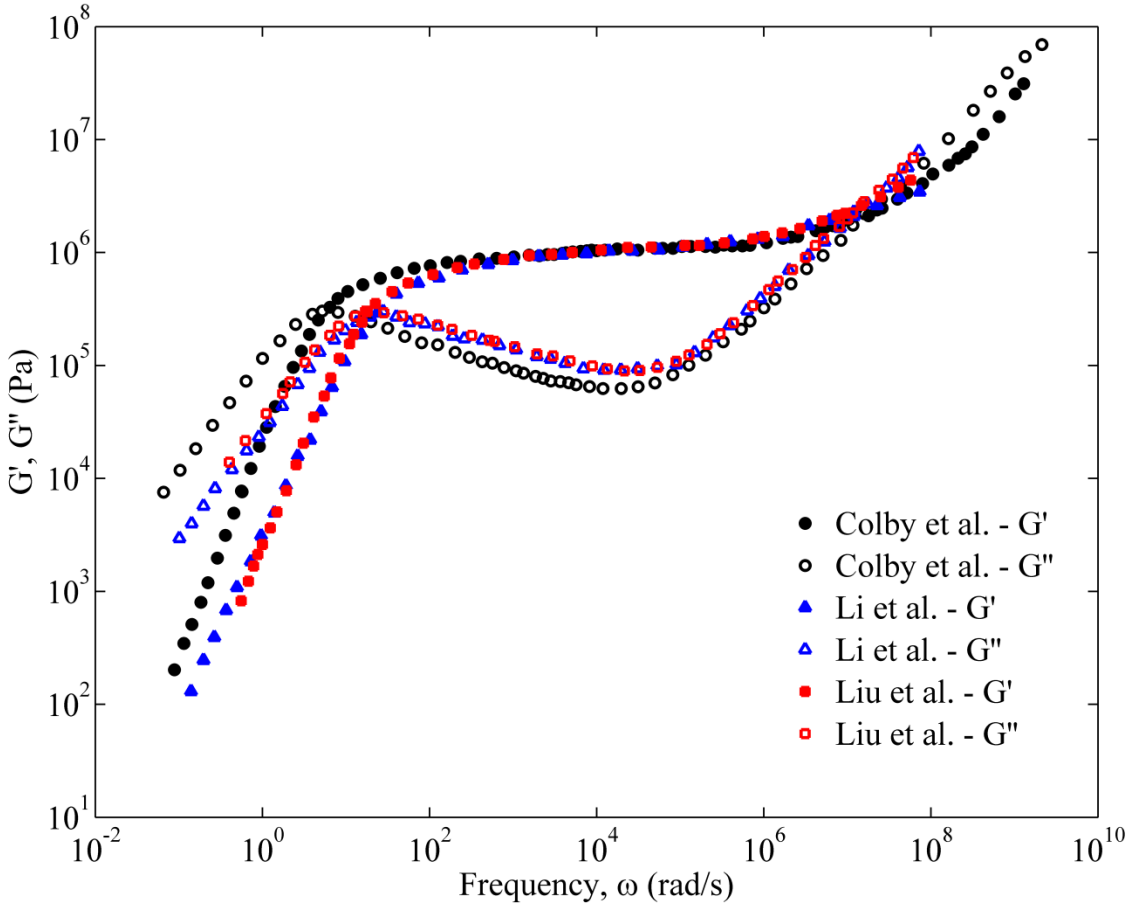

Figure 4.2. Storage and loss moduli of linear 1,4-polybutadienes at T=25°C. The polybutadienes of Colby *et al*.[22] and Liu *et al*.[28] are nearly monodisperse. The polybutadiene of Li *et al*.[29] is a 1:9 binary mixture of 130,000 and 92,000.

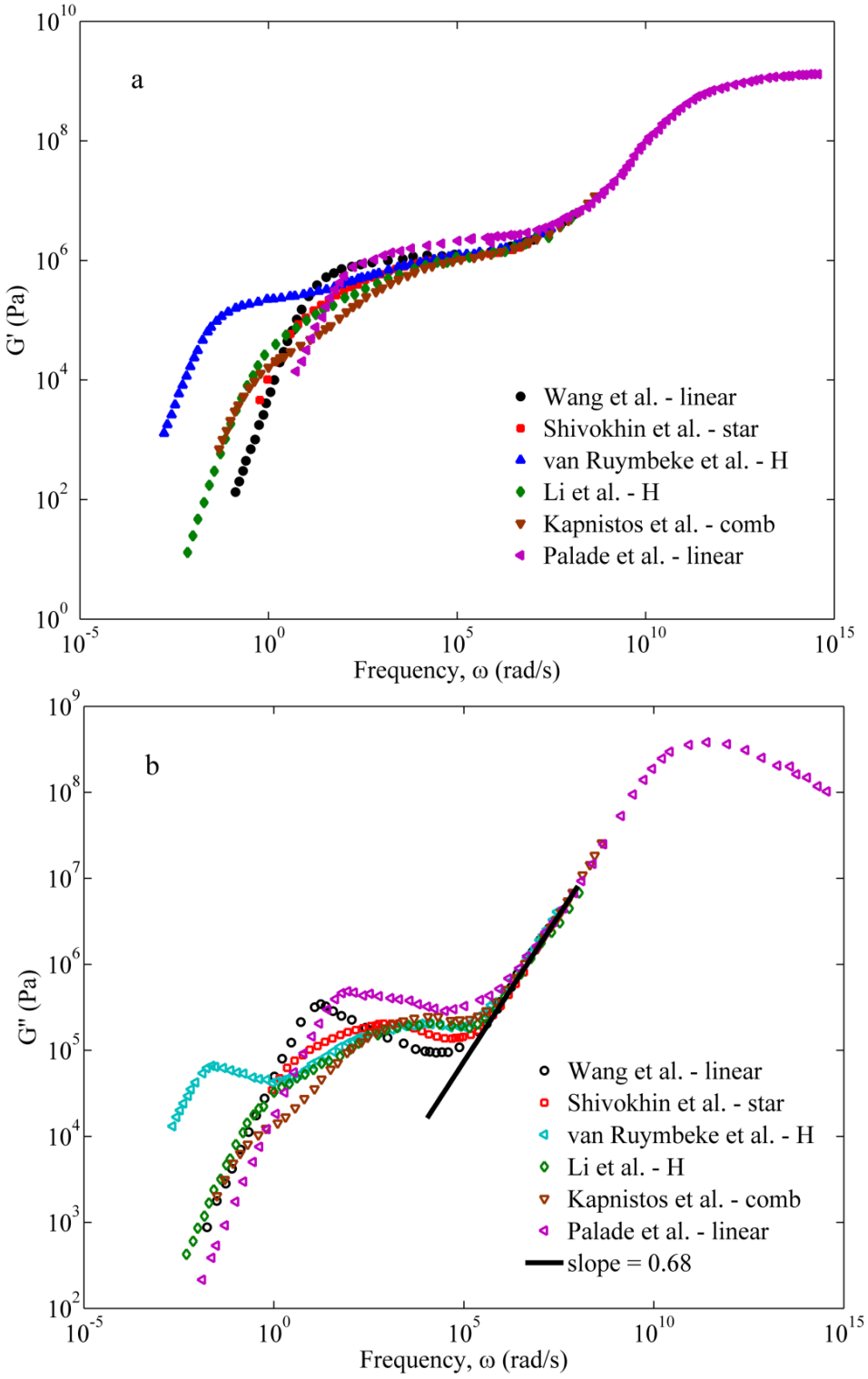

Figure 4.3. (a) storage and (b) loss moduli of linear and branched 1,4-polybutadienes at T=25°C. The data of Kapnistos *et al.*[13] and van Ruymbeke *et al.*[31] were shifted from T=0°C and T=20°C, respectively to T=25°C using the shift factors calculated by the WLF equation using WLF parameters given in the respective publications. In the transition frequency region the loss modulus shows a power-law dependence with an exponent of 0.68.

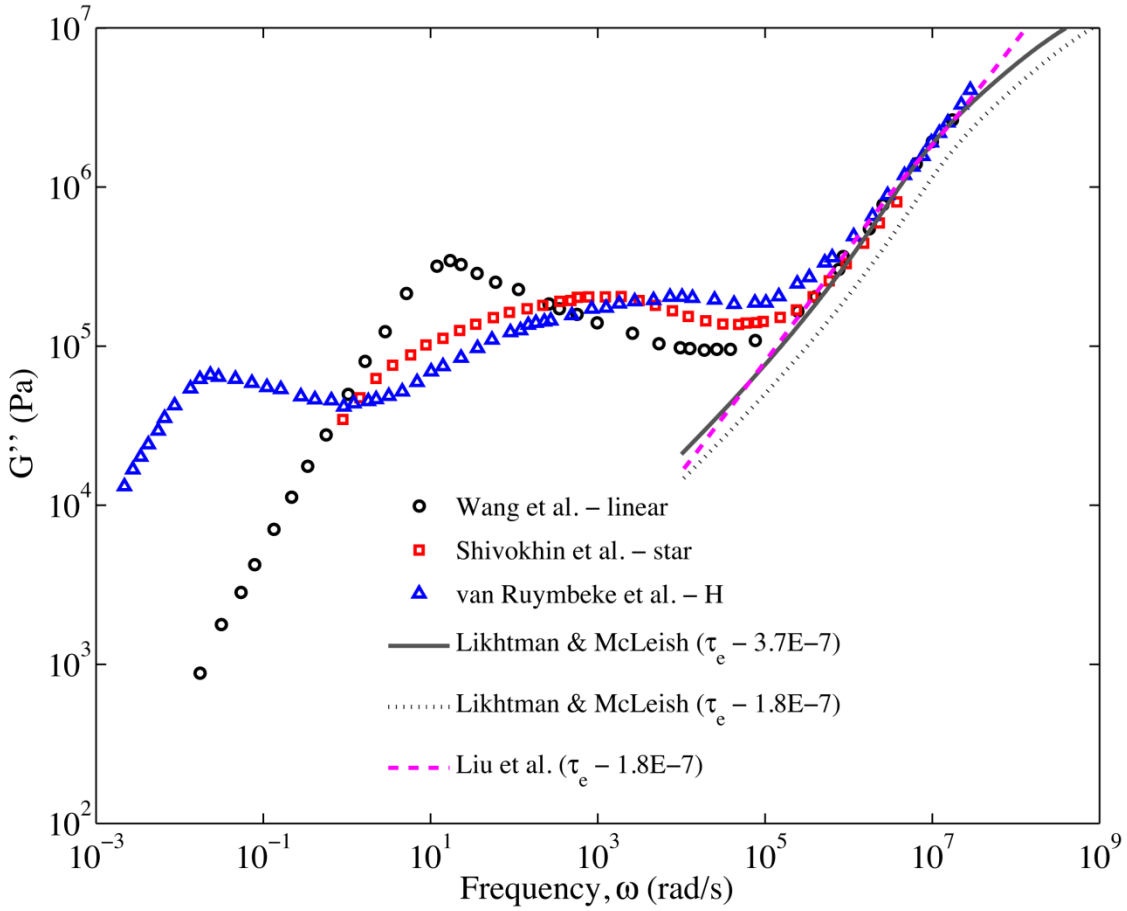

Figure 4.4. Comparison of model predictions of Liu *et al.*[17] (red dashed line) and Likhtman and McLeish[8] (black dotted and solid lines) using Eq. (2) and Eq. (3), respectively, for loss moduli of polybutadienes in the transition frequency region at T=25°C.

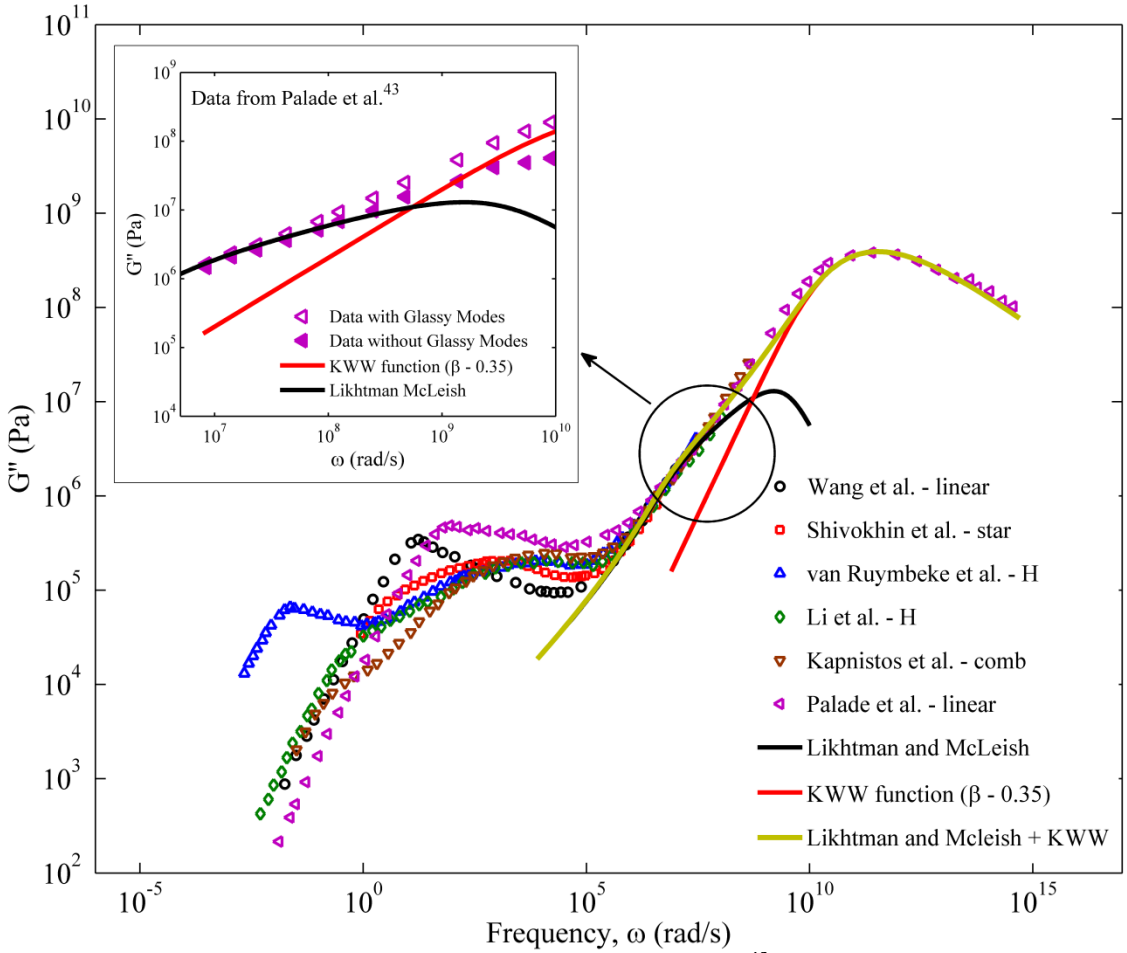

Figure 4.5. Comparison of model predictions of KWW[43] (red solid line) using Eq. (4) and Likhtman and McLeish[8] (solid black line) using Eq. (3), respectively, and their sum (solid yellow line) for loss moduli of polybutadienes in the high frequency region at T=25°C. Inset shows experimental G" data by Palade *et al.*[43] as is (open left triangles) and with glassy modes subtracted (closed left triangles) for linear polybutadiene. Solid black line in the inset indicates Rouse model prediction while solid red line gives the KWW function prediction for loss moduli, G", in the high frequency region at T=25°C.

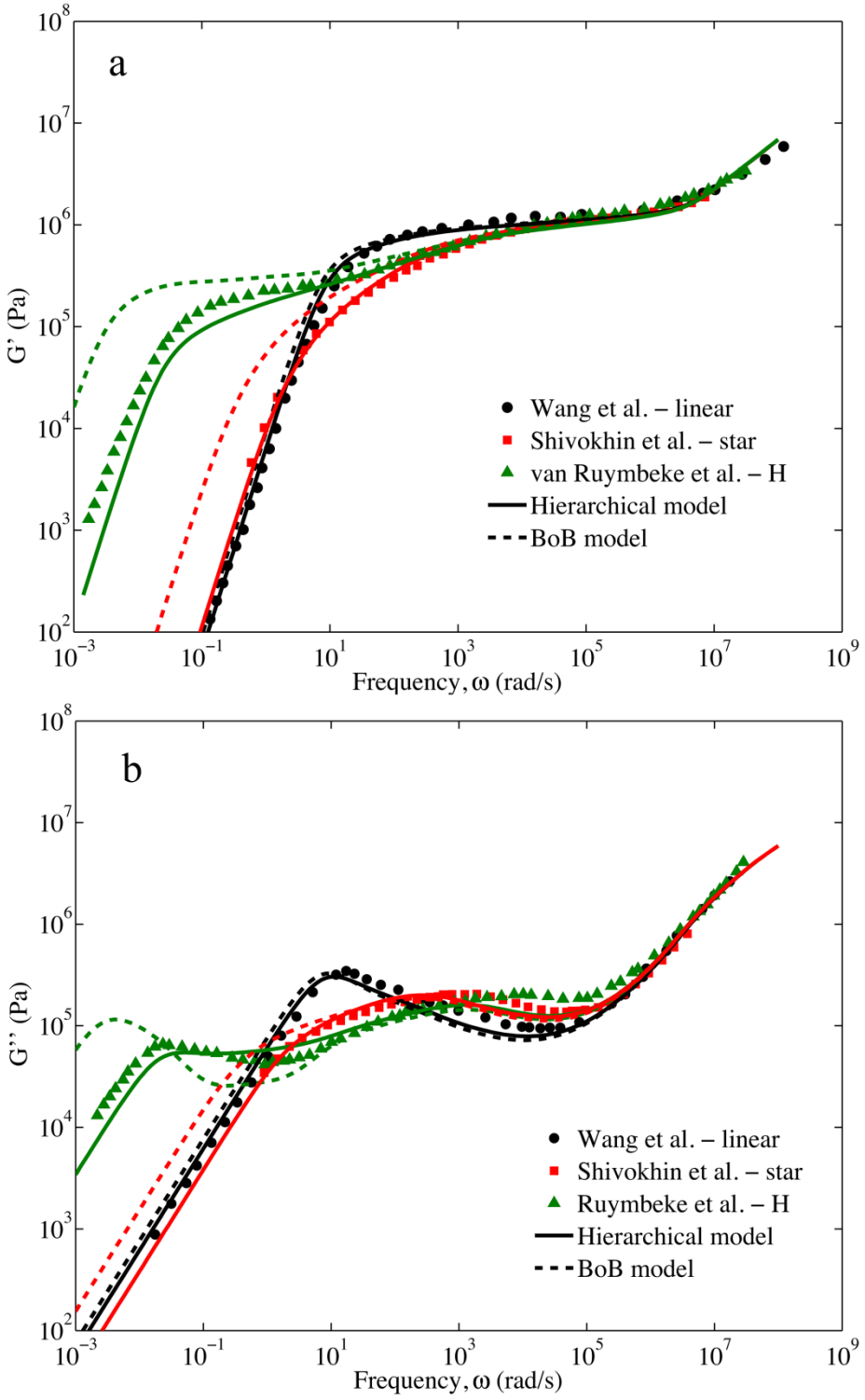

Figure 4.6. Comparison of model predictions of (a) storage modulus and (b) loss modulus with measurements at T=25°C using the hierarchical model (solid lines) and bob model (dashed lines) for linear, star, and H polybutadienes. Parameter values of $G_N^0 = 1.15\times10^6(Pa)$, $M_e = 1543$, and $\tau_e = 3.7\times10^{-7}(s)$ are used in model predictions. The molecular weights are given in Tables 4.1 and 4.2.

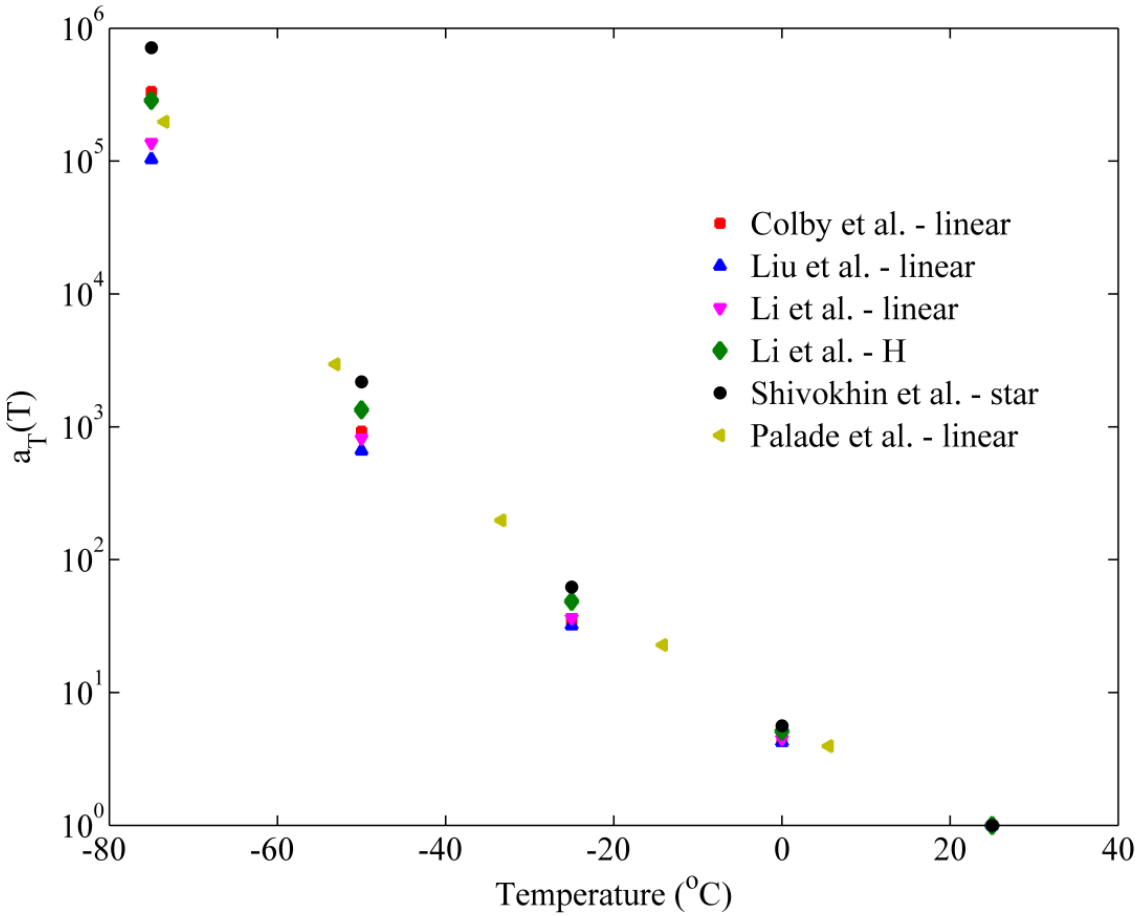

Figure 4.7. Comparison of shift factors of linear and branched 1,4-polybutadienes having the same reference temperature of T=25°C.

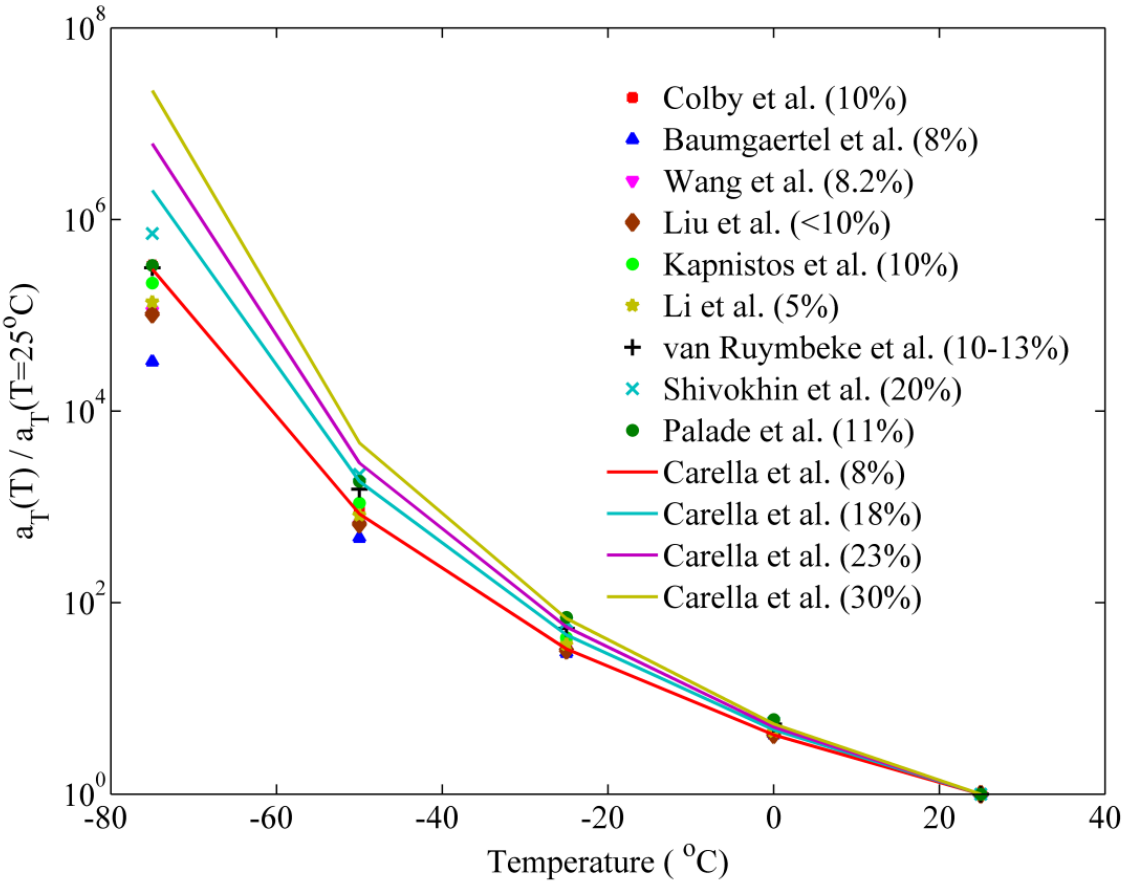

Figure 4.8. Comparison of the normalized shift factors, which is defined as the ratio of shift factor at a given temperature to the shift factor at T=25°C for linear and branched 1,4-polybutadienes. The numbers in parenthesis represent the 1,2 contents.

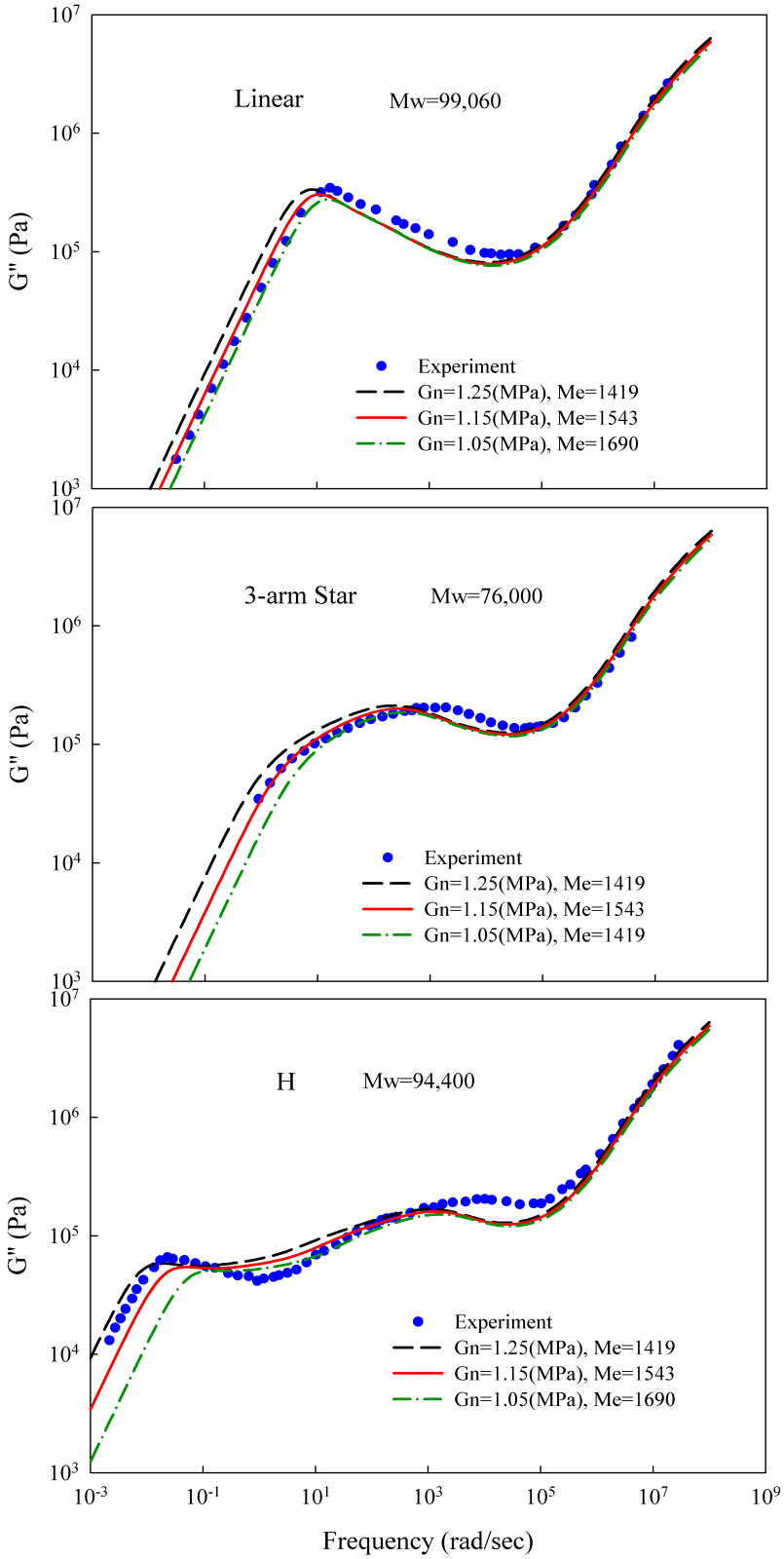

Figure 4.9. Effect of changing the plateau modulus and the entanglement molecular weight on the hierarchical model prediction of loss modulus for linear, star, and H 1,4-polybutadienes.

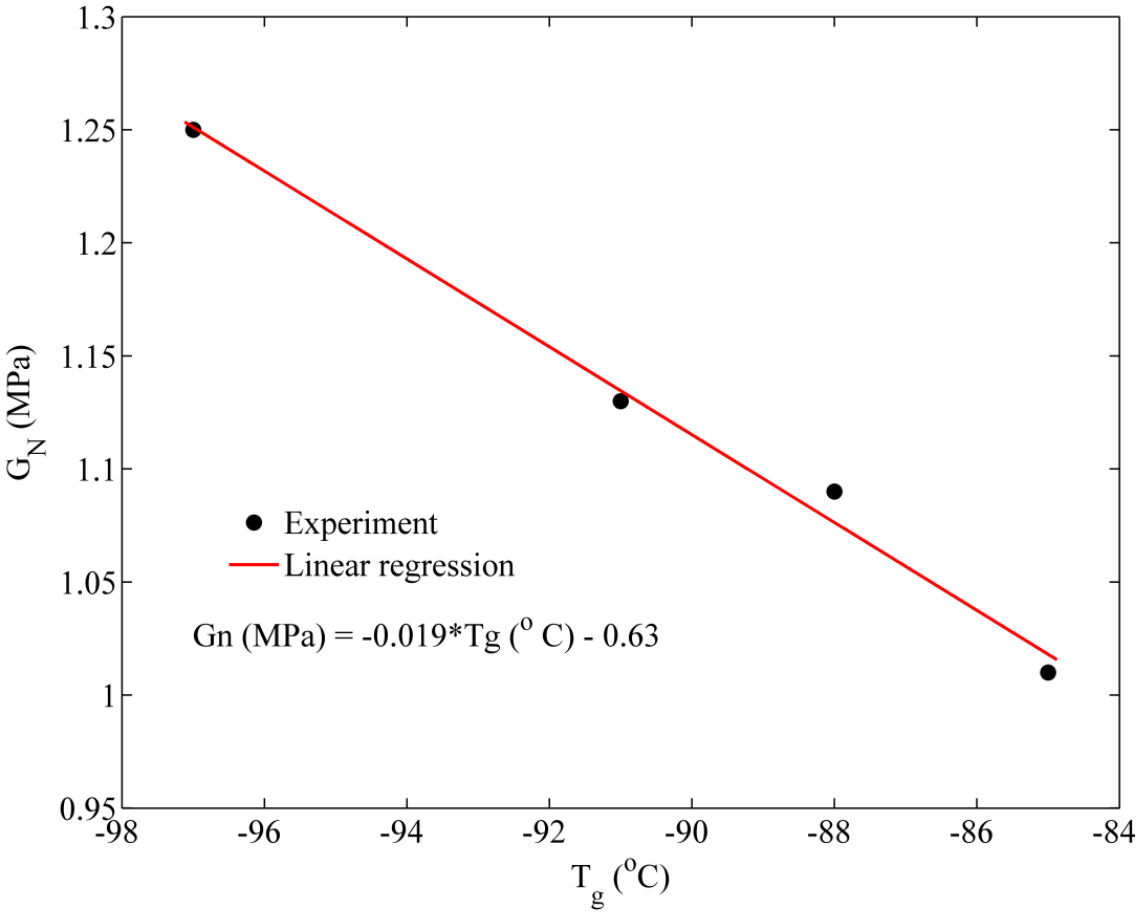

Figure 4.10. Variation of the plateau modulus with the glass transition temperature for polybutadienes as reported by Carella *et al.*[40]

CHAPTER 5

Challenging tube and slip-link models: Predicting the linear rheology of 1,4-polybutadiene blends of well-characterized star and linear 1,4-polybutadienes

5.1. Abstract

This chapter compares predictions of the two most advanced versions of the tube model, namely the "Hierarchical model" by Wang *et al.* (*J. Rheol.* 54:223, 2010) and the BoB (branch-on-branch) model by Das *et al.* (*J. Rheol.* 50:207-234, 2006), against linear viscoelastic G' and G" data of binary blends of monodisperse 1,4-polybutadiene star polymer of arm molecular weight 24,000 g/mol with a monodisperse linear 1,4-polybutadiene of molecular weight 58,000 g/mol. The star was carefully synthesized and characterized by temperature gradient interaction chromatography, and by linear rheology in the high frequency region through time-temperature superposition. We found massive failures of both the Hierarchical and BoB models to predict the terminal relaxation behavior of the star/linear blends, despite their success in predicting the rheology of the pure star and pure linear. This failure occurred regardless of the choices made concerning constraint release, such as assuming arm retraction in "fat" or "skinny" tubes, or allowing for "disentanglement relaxation" to cut off the constraint release Rouse process at long times. In addition, these blends were also tested against a coarse-grained slip link model, the "Cluster Fixed Slip-link Model (CFSM)" by Schieber and coworkers (Andreev *et al.*, *J. Rheol.* 58, 723–736, 2014) in which several Kuhn steps are clustered together for computational efficiency. The CFSM with only two molecular-weight and chain-architecture-independent parameters, namely, τ_c, the characteristic shuffling time of the cluster of Kuhn steps through the entanglement and M_c, the molecular weight of a cluster, was able to give excellent agreement with experiments. The failures of the tube models call into question whether constraint release can be described as a combination of constraint release Rouse processes and dynamic tube dilation within a canonical tube model of entanglement interactions. In light of its success, the

DSM slip link model may be used to address the constraint release issue more rigorously and potentially to help fix the tube models.

In this Chapter, the synthesis of 24K star polymer was carried out by Beom-Goo Kang from Jimmy May's group at University of Tennessee. The TGIC characterization of 24K star polymer was done by Sanghoon Lee from Taihyun Chang's group in Pohang University of Science and Technology, Korea. Maria Katzarova from Jay Schieber's lab at Illinois Institute of Technology performed the CSFM slip-link predictions. The low temperature rheology measurements on the pure 24KS star and 58K linear polymers were conducted by Priyanka Desai and Ryan Hall on the RMS-800 rheometer in David Venerus' lab at Illinois Institute of Technology. Priyanka Desai acknowledges all of their contributions. (**Text and figures in this chapter are from the following manuscript – Desai, P.S, Kang, B-G, Katzarova, M., Hall, R., Huang, Q., Lee, S., Chang, T., Venerus, D.C., Mays, J., Schieber, J.D., Larson, R.G. (2015)** ***(manuscript submitted)***

5.2. Introduction

The introduction of a mean-field entanglement "tube" to describe constraints on polymer motion by de Gennes[1], and Doi and Edwards[2], has greatly advanced our understanding of the dynamics and rheology of polymers with various complex architectures and of their blends. In the tube model, relaxation occurs by chain motion within the tube, and by release of the entanglement constraints that define the tube. Motion within the tube has been successfully described by a combination of reptation or sliding of the whole chain along the tube and by contour length fluctuations, or "breathing modes," which allow the ends of the chain to escape the ends of the tube and relax stress faster than by reptation alone. Constraint release can be modeled for polydisperse linear polymers by allowing the tube itself to undergo local diffusion due to repeated release of constraints along its contour. The motion of the tube produced by the accumulation of local constraint-release events is mathematically identical to Rouse relaxation, except that "viscosity" of the medium through which the Rouse "chain" (actually tube) drifts is set by the rate at which constraints are released by the surrounding chains[3]. Hence, this mechanism is called "constraint-release (CR) Rouse relaxation." CR-Rouse relaxation, however, is not adequate to describe constraint release effects in monodisperse star polymers. It has thus been necessary to introduce the concept of "tube dilation" (also known as dynamic dilution[4]), which envisages that constraint release gradually enlarges the diameter of the tube constraining the polymer, shortening its length, and thus accelerating the relaxation of the chain within it.

A "universal" tube model capable of describing all well entangled polymers, including mixtures of branched and linear polymers is the "Holy Grail" of rheological modeling, since such a theory would allow commercial polymer melts to be modeled reliably. In an effort to develop such a model, it is necessary to describe constraint release for blends of branched and linear polymers. As a first effort in this direction, Milner, McLeish and coworkers[5] used a combination of tube dilation and CR-Rouse relaxation to predict constraint release dynamics of a blend of a monodisperse star polymer with a monodisperse linear polymer, with CR-Rouse processes controlling the rate at which the dynamic dilution of the star arms proceeds. Their work was a crucial step towards the development of general tube theories for relaxation of mixtures of linear and long-chain-branched polymers of arbitrary branching structure. Two such general theories, the "Hierarchical" model of Larson and coworkers, and the "BoB" (Branch-on-

Branch) model of Das, McLeish, Read, and coworkers, are now publically available, and have enjoyed some success in predicting the rheology of complex mixtures of branched and linear polymers.

Despite these advances in understanding, there are significant challenges in accounting for constraint release within tube models. Sometimes reptation or fluctuations of the chain are taken to occur in an un-dilated "skinny" tube[6], and sometimes in the dilated "fat" tube[7], and it is unclear in general which tube diameter to use. In the original work of Milner *et al.*[5] that first addressed star-linear blends, constraint release caused by relaxation of the linear chains dynamically widens the tube containing the star arm, but during this widening the fluctuations of that arm are mysteriously shut off, until the widening comes to an end. This is the so-called "arm frozen" assumption, also adopted by Park *et al.*[8]. Apart from relatively good agreement between theory and experiment for the particular set of star/linear blends studied by Milner and McLeish, there seems to be little justification for this assumption. In addition, during constraint release caused by relaxation of the linear chains, Milner *et al.*[5] chose $\alpha = 4/3$ for the tube diameter "dilution exponent" relating tube diameter to the fraction of un-relaxed melt. This value can be obtained by scaling arguments, and contrasts with $\alpha = 1$ arising from the assumption that entanglements are binary events. In general, the value $\alpha = 1$ appears to be required to obtain agreement with experimental data for binary blends of linear polymers, while accurate prediction of the rheology of star polymers seems to require setting $\alpha = 4/3$, at least in some tube models[9]. When the artificial "arm frozen" assumption is removed and the arms are allowed to fluctuate in a thin tube during the CR-Rouse process, tube theories are able to predict the rheology of both pure linear and pure star polymers when $\alpha = 4/3$, but blends of the two are rather poorly described, as shown in Figure 6 of the paper by Wang *et al.*[9] and which we show again here, as Figure 5.1, to compare in what follows to experimental data and predictions for our newly prepared star/linear blends studied here.

In addition to these issues with star/linear blends, recent work by van Ruymbeke and Watanabe[10] on linear/linear binary blends suggests that the dilution exponent α might be a function of time, varying from 1 at early times to 4/3 at long times. Khaliullin and Schieber[11] recently showed that two different versions of the tube model were unable to yield an accurate prediction of binary linear blends. In addition, recent work of Watanabe and coworkers[12]

suggests that previous theories of constraint release are inadequate even for "simple" cases of linear/linear blends. Thus, the inclusion of constraint release mechanisms into the tube model is problematic, especially for star/linear blends, where constraint release is described by a combination of CR-Rouse processes and tube dilation.

We note, however, that there are only two "complete" data sets in the current literature for blends of monodisperse star and linear polymers. The first is the 1,4-polybutadiene star/linear blend studied theoretically by Milner, McLeish and co-workers that we here call "PBd42KS-100KL," with a monodisperse star polymer having arm molecular weight 42,333 g/mol and a monodisperse linear polymer of molecular weight 100,000 g/mol. This data set was taken from the work of Struglinski *et al.*[13]. There is also a very recent 1,4-polybutadiene data set, here called "PBd24.5KS-6.5KL" with star arm having molecular weight 24,500 g/mol, and the linear molecule having molecular weight of 6,500 g/mol, which is just high enough to be modestly self-entangled[14]. Other, less complete, data sets for star/linear blends include that of Lee and Archer[15], and of Roovers *et al.*[16]. However, the former data set does not include rheological data for the pure star, while the latter contains only data for a blend of 2.5% star in a linear matrix. Hence, to assess tube models more thoroughly, there is a great need for additional data on well entangled blends of nearly monodisperse star and linear polymers, which motivated our acquisition of a new, complete, data set here.

In part because of the unsatisfactory treatment of constraint release within the tube model, an alternative to the tube model, the so-called "slip-link" class of models, has attracted increasing attention in recent years[17-19]. Slip-link models track the stochastic motion of individual chains and average over many such chains to obtain the rheological response. Most importantly, in slip link models the constraints on chain motion imposed by entanglements are accounted for individually, rather than collectively, as in the tube model[20]. Thus, the "tube," which confines the chain *globally* along its length, is replaced by "slip-links" that *locally* constrain chain sliding to pass through the position of each slip link. Both reptation and local Rouse motions along chains can be allowed in slip link models. Constraint release arises through the disappearance of slip-links when chain ends pass through a slip-link, and is balanced by the appearance of new slip-links via detailed balance. A major advantage of slip-link models is that, in doing away with the tube, no explicit accounting need be made of "tube dilation" or of CR-

Rouse tube motion. Instead, these processes are allowed to arise naturally from the constrained motion of the chains and the appearance and disappearance of slip links.

While slip-link models remove many of the questionable assumptions involved in the tube model discussed above, they replace them with other assumptions, namely: i) binary entanglements that involve only two chains[21]; and ii) approximations that relate the behavior of one chain to that of its neighbors, either through a mean-field assumption, or by enacting rules to determine when and how neighboring chains become "entangled" and new slip-links are added[17,22,23]. In addition, slip-link models are computationally much more demanding than tube models. In fact, for star molecules, which relax very slowly, most slip-link models can only simulate molecules with only 5 or 10 entanglements per branch[24], although a recent more coarse-grained slip-link model by Schieber and coworkers, the Clustered Fixed Slip-link Model[25] (CFSM), can simulate stars with 19 or more entanglements, as is the case for the star studied in this work. Recent implementation of a GPU algorithm[26] for simulations using the slip-link model will increase the model's capabilities further still.

To progress further, it is important to obtain additional high quality data for well-entangled blends of monodisperse star and monodisperse linear polymers, and to compare these data against the most advanced tube and slip-link models. To make the blends more accessible to analysis by slip-link models, it is important that the star arms be reasonably short, while remaining well entangled.

In this chapter, we therefore, describe the synthesis and characterization of a monodisperse 1,4-polybutadiene star of arm molecular weight around 24,000 g/mol. Since the rheological data obtained from this material are intended to be used to test models, and since star polymers are extremely sensitive to impurities, especially of linear contaminants, this star is characterized by both size exclusion chromatography (SEC) and temperature gradient interaction chromatography (TGIC). Even if some fraction of the molecules lack an arm, or have an excess arm, there will be little effect on the rheology given that the star contains four arms. In fact, it is now well established that the rheology of star polymers is mainly sensitive to the arm molecular weight, as opposed to the number of arms[27]. The relatively modest molecular weight of this star polymer makes it amenable to analysis using slip-link models, especially when blended with linear polymer. In order to prepare well-controlled blends, a linear 1,4-polybutadiene polymer of molecular weight 58,000 g/mol is acquired commercially and characterized rheologically to

ensure its quality. The rheological measurements on the pure star and pure linear polymers are carried out on two rheometers, one of which is equipped with a low-temperature fixture so that high-frequency data can be obtained by time-temperature superposition (TTS). The experiments are performed at low temperatures for three reasons: i) to ensure that rheological data for the two materials superpose in the high-frequency regime; ii) to ensure that the material remains chemically stable during the rheological measurements; and iii) to confirm the established value of the "equilibration time" for 1,4-polybutadiene.

Mixtures of these star and linear materials, forming "PBd24KS-58KL" blends, are then also studied rheologically, and the data used to test two modern tube theories for linear viscoelastic properties, namely the "Hierarchical 3.0" model by Wang *et al.*[9] and BoB (branch-on-branch) model by Das *et al.*[6]. Both models have previously been shown to be successful in quantitatively describing the rheological properties of a range of polymers, including "combs", hyperbranched polymers, and commercial polyolefins made by single-site metallocene catalysis, but were not able to describe accurately the rheology of the PBd42KS-100KL blends. However, the PBd42KS-100KL is not amenable to analysis by slip-link models at present, because of the large number of entanglements in the star polymer. Our aim here is to see how well both the tube model and the slip-link model can predict the rheology of a star-linear blend. The PBd24KS-58KL blends are ideal for this purpose, given the development of a relatively fast slip-link model, the Clustered Fixed Slip-link Model (CFSM) slip-link model proposed recently by Schieber and coworkers[25].

The chapter is outlined as follows. Section 5.3 describes the detailed synthesis and TGIC characterization of the pure 4-arm star 1,4-PBd of arm molecular weight 24,000 g/mol and the preparation of its blend with a linear 1,4-PBd of molecular weight 58,000 g/mol along with their experimental rheology characterization. In Section 5.4, we describe the tube model theory and the slip-link simulations. In Section 5.5, we present and discuss experimental rheological measurements, and compare and contrast the massive failure we observe of the tube theories to predict the star/linear rheological data with the successful predictions of the slip-link. Conclusions and perspectives are presented in Section 5.6.

5.3. Materials and experimental methods

5.3.1. Materials and blends preparation

Two 1,4-polybutadienes, namely a linear and a star sample, as well as their blends, were used in this study. The linear 1,4-PBd was purchased from Polymer Source, Inc. Its number average molecular weight and molecular weight distribution were reported by Polymer Source to be 58,000 g/mol and 1.03, respectively, and its chemical composition of cis-1,4, trans-1,4, and 1,2-vinyl was given as 68%, 27%, and 5%, respectively. We refer to the linear sample as '58KL'. A four-arm symmetric 1,4-PBd star was synthesized as described in detail in the following section. Its arm number-average molecular weight and molecular weight distribution are 24,000 g/mol and 1.04, respectively and we refer to it as '24KS'. The molecular characteristics of the symmetric 4-arm star sample are given in Table 1. 1,4-PBd star/linear blends were prepared at star weight fractions 80%, 60%, 40%, 20% and 10%. Weighed amounts of linear and star melts were dissolved in excess dichloromethane (sourced from Sigma Aldrich). The solvent was initially allowed to evaporate from the sample at atmospheric pressure in a fume hood for about a week and then the sample was transferred to a vacuum chamber held at room temperature for another two weeks or more to ensure complete removal of excess dichloromethane. The blends were checked for remaining solvent via smell after drying under vacuum, and the weight of the samples was monitored over three days to ensure complete solvent removal and to produce the final star/ linear melt blends with desired compositions. After vacuum drying, the blends were stored in the freezer prior to rheological measurements.

5.3.1.1. Synthesis and purification[1]

1,3-Butadiene (Bd) (Aldrich, 99%), benzene (Aldrich, 99.8%), and methanol (terminating agent, Aldrich, 99%) were purified according to experimental techniques common in high-vacuum anionic polymerization[28-31]. 1,2-Bis(methyldichlorosilyl)ethane (BMDCSE) (linking agent, Gelest, 95%) was distilled several times over CaH_2 on a vacuum line. *s*-Butyllithium (*s*-BuLi, 1.4 M in cyclohexane, Aldrich) was used without purification and was diluted with dry *n*-hexane. The diluted reagents were stored at –30 °C in ampules equipped with break-seals before use. The polymerization and linking reaction were performed under high vacuum condition in the sealed all-glass reactors equipped with break-seals. The reactors were pre-washed with *n*-BuLi solution after sealing off from the vacuum line.

[1]Beom-Goo Kang from Jimmy May's group at the University of Tennessee performed the synthesis and purification of 24KS. The corresponding sections in this chapter were also prepared by him. Priyanka Desai acknowledges his contributions.

5.3.1.2. Synthesis of living PBd

The polymerization of Bd (12 g, 222 mmol) was performed using *s*-BuLi (0.55 mmol) in benzene at room temperature for 24 h (Scheme 5.1(a)). Then, a small portion of living PBdLi was sampled by heat-sealing the constriction for characterization. The rest of living polymer solution was subsequently gathered in a pre-calibrated ampule equipped with break-seals for the linking reaction with BMDCSE. The resulting PBd was characterized by SEC, giving PBd (M_n(obsd) = 24 kg/mol, M_w/M_n = 1.04 (Table 5.1)).

5.3.1.3. Synthesis of 4-arm star PBd (24KS)

The linking reaction of a benzene solution of living PBd (24 kg/mol, 0.5 mmol) with the linking agent BMDCSE (0.11 mmol) was performed in benzene (500 mL) at room temperature for 3 weeks with rigorous stirring to form well-defined 4-arm star PBd. The reaction was monitored by sampling a small amount of reaction solution via constrictions for SEC characterization. After terminating the linking solution with degassed methanol, the polymer solution was stabilized with butylated hydroxytoluene (BHT) and then poured into a large excess of methanol to precipitate the polymers. The fractional precipitation was repeated using toluene/MeOH to isolate highly pure 4-arm star PBd. The fractionated star polymer was further precipitated in methanol and dried under high vacuum condition for characterization. The resulting 4-arm star PBd was characterized by SEC, giving 24KS (M_n(obsd) = 97 kg/mol, M_w/M_n = 1.05 (Table 5.1)).

5.3.2. SEC and TGIC characterization[2]

5.3.2.1. Size exclusion chromatography (SEC)

Size exclusion chromatography/two-angle laser light scattering (SEC-TALLS) connected with a refractive index (RI) detector and Viscotek differential viscometer was used to characterize the star arm, PBd, and 4-arm star PBd, 24KS. Tetrahydrofuran (THF) was used as the mobile phase at a flow rate of 1.0 mL/min at 40 °C. This system features a Waters 1525 high-

[2] Sanghoon Lee from Taihyun Chang's group at Pohang University of Science and Technology, Korea performed TGIC characterization on 24KS and prepared the corresponding TGIC characterization section in this chapter. Beom-Goo Kang from Jimmy May's group at the University of Tennessee performed SEC characterization. Priyanka Desai acknowledges their contributions.

pressure pump, Waters Ultrastyragel columns (HR-2, HR-4, HR-5E, HR-5E, and HR-6E with pore sizes 10^3, 10^4, and 10^5 Å), a Waters 2410 differential refractometer detector (at 680 nm), a Precision Detectors PD-2040 two-angle (15°, 90°) light scattering detector, and a Viscotek differential viscometer. The Precision Detectors software "Discovery 32" was utilized to calculate the M_w values from SEC-TALLS data. The refractive index increment (dn/dc) value was measured on a Wyatt Optilab DSP detector at a wavelength of 690 nm and temperature of 40 °C in THF. After dn/dc was measured for five different concentrations of each sample, the average value 0.130 mL/g was used.

5.3.2.2. Temperature gradient interaction chromatography (TGIC)

TGIC is an HPLC technique controlling the interaction strength of the analytes with the stationary phase by changing the temperature of the column[32,33]. TGIC experiments were carried out with a typical HPLC system equipped with a C18 bonded silica column (Nucleosil C18, 250 × 4.6 (i.d.) mm, 500 Å, 7 μm particle size). The eluent was 1,4-dioxane (Samchun, HPLC grade) at a flow rate of 0.4 mL/min. The temperature of the column was controlled by circulating a fluid from a programmable bath/circulator (Thermo-Haake, C26P) through a homemade column jacket. All TGIC analyses were done with a linear temperature gradient from 15 to 30 °C in 60 min (0.25 °C/min). Sample solutions in 1,4–dioxane (~3 mg/mL, dn/dc = 0.104 mL/g) were prepared by dissolving the polymers in a small volume of the eluting solvent and the injection volume was 100 μL[34]. The TGIC chromatograms were recorded with a differential refractometer (RI) detector (Shodex, RI-101) and a light scattering (LS) detector (Wyatt, miniDawn).

5.3.3. Synthesis of 4-arm star PBd (24KS), SEC and TGIC characterization results

5.3.3.1. Synthesis of 4-arm star PBd (24KS)

Scheme 5.1 shows the synthetic strategy to prepare the 4-arm star PBd. The polymerization of Bd was first performed using *s*-BuLi in benzene under high vacuum (Scheme 5.1(a)). The colorless polymerization solution was maintained at room temperature for 24 h. After completion of the polymerization, the living PBd solution was collected in a pre-calibrated ampule equipped with break-seals for the subsequent linking reaction with chlorosilane derivative (BMDCSE). The polymerization results shown in Scheme 5.1 and Table 5.1 suggest that well-defined PBd was synthesized, as expected. The observed M_n value agrees well with

predicted one based on monomer to initiator ratios and the SEC curve of PBd shows a unimodal shape with narrow M_w/M_n (Figure 5.2(a)).

The synthesis of 24KS was performed by the reaction of excess living PBd with linking agent BMDCSE in the glass reactor sealed off from the vacuum line. In this procedure, it should be noted that careful purification of BMDCSE by repeated distillations on a vacuum line is necessary to obtain a highly pure linking agent, which is the key factor for synthesis of the desired 24KS. The living PBd was added to BMDCSE solution in benzene and the linking reaction was maintained at room temperature with rigorous stirring. The reaction was then monitored by removing small aliquots, followed by SEC analysis. The reaction was considered complete when the SEC peak of PBd used in excess did not change (Figure 5.2(b)). Highly pure 24KS was isolated by fractional precipitation using toluene/MeOH, as was confirmed by SEC analysis (Figure 5.2(c)). Although the controlled M_n and narrow M_w/M_n of 24KS suggest that a well-defined 4-arm star PBd was obtained under the reaction conditions employed in this study (Table 5.1), SEC is not able to distinguish impurities caused by incomplete or excess linkage of arms to the linking agent. We therefore also characterize the sample by temperature gradient interaction chromatography (TGIC), which is able to detect such impurities, as discussed below.

5.3.3.2. Characterization of 4-arm star PBd (24KS) by TGIC

TGIC is known to separate polymers according to their molecular weight (MW) while SEC separates them according to the hydrodynamic size[32]. In addition, TGIC shows much higher resolution than SEC in resolving the branched polymers prepared by anionic polymerization according to their MW[35-37]. Therefore, we employed TGIC to further characterize the 24KS sample since rheological properties are very sensitive to the chain branching and TGIC can resolve the star-shaped polymers far better than can SEC[38,39].

Figure 5.3 shows TGIC chromatogram of 24KS. It was recorded by an RI detector (Δn) and LS detector at 90^o scattering angle (R_{90}) to measure the absolute MW. The peak MW (M_p) of 24KS was measured to be 89 kg/mol, which agrees reasonably well with the value determined by SEC-TALLS, which was 97 kg/mol and the PBd did not elute as a narrow single peak. 24KS shows a main peak eluting out at 30–35 min and a large fronting shoulder eluting out at 25–30 min (Figure 5.3). The shape of the peak indicates that 24KS contains a significant amount of

byproduct eluting in its shoulder, but it appears quite uniform in MW judging from the well-overlapped RI and LS signals. Such an overlap of concentration and LS signals is a good indication of very narrow MW distribution[39]. A possible explanation of the peculiar behavior is that the polymers eluting in the fronting shoulder are the same in molecular weight as those in the main peak, but contain a functionality which is repulsively interacting with the C18 stationary phase[40].

The linking agent, BMDCSE, can undergo hydrolysis/oligomerization during the storage to become a linker with more than 4 chlorosilyl groups. The oligomerized BMDCSE could result in byproducts of stars with more than 4-arms and/or additional functionality such as hydroxy group(s). The high MW species (stars with more than 4-arms) were well removed by the fractional precipitation, but 4-arm star PBd with additional functionality remains and might be detected in the TGIC analysis[41]. This scenario is supported by the TGIC chromatogram of 24KS shown in Figure 5.3. In the chromatogram, a trace of high MW species was found after the main peak. The amount is almost negligible, but certainly higher than the noise level. The values of Mw given by SEC-TALLS and TGIC are 97 kg/mol and 89 kg/mol, respectively, both of which are within experimental error of the target molecular weight of 24,000 g/mol per arm, or 96,000 g/mol for the whole polymer.

5.3.4. Rheology experiments

Dynamic storage, G' and loss, G" moduli for the star/linear PBD blend samples were measured in small-amplitude oscillatory shear flow using the strain-controlled ARES-LS rheometer with an 8mm diameter parallel plate and at a sample gap of 1 mm. Dynamic strain sweep measurements were first conducted to select the strains in the range of linear regime. Dynamic frequency sweeps at a selected linear strain percent were conducted at a constant temperature of 25°C at frequencies ranging from 0.01 to 100 rad/s. In order to ensure sample stability, a gaseous nitrogen atmosphere was used. For the case of pure star, 24KS, and pure linear 58KL samples, linear viscoelastic oscillatory shear tests were repeated on another rheometer, the Rheometrics Mechanical Spectrometer RMS-800, using an 8mm parallel plate geometry at frequencies ranging from 0.1 to 100 rad/s and temperatures from +25°C to -80 °C under a liquid nitrogen blanket. Linear viscoelastic G' and G" curves from oscillatory experiments at various low temperatures were then horizontally shifted using the time-

temperature superposition (TTS) software on the rheometer using a two-dimensional residual minimization technique to form a master curve at a reference temperature of +25°C. From this, the WLF shift factors $a_T(T)$ were obtained at multiple measurement temperatures for both 24KS and 58KL samples.

5.4. Theory, modeling and simulations

5.4.1. Tube models

We test constraint release dynamics using two coarse-grained mean-field tube models that were developed for predicting the linear rheology of general mixtures of branched polymers. The first is the Hierarchical 3.0 model by Wang *et al.*[9] and the second is the BoB (branch-on-branch) model by Das *et al*.[6]. Even though both models are based on similar hierarchical relaxation mechanisms and treatment of constraint release dynamics, they differ in their computational algorithms and implementation, a detailed comparison of which is presented in Wang *et al.*[9].

The predictions are carried out using two sets of parameter values summarized in Table 2. The so-called "Park" values, from the work of Park *et al.*[8] and Wang *et al.*[9], are used as input parameters for the Hierarchical model and the "Das" values, from Das *et al*.[6], are used with the BoB model. In both of the models, the two most important material dependent parameters, the plateau modulus G_N^0 and the entanglement molecular weight M_e, are related to each other by the definition . $M_e = 4/5 \times \rho RT / G_N^0$ Another fundamental tube model parameter, τ_e, the equilibration time or Rouse relaxation time of a chain containing one entanglement, was obtained by adjusting its value to best fit the low frequency data in both the models. By fitting the Rouse model to the high-frequency transition linear viscoelastic data for a series of 1,4-PBd samples, Park *et al.*[42] recently determined the value of τ_e and its uncertainty as (3.7 ± 0.93) × 10^{-7} s at T = 25 °C for 1,4-PBd, and both the Park and Das values for τ_e lie within these limits. Perhaps the best-known difference between both these parameter sets is in the value of the so-called "dilution exponent" α, which controls the rate at which the tube expands its diameter as polymer chains relax[43]. Details describing the tube dilation process can be found in Milner and McLeish[44]. Two different theoretical concepts, one that focuses on entanglements as pair-wise interactions

between chains and the other one treating entanglements as a collective phenomenon,[45] give the two values $\alpha = 1$ and $\alpha = 4/3$ that are used in the Das and Park parameter sets, respectively. While these two values are similar, they are exponents on a quantity that is itself inside an exponential function, and therefore a small difference between them has a big impact on predictions.

The Hierarchical model gives the user the freedom to choose between three different arm retraction algorithms, wherein the arm contained within the tube may relax by retraction while the confining tube itself undergoes CR-rouse motion. These options are the following. 1) No arm retraction - arm retraction is not allowed or is "frozen" during tube dilation. 2) Arm retraction in the 'thin' tube – arm retraction occurs in the thin tube whose diameter is defined by the un-relaxed volume fraction, ϕ just before the onset of CR-Rouse motion. 3) Arm retraction in the 'fat' tube – the arm retracts in a "fat" tube whose diameter is set by $\phi_{ST}(t)$, which is the fraction of original entanglements that define the tube that the arm is able to explore by constraint release during a time t. Details regarding these options are given in Wang *et al.*[9]. Here we test the "thin tube" and the "fat tube" as well as the "arm frozen option" in the Hierarchical model and results are discussed below. The BoB model, on the other hand, does not give these options and arm retraction proceeds in the 'thin' tube, which is the same as option 2 in the Hierarchical model.

5.4.2. Slip-link predictions[3]

5.4.2.1. The discrete slip-link model

The discrete slip-link model (DSM) is a single-chain mean-field model for entanglement-dominated polymer dynamics proposed by Schieber *et al.*[22,46,47]. The model has been shown to be consistent with thermodynamics[48]. With just three parameters - the molecular weight of a Kuhn step, M_K, the "entanglement activity," β, and the Kuhn step frictional time, τ_K - the DSM is able to predict simultaneously both nonlinear rheology and the linear viscoelasticity and dielectric relaxation of monodisperse linear, polydisperse linear and branched polymers[11,21,49,50] and cross-linked networks[19,51]. Recently, a hierarchy of mathematically well-defined slip-link models was

[3]Maria Katzarova from Jay Schieber's group at Illinois Institute of Technology carried out the slip-link predictions for pure components and prepared the corresponding Slip-link simulations sections in this chapter. Priyanka Desai acknowledges her contributions.

developed[18,51,52], all but one of whose parameters can be obtained from atomistic simulations. Moreover, the most coarse-grained member of the hierarchy, the CFSM, has only two parameters which can be estimated from the low-frequency crossover, (ω_x, G_x), of the dynamic modulus, G^*, of linear monodisperse chains[53]. Here, the DSM is applied to 1,4-polybutadiene blends of star-branched and linear polymer chains.

In the DSM, polymer chains are described by random walk statistics. This is expected to hold for polymeric chains with contour length and entanglement spacing larger than several Kuhn steps. By assuming that the chain relaxation is slower than the relaxation of a strand between entanglements, the chains are then further coarse-grained to the primitive path defined by the entanglements. The entanglements are randomly distributed along the chain with uniform probability $1/(1+\beta)$, where $\beta = e^{-\mu^E/k_BT}$, μ^E is the "entanglement activity." is the chemical potential conjugate to the entanglement number and k_B is the Boltzmann constant. The entanglement activity of the surrounding chains sets the average entanglement density, but allows fluctuations in the number of entanglements on the probe chain.

The probe chain is subject to two dynamic processes: sliding dynamics (SD) and constraint dynamics (CD). In SD, Kuhn steps shuffle through slip-links with a characteristic time τ_K. This Kuhn step shuffling between entangled strands is due to Brownian forces and free energy differences. When this process occurs at the ends of a linear chain, or at the free end of a star-branched chain, entanglements can be destroyed or created. The probability of creating an entanglement at the end of the chain is connected with the destruction process through detailed balance. CD is the creation and destruction of entanglements due to SD of the surrounding invisible matrix chains. CD is implemented self-consistently with SD, as described in detail elsewhere[25]. Destruction and creation of entanglements by CD occurs anywhere along the chain. For the star-branched chains, entanglements can be created and destroyed by SD only at the free ends of the star arms and by CD anywhere along the chain[24]. For the linear chains, entanglements are created and destroyed by SD on both ends of the chain and by CD anywhere along the chain.

The characteristic lifetime of the i^{th} entanglement, τ_i^{CD}, is introduced to implement a mean-field self-consistent realization with independent chains in the ensemble. The lifetimes, τ_i^{CD}, are chosen from the distribution of lifetimes, $p^{CD}(\tau_i^{CD})$. This distribution is determined self-

consistently from destruction of entanglements by SD. The p^{CD} for the blends considered in this work is given by

$$p^{CD}(\tau^{CD}) = w_{sb}p_{sb}^{CD}(\tau^{CD}) + w_{lc}p_{lc}^{CD}(\tau^{CD}) \quad (1)$$

where *w* is the weight fraction, and the sub-indexes, sb and lc stand for star-branched and linear chains, respectively. Therefore, in the DSM, each component of the blend is modeled in a self-consistent realization with independent chains in the ensemble. The effect of other chains is given by the self-consistent mean-field defined in Eq. (1). In other words, in the DSM, each component of the blend, with different architectures, can be realized independently while the effect of other architectures is given by the constraint dynamics mean-field.

The DSM is a well-defined mathematical model in which the probability density of chain conformations evolves in time according to a differential Chapman-Kolmogorov equation[17]. To perform calculations of dynamic observables, a probe chain or an ensemble of independent probe chains is evolved in time using a numerical algorithm[26]. The stress tensor is calculated from the simulated chain conformations using an expression derivable from a virtual work argument[48]. Two types of rheological calculations can be performed, equilibrium (or Green-Kubo) calculations in which the rate of deformation tensor is set to zero and the autocorrelation function of stress at equilibrium is followed; or flow calculations in which a specific flow field is applied and the stress as a function of time is recorded.

Using the blend $p^{CD}(\tau^{CD})$, the relaxation modulus for each probe chain in the blend is calculated with a Green-Kubo simulation. The relaxation modulus of the blend, *G(t)*, is expressed in terms of the relaxation modulus of each of the components in the blend as,

$$G(t) = w_{sb}G_{sb}(t) + w_{lc}G_{lc}(t) \quad (2)$$

Universality observed in experimental data suggests that the shape of the dynamic modulus of linear, monodisperse, entangled polymers is mostly determined by one parameter, namely the average number of entanglements. This universality has been exploited in predictions of the DSM, which resulted in the development of the Clustered Fixed Slip-link Model (CFSM)[25], a less detailed level of description than the DSM, that provides a mapping of β and N_K , the number of Kuhn steps, to one parameter, N_c, the number of clusters. The CFSM is simply the DSM with $\beta = 1$ and making the following substitutions in the original model:

$$M_{\mathrm{K}} \rightarrow M_{\mathrm{c}} \approx 0.56(\beta+1)M_{\mathrm{K}} \quad (3)$$

$$\tau_K \rightarrow \tau_{\mathrm{c}} \approx 0.265\tau_{\mathrm{K}}\beta^{8/3} \quad (4)$$

where $M_{\mathrm{K}} = M_W/N_{\mathrm{K}}$, $M_{\mathrm{c}} = M_W/N_{\mathrm{c}}$ is the molecular weight of a cluster, τ_{c} is a cluster-shuffling characteristic time and M_W is the molecular weight of a chain. The CFSM can describe well both equilibrium viscoelasticity and shear flow for linear and star-branched polymer melts[25]. The CFSM predictions are nearly identical to those of the DSM and it offers significant computational savings.

5.5. Results and discussion

5.5.1. Tube model predictions

5.5.1.1. Dynamic modulus predictions of the star/linear blends

Figure 5.4 shows the WLF shift factors, $a_T(T)$, obtained from shifting the experimental linear viscoelastic G', G" curves obtained at various low temperatures to the same reference temperature of 25°C using TTS for both the star, 24KS and the linear, 58KL samples. The shift factors for the star and linear 1,4-PBd samples are very similar near the reference temperature, but differ increasingly with decreasing temperature, especially below -50°C as seen. This variation in the shift factors at low temperatures can be attributed to a slight difference in the 1,2 content values for the star and linear samples and are well within the limits obtained for 1,4-PBds with 1,2 content ranging between 5 to 11% as recently shown by Park *et al.*[42]. Additionally, the shifted G' and G" curves for both the 24KS and 58KL samples show good agreement in their high frequency G' and G" crossover and superpose very well in the high frequency region as shown in Figure 5.5, indicating successful time-temperature superposition.

Figure 5.5 features linear viscoelastic G', G" relaxation master curves at a reference temperature of 25°C obtained using TTS for pure monodisperse star, 24KS and linear, 58KL samples. The tube model predictions, from the Hierarchical 3.0 model, which are represented as solid (G') and dash (G") lines, are in good agreement with the experimental data, where for the star, we assume an arm molecular weight of 24 kg/mol rather than the TGIC peak molecular weight of 89,000/4 = 22.25 kg/mol. The molecular weight 24 kg/mol is within experimental error of 22.25 kg/mol, and gives slightly better agreement with the experimental rheology than does

22.25 kg/mol. Given the demonstrated good success of the tube model in predicting pure star rheology for 1,4-PBd, we believe that the value of 24 kg/mol per arm for the star polymer is accurate. The molecular weight of the linear polymer was taken to be the value provided by the supplier, 58 kg/mol. These molecular weights were held fixed in all calculations that follow. The good agreement between theory and experiment for pure star and pure linear is not a surprise because various versions of the tube model have done well in predicting monodisperse linear and star polymers[9].

While the tube model works well for pure 24KS star and for pure 58KL linear polymers with the same model parameters, the model breaks down badly for binary blends of the two, as shown in Figure 5.6. As can be seen in the G' curves (Figure 5.6A), for the cases with star fractions ϕ_s - 0.6, 0.4, 0.2, 0.1, the model predicts a much slower decay in G' in the low frequency region than is shown in the experimental data. Furthermore, this terminal behavior in G' is slower than even the pure 100% star component. The discrepancy between the experiments and theory is less pronounced in the G" predictions shown in B in Figure 5.6. The insert in Figure 5.6B shows the non-monotonic variation in terminal relaxation time, τ_d as a function of the star volume fraction, ϕ_s, extracted from Hierarchical model predictions for the same set of data shown in Figure 5.6. This massive disagreement between model predictions and experimental data is much larger than shown in the earlier studies of 42KS/100KL 1,4-polybutadiene blends, as shown in Figure 5.1, where the tube model at least predicted a monotonic dependence of the terminal relaxation behavior on star volume fraction.

This failure of the tube model is related to its inability to capture constraint release properly as a combination of CR-Rouse relaxation and tube dilation. In an attempt to "fix" the model predictions, we activate a "disentanglement relaxation threshold" that allows the star arm to completely relax when the tube in which it fluctuates has dilated to the point that it has only 3 remaining entanglements, which is an entanglement density at which a transition to strong entanglement effects typically occurs. A discussion of this disentanglement relaxation mechanism can be found in Wang *et al.*[9]. For consistency, the disentanglement threshold, discussed above, is also applied to the linear components. In the blends studied here, the linear chains are quite short and for the case shown in Figure 5.7 where the star volume fractions are

very low, the linear chains make up the majority of the system. Once they reach the disentanglement threshold of 3 entanglements, they are allowed to relax their stress even before they reach their reptation time. Once the linear chains are fully relaxed, they dilate the tube containing the star arms, allowing them to retract faster and quickly reach their disentanglement relaxation threshold of 3 entanglements and also relax. This leads to G' predictions for $S_{a,\min} = 3$ that are even lower than the experiments, for the four cases considered here. While this might be corrected by either applying the disentanglement mechanism only to the star polymers, or by changing the value of the threshold to a lower value, $S_{a,\min} = 1$ as done by Larson[7], such manipulations would be arbitrary.

According to tube theory, after the linear chains relax, the remaining unrelaxed star arms explore a widening tube called the "supertube", by constraint-release Rouse (CR-Rouse) motion. The Hierarchical model allows different options for the choice of the diameter of the confining tube in which the star arm retracts in the CR-Rouse regime. The arm can undergo retraction in the *thin* tube whose diameter is set by the un-relaxed volume fraction ϕ of all chains, including the linear ones, just before the onset of CR-Rouse, relaxation. Alternatively, arm retraction can take place in the *fat* tube (or supertube) whose diameter is set by ϕ_{ST} and is continuously evolving within the CR-Rouse regime. Or the arm can be assumed not to retract at all during period of supertube exploration, which is the so-called "arm frozen" assumption initially invoked by Milner and McLeish. Figure 5.8A shows that for the same four blends considered in Figure 5.7, the model over predicts the data if the star arm is allowed to relax within the thin tube (solid lines). However, when the star arm is allowed to relax in the fat tube (dashed lines), the modulus decreases rather quickly and is closer to the experimental data, although still not matching the data well. Figure 5.8B shows increasingly worse predictions as the star volume fraction decreases when the arm is 'frozen' or not allowed to retract at all during the CR-Rouse regime. The results in Figure 5.8B show that while the ad hoc "arm frozen" assumption seems to have yielded good predictions for the set of star/linear blends studied by Milner and McLeish, it does not provide consistently accurate predictions.

To investigate a different version of the tube model, the BoB model was tested using the Das parameters normally used for this model. As can be seen in Figure 5.9, the BoB model

predicts the rheology of blends with star fractions $\phi_s \geq 0.6$ better than the Hierarchical model, but predictions for all other blends are just as poor. Interestingly, unlike the Hierarchical model, the BoB model is unable to predict the pure linear 58KL correctly.

5.5.2. DSM slip-link simulations

5.5.2.1. Determination of the DSM parameters for PBd

Using the procedure described by Katzarova *et al.*[53], the two CFSM parameters, τ_c= 0.15μs and M_c = 618Da, were obtained by matching the CFSM G^* analytic expressions to the low-frequency crossover (ω_x, G_x) of the linear monodisperse G^* experimental data in Figure 5.10. Both of these values are architecture and molecular weight independent. The DSM parameters for PBd, β = 9.6 and τ_K = 1.3ns, which are needed to add the Rouse dynamics, were estimated using the scaling relations given in Equations 3 and 4, respectively. A comparison between the prediction using this procedure and experimental data for 58L at T = 25°C is shown in Figure 5.10. For PBd, M_K = 103.9 Da[54]. The resulting value for the number of clusters is N_c^{lc} = 94. Without further adjustments, these parameters were used for the prediction of the symmetric 4-arm PBd star, 24KS. Predictions with β = 1 were done with coarse-grained parameters N_c^{sb} /arm = 39. The resulting prediction is shown in Figure 5.10B and agrees well in the region of frequencies measured. For both the star and linear chains, the entanglement plateau can be observed at high frequencies. Note that the crossover frequency for the star, which is a rough indicator of the longest relaxation time, occurs at lower frequencies than that for the linear chains since the star chains cannot relax by SD at the branch point.

5.5.2.2. Dynamic moduli predictions for star/linear blends

Using the model parameters found in the previous section, for the pure components, the self-consistent CD mean field can be constructed according to Eq. (1). Then, each type of chain in the ensemble (irrespective of architecture and molecular weight) can be simulated independently using this blend p^{CD} field, Eq. (1). The relaxation modulus for the blend of star and linear chains is then constructed by performing a weighted average, Eq. (2), of the relaxation moduli of each architecture. The parameters, M_c and τ_c, are architecture independent. Therefore,

for consistent predictions, the parameters obtained for linear chains were used for the predictions of star/linear blends of 24KS-58KL chains at a reference temperature, T = 25°C. The dynamic modulus is then obtained by transforming the relaxation modulus to the frequency domain analytically[53]. The resulting storage moduli, G', for each of the different blends as well as 100% star and 100% linear systems are shown in Figure 5.11A and the corresponding loss moduli, G" are shown in Figure 5.11B.

The CFSM gives considerably improved predictions for bidisperse 24KS-58KL blends over any of the available tube (Hierarchical and BoB) models, as shown in Figure 5.11. This success may be due to the fact that the CFSM models polymer chain dynamics at a more detailed level than do tube models. Instead of tracking specific constraint release mechanisms and longitudinal motions, the CFSM only tracks the primitive path and fluctuating monomer densities. All CD mechanisms arise naturally, once binary interactions are assumed. As mentioned previously, the model first tracks the movement of Kuhn segments through entanglements without constraint release. The dynamics obtained are then used to construct the constraint release rate which is used in a second simulation of the sliding dynamics. In this way, the CFSM captures constraint release at a level of detail that eludes the current tube models. We note here that an alternative slip link model, the "slip-spring" model of Likhtman and coworkers[14], accounts for constraint release in a single simulation by explicitly pairing a partner matrix chain and one of its slip links to each slip link on the "test" chain, so that the slip link on the test chains disappears if either the test chain slides through its slip link, or the partner chain slides through its paired slip link. This "slip-spring" model[14] was able to predict successfully the linear rheology of the PBd24.5KS-6.5KL star/linear data set discussed early. It would be of interest to apply the CFSM to this data set to see if it is as successful in predicting as is the slip-spring model, and, vice versa, to apply the slip-spring model to our new PBd24KS-58KL data set. If both slip spring models can predict both data sets well, this would suggest that the differences in how these slip spring models handle constraint release matter little, and would show that slip link models possess a robustness in this respect that is lacking from current tube models. In addition, by using the CFSM or slip-spring model to investigate the molecular physics of constraint release in detail, it might be possible to gain an improved understanding that might be captured in a tube model.

5.5.3. Inspection of entanglement volume fractions in the tube model

For the star-linear blends, if the volume fraction of stars is lower than around 20%, both the Hierarchical and BoB models, using the "thin tube" assumption (and not activating disentanglement) predict stress relaxation that is much slower than that observed in experiments. The reason is that that once the short linear chains are relaxed by reptation, there is a sudden drop of the un-relaxed volume fraction ϕ (by about 90%) and the system enters the supertube relaxation regime in which the star relaxes by the CR-Rouse motion of the thin confining tube, and ϕ_{ST} follows a power law $\phi_{ST} \propto t^{-1/2\alpha}$. Only when ϕ_{ST} drops below ϕ is the CR-Rouse relaxation process deactivated. Since for small star volume fractions, ϕ is very low when the linear chains relax, it takes an extremely long time for ϕ_{ST} to drop down to ϕ, which leads to an artificially prolonged supertube regime. This results in the overestimation of the terminal stress relaxation time and to the long tail in G' for the blends as seen in Figure 5.9 for blends with $\phi_s \leq$ 0.2 and in Figure 5.6A for blends with $\phi_s \leq 0.6$.

The density of the remaining entanglements on the un-relaxed star arms after the linear chains have relaxed varies with star volume fraction. More specifically, the remaining number of entanglements are obtained by dividing the molecular weight of the star arm, M_a, by the entanglement molecular weight, M_e, and multiplying the resulting value by the total un-relaxed volume fraction, ϕ. For all the cases shown in Figure 5.12, the linear chains reach their reptation time at around t = 0.0145s and completely relax. For the case where the star volume fraction is relatively high for example, ϕ_s = 0.8 as shown in Figure 5.12B, the total un-relaxed volume fraction ϕ suddenly drops at t = 0.0145s from 0.536 to 0.417, a drop of only about 22%. For this case, since the density of remaining entanglements per arm is around 6 which is still considerable the star arm is still sufficiently entangled and ϕ_{ST} is able to catch up to ϕ in a reasonably short time during the CR-Rouse regime. Consequently, the storage modulus G' for this blend in Figure 5.6A does not relax slower than the pure star does. However, if the star volume fraction is dilute, for example, ϕ_s = 0.1 as shown in Figure 5.12E, the sudden drop at t = 0.015s in the total un-relaxed volume fraction ϕ is much appreciable, from a value of 0.591 down to only 0.053. The corresponding density of entanglements abruptly drops by about 91% and there are only about

0.8 surviving long-time entanglements on each star arm. For this low enough number of surviving entanglements, ϕ_{ST} never drops down to ϕ and this leads to a prolonged supertube regime. Consequently, the modulus relaxes very slowly as seen in Figure 5.6A. A similar trend is observed in Figure 5.12D, for star volume fraction, $\phi_s = 0.2$.

5.6. Conclusions and perspective

We have presented a detailed comparison of the linear rheology of carefully synthesized and characterized bidisperse star and linear blends, 24KS-58KL, with both the tube theory based on the Hierarchical and BoB models and with the recently developed CFSM slip-link model. While the predictions of the tube models agree in many cases with measured rheological properties for monodisperse linear, star, H, and other polymers, they fail badly for blends of a monodisperse star polymer with a monodisperse linear polymer. While earlier studies have shown that star/linear blends present problems for tube models, we find here that failure is extreme when the star volume fraction is low enough the star arms are sparsely self entangled and there are fewer than 3 entanglements per arm after the relaxation of linear chains.

This failure can be attributed to the inability of the tube models to describe constraint release events accurately in situations where rather abrupt relaxation of a portion of the entanglement network occurs by reptation of linear chains, but the remainder relaxes gradually by arm fluctuations. Tube models with several modifications were used to test the constraint release effects, including: 1) using two different sets of input parameters, namely, the Park ($\alpha=4/3$) and Das ($\alpha=1$) parameters, 2) performing arm retraction in both the *thin* and *fat* tubes in CR-Rouse motion, 3) including a disentanglement mechanism, 4) using two different computational models, namely, Hierarchical and BoB, that differ in their numerical implementations but that use the same basic relaxation mechanisms. None of these alternatives provided a quantitative description of the dynamics and rheology of the star/linear blend studied here

Finally, a slip-link model, the Clustered Fixed Slip-link Model (CFSM) proved to be highly successful in predicting the linear rheology of this star-linear blend. The slip-link model incorporates both sliding dynamics (SD) of individual chains through the entanglement mesh by reptation and contour length fluctuations, and constraint dynamics (CD), which captures both the

"dynamic dilution" and "constraint-release Rouse" mechanisms of the tube model in simple limiting cases and transcends these mechanisms in more complex situations.

Both the CSFM slip-link simulations and the Hierarchical tube models describe relaxation due to sliding dynamics (reptation and contour length fluctuations) of the "test" chain and constraint release due to motion of the matrix chains. In tube models, the sliding dynamics and constraint dynamics are accounted for using a mean-field relaxation function for each of these and then combining these to produce predictions of stress relaxation. In the CSFM there is a function $p^{CD}(\tau)$ for "sliding dynamics" which is a probability distribution for constraint release times. However, there is no attempt to decompose the stress relaxation into a combination of two functions; instead both constraint release and sliding dynamics are accounted for locally – at each entanglement point in the simulated melt. The DSM can be used to obtain separate relaxation functions for sliding dynamics and constraint dynamics, by turning off, respectively, the constraint dynamics, and the sliding dynamics, and computing the resulting relaxation modulus in each case. These modulus functions, each normalized by the zero-time modulus, can be multiplied together to obtain a normalized relaxation modulus, which can be compared to the modulus obtained from the full DSM theory. The idea is to determine if the DSM modulus can be represented as a simple product of moduli produced by sliding dynamics and constraint dynamics. This comparison has been carried out by Khaliullin and Schieber[11] and by Pilyugina *et al.*[24] and found to work reasonably well for bidisperse linear chains, but not for star-branched chains. For the star/linear blends studied here, we carried out analogous tests with the CSFM and find that the factorization fails progressively more severely as the concentration of star polymer increases (results not shown). While the tube models considered here involve computing products of functions describing sliding dynamics and constraint dynamics, even in these tube models the relaxation modulus of a star/linear blend is not a simple product of two such functions, because in the tube model constraint dynamics are described using both tube dilation and constraint release Rouse processes, whose relative importance depends on how rapidly constraint release occurs. In fact, the worst failures of the tube model are at the lowest non-zero fraction of star polymer, where factorization, using the DSM model, works best. For pure star or pure linear melts, both CSFM and tube models are successful in predicting linear rheology, and the tube models are not very sensitive to the details of how relaxation is treated during the constraint release Rouse process. For the star/linear blends, however, the sudden release of

entanglements that occurs when the linear chains relax while stars are largely un-relaxed exposes the deficiencies of how current tube models manage relaxation that is dominated by constraint release. As discussed, none of the assumptions about relaxation during the period after sudden relaxation of the linear chains give accurate predictions.

Given the much greater computational speed of tube models, however, it would be of great interest to see if there is a deeper understanding of constraint release that can be obtained from a careful interrogation of the CSFM, and use this to develop an improved tube model, or at least to determine the conditions under which tube models can be expected to be successful, and when they can't be. After all, tube models such as the Hierarchical model and the BoB model have successfully predicted the rheology of many polymer melts, including compositionally complex commercial melts[6,55]. Commercial polymers are invariably polydisperse, and it appears that the severe errors that occur when applying tube models to blends of monodisperse stars with monodisperse linear polymer are not nearly as severe for polymers with broad polydispersity. However, without either an improvement in the underlying description of constraint release in tube models, or at least a clear delineation of the conditions under which tube models will and will not work well, we must remain skeptical of their reliability.

5.7. References

1. de Gennes, P. G., "Reptation of a polymer chain in the presence of fixed obstacles," *J. Chem. Phys*. *55*, 572 (1971)
2. Doi, M., Edwards, S. F. *The theory of polymer dynamics,* 2nd ed.; Clarendon: Oxford (1988)
3. Viovy, J. L., Rubinstein, M., Colby, R. H., "Constraint release in polymer melts: tube reorganization versus tube dilation," *Macromolecules* 24, 3587 (1991)
4. Marrucci, G., "Relaxation by reptation and tube enlargement - a model for polydisperse polymers," *J. Polym. Sci., Polym. Phys. Ed.* 23, 159 (1985)
5. Milner, S. T., McLeish, T. C. B., Young, R. N., Hakiki, A., Johnson, J. M., "Dynamic dilution, constraint release, and star-linear blends," *Macromolecules* 31, 9345 (1998)
6. Das, C., Inkson, N. J., Read, D. J., Kelmanson, M. A., McLeish, T. C. B., "Computational linear rheology of generally branch-on-branch polymers," *J. Rheol.* 50, 207 (2006)
7. Larson, R. G., "Combinatorial rheology of branched polymer melts," *Macromolecules* 34, 4556 (2001)
8. Park, S. J., Shanbhag, S., Larson, R. G., "A hierarchical algorithm for predicting the linear viscoelastic properties of polymer melts with long-chain branching," *Rheol. Acta* 44, 319 (2005)
9. Wang, Z., Chen, X., Larson, R. G., "Comparing tube models for predicting the linear rheology of branched polymer melts," *J. Rheol.* 54, 223 (2010)
10. van Ruymbeke, E., Masubuchi, Y., Watanabe, H., "Effective value of the dynamic dilution exponent in bidisperse linear polymers: From 1 to 4/3," *Macromolecules* 45, 4, 2085 (2012)
11. Khaliullin, R. N., Schieber, J. D., "Application of the slip-link model to bidisperse systems," *Macromolecules* 43, 6202 (2010)
12. Watanabe, H., "Slow dynamics in homopolymer liquids," *Polym. J.* 41, 929 (2009)
13. Struglinski, M. J., Graessley, W. W., Fetters, L. J., "Effects of polydispersity on the linear viscoelastic properties of entangled polymers. 3. Experimental observations on binary mixtures of linear and star polybutadiene," *Macromolecules* 21, 783 (1988)
14. Shivokhin, M. E., van Ruymbeke, E., Bailly, C., Kouloumasis, D., Hadjichristidis N., Likhtman, A. E., "Understanding constraint release in star/linear polymer blends," *Macromolecules* 47, 2451 (2014)
15. Lee J. H., Archer L.A., "Stress relaxation of star/linear polymer blends," *Macromolecules* 35, 17 (2002)
16. Roovers, J., "Tube renewal in the relaxation of 4-arm star polybutadienes in linear polybutadienes," *Macromolecules* 20, 148 (1987)
17. Masubuchi, Y., "Simulating the flow of entangled polymers," *Annu. Rev. Chem. Bio. Eng.* 5, 11 (2014)
18. Schieber, J. D., Andreev, M., "Entangled polymer dynamics in equilibrium and flow modeled through slip links," *Annu. Rev. Chem. Bio. Eng.* 5, 367 (2014)
19. Jensen, M. K., Khaliullin, R., Schieber, J. D., "Self-consistent modeling of entangled network strands and linear dangling structures in a single strand mean-field slip-link model," *Rheol. Acta* 51, 21 (2012)
20. Khaliullin, R. N., Schieber, J. D., "Self-consistent modeling of constraint release in a single-chain mean-field slip-link model," *Macromolecules* 42, 7504 (2009)

21. Andreev, M., Khaliullin, R. N., Steenbakkers, R. J., Schieber, J. D., "Approximations of the discrete slip-link model and their effect on nonlinear rheology predictions," *J. Rheol.* 57, 535 (2013)
22. Schieber, J. D., "Fluctuations in entanglements of polymer liquids," *J. Chem. Phys.* 118, 5162 (2003)
23. Likhtman, A. E., "Single−chain slip−link model of entangled polymers: Simultaneous description of neutron spin−echo, rheology, and diffusion," *Macromolecules* 38, 14 (2005)
24. Pilyugina, E., Andreev, M., Schieber, J. D., "Dielectric relaxation as an independent examination of relaxation mechanisms in entangled polymers using the discrete slip-link model," *Macromolecules* 45, 5728 (2012)
25. Andreev, M., Feng, H., Yang, L., Schieber, J. D., "Universality and speedup in equilibrium and nonlinear rheology predictions of the fixed slip-link model," *J. Rheol.* 58, 723 (2014)
26. Andreev, M., Schieber, J. D., "Accessible and quantitative entangled polymer rheology predictions, suitable for complex flow calculations," *Macromolecules* 48, 5, 1606 (2015)
27. Pattamaprom, C., Larson, R. G., "Predicting the linear viscoelastic properties of monodisperse and polydisperse polystyrenes and polyethylenes," *Rheol Acta* 40, 516 (2001)
28. Hadjichristidis, N., Iatrou, H., Pispas, S., Pitsikalis, M., "Anionic polymerization: High vacuum techniques," *J. Polym. Sci., Part A: Polym. Chem.* 38, 3211 (2000)
29. Uhrig, D., Mays, J. W., "Experimental techniques in high-vacuum anionic polymerization," *J. Polym. Sci., Part A: Polym. Chem.* 43, 6179 (2005)
30. Rahman, M. S., Aggarwal, R., Larson, R. G., Dealy, J. M., Mays, J., "Synthesis and dilute solution properties of well−defined H−shaped polybutadienes," *Macromolecules* 41, 8225 (2008)
31. Rahman, M. S., Lee, H., Chen, X., Chang, T., Larson, R., Mays, J., "Model branched polymers: Synthesis and characterization of asymmetric H-shaped polybutadienes," *ACS Macro Lett.* 1, 537 (2012)
32. Chang, T., "Polymer characterization by interaction chromatography," *J. Polym. Sci., Part B: Polym. Phys.* 43, 1591 (2005)
33. Ryu, J., Chang, T., "Thermodynamic prediction of polymer retention in temperature-programmed HPLC," *Anal. Chem.* 77, 6347 (2005)
34. Lee, W., Park, S., Chang, T., "Liquid chromatography at the critical condition for polyisoprene using a single solvent," *Anal. Chem.* 73, 3884 (2001)
35. Lee, H. C., Lee, W., Chang, T., Yoon, J. S., Frater, D. J., Mays, J. W., "Linking reaction kinetics of star shaped polystyrene by temperature gradient interaction chromatography," *Macromolecules* 31, 4114 (1998)
36. Perny, S., Allgaier, J., Cho, D., Lee, W., Chang, T., "Synthesis and structural analysis of an H-shaped polybutadiene," *Macromolecules* 34, 5408 (2001)
37. Ratkanthwar, K., Hadjichristidis, N., Lee, S., Chang, T., Pudukulathan, Z., Vlassopoulos, D., "Synthesis and characterization of an exact comb polyisoprene with three branches having the middle branch twice the molecular weight of the other two identical external branches," *Polym. Chem.* 4, 5645 (2013)
38. Lee, H. C., Chang, T., Harville, S., Mays, J. W., "Characterization of linear and star polystyrene by temperature-gradient interaction chromatography with a light-scattering detector," *Macromolecules* 31, 690 (1998)
39. Chen, X., Rahman, S., Lee, H., Mays, J., Chang, T., Larson, R., "Combined synthesis, TGIC characterization, and rheological measurement and prediction of symmetric H polybutadienes

and their blends with linear and star-shaped polybutadienes," *Macromolecules* 44, 7799 (2011)
40. Im, K., Park, S., Cho, D., Chang, T., Lee, K., Choi, N., "HPLC and MALDI-TOF MS analysis of highly branched polystyrene: Resolution enhancement by branching," *Anal. Chem.* 76, 2638 (2004)
41. Kim, Y., Ahn, S., Chang, T., "Martin's rule for high-performance liquid chromatography retention of polystyrene oligomers," *Anal. Chem.* 81, 5902 (2009)
42. Park, S. J., Desai, P. S., Chen, X., Larson, R. G., "Universal relaxation behavior of entangled 1,4-polybutadiene melts in the transition frequency region," *Macromolecules* 48, 4122 (2015)
43. Colby, R. H., Rubinstein, M., "Two-parameter scaling for polymers in solvents," *Macromolecules* 23, 2753 (1990)
44. Milner, S. T., McLeish, T. C. B., "Parameter-free theory for stress relaxation in star polymer melts," *Macromolecules* 30, 2159 (1997)
45. Milner, S. T., "Predicting the tube diameter in melts and solutions," *Macromolecules* 38, 4929 (2005)
46. Neergaard, J., Schieber, J. D., "A full-chain network model with sliplinks and binary constraint release," *Proc. XIIIth Intl. Cong. Rheol.* (2000)
47. Schieber, J. D., Neergaard, J., Gupta, S., "A full-chain, temporary network model with sliplinks, chain-length fluctuations, chain connectivity and chain stretching," *J. Rheol.* 47, 213 (2003)
48. Schieber, J. D., "GENERIC compliance of a temporary network model with sliplinks, chain-length fluctuations, segment-connectivity and constraint release," *J. Non-Equilib. Thermodyn.* 28, 179 (2003)
49. Andreev, M., Feng, H., Yang, L., Schieber, J. D., "Universality and speedup in equilibrium and nonlinear rheology predictions of the fixed slip-link model," *J. Rheol.* 58, 723 (2014)
50. Pilyugina, E., Andreev, M., Schieber, J. D., "Dielectric relaxation as an independent examination of relaxation mechanisms in entangled polymers using the discrete slip-link model," *Macromolecules* 45, 5728 (2012)
51. Katzarova, M., Andreev, M., Sliozberg, Y. R., Mrozek, R. A., Lenhart, J. L., Andzelm, J. W., Schieber, J. D., "Rheological predictions of network systems swollen with entangled solvent," *AIChE J.* 60, 1372 (2014)
52. Schieber, J. D., Indei., T., Steenbakkers, R. J. A., "Fluctuating Entanglements in Single-Chain Mean-Field Models," *Polymers* 5, 643 (2013)
53. Katzarova, M., Yang, L., Andreev, M., Córdoba, A., Schieber, J. D., "Analytic slip-link expressions for universal dynamic modulus predictions of linear monodisperse polymer melts," *Rheol. Acta* 54, 169 (2015)
54. Steenbakkers, R. J., Tzoumanekas, C., Li, Y., Liu, W. K., Kröger, M., Schieber, J. D., "Primitive-path statistics of entangled polymers: Mapping multi-chain simulations onto single chain mean-field models," New Journal of Physics 16, 015027 (2014)
55. Chen X., Costeux, C., Larson, R. G., "Characterization and prediction of long-chain branching in commercial polyethylenes by a combination of rheology and modeling methods", *J. Rheol* 54, 6, 1185 (2010)

Table 5.1. Synthesis of 4-arm star PBd at room temperature in benzene[a]

sample	*s*-BuLi	Bd	BMDCSE	4-Arm Star PBd (PBd)		
				M_n (kg/mol)		M_w/M_n[c]
	mmol	mmol	mmol	calcd[b]	obsd[c]	
24KS	0.55	222	0.11	88 (22)	97 (24)	1.05 (1.04)

[a] Yields of polymers were quantitative. [b] M_n(calcd) of PBd = (molecular weight of monomer) × [monomer] / [initiator]. M_n(calcd) of 24KS = M_n(calcd) of PBd × 4. [c] M_n(obsd) and M_w/M_n were obtained by SEC-TALLS using THF as an eluent.

Table 5.2. Input parameters used in Hierarchical and BoB model calculations of 1,4-PBd at T=25°C

Parameters	Hierarchical 3.0 Park Parameters	BoB Das Parameters
α	4/3	1
G_N^0 (MPa)	1.15	0.97
M_e (Da)	1650	1836
τ_e (sec)	3.7×10^{-7}	2.75×10^{-7}

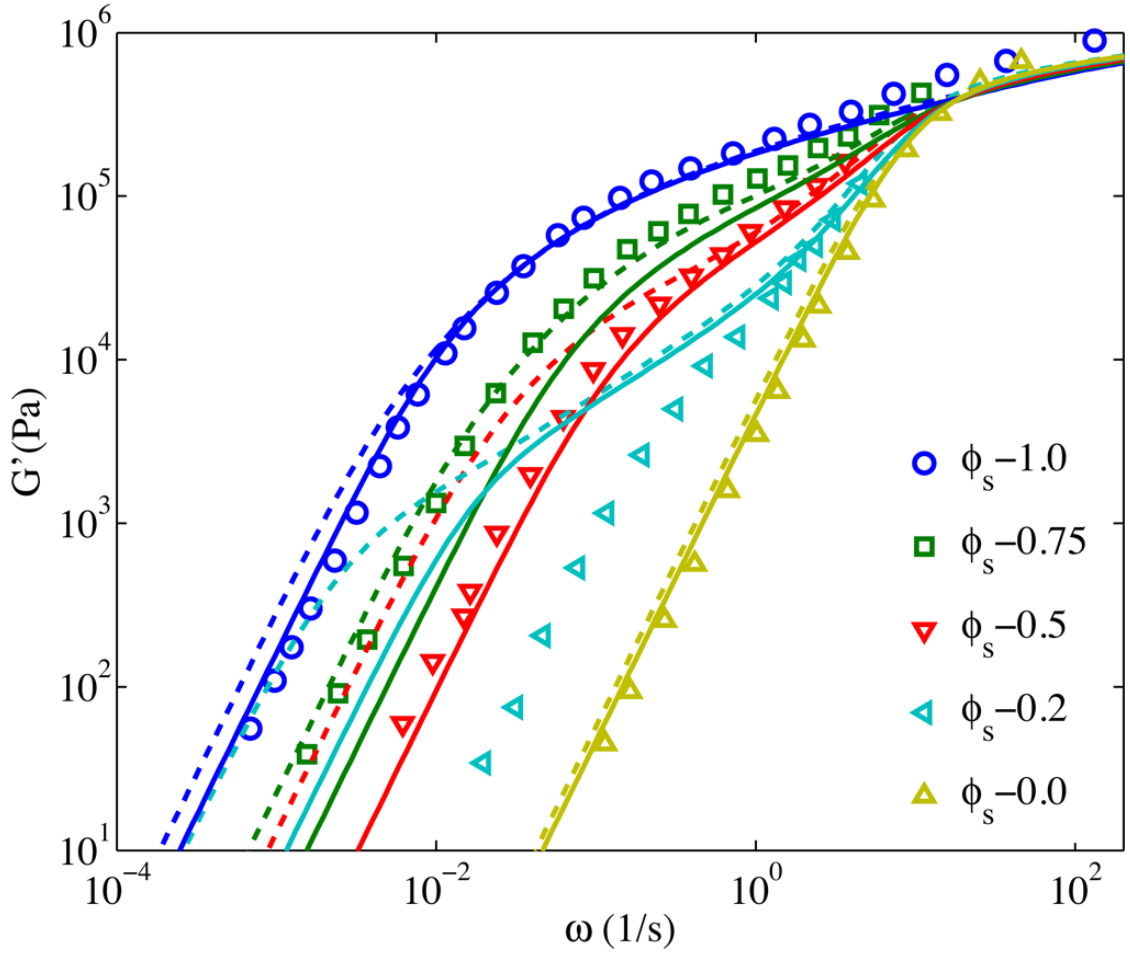

Figure 5.1. Storage moduli, G' for 1,4-PBd42KS-100KL blends at five different star volume fractions as shown. The symbols are experimental data at T=25°C. Solid lines are Hierarchical tube model predictions and dashed lines are BoB tube model predictions both obtained using the 'Park' input parameters and assuming arm retraction in thin tube in the CR-Rouse regime. The data are from Struglinski *et al.*[13]

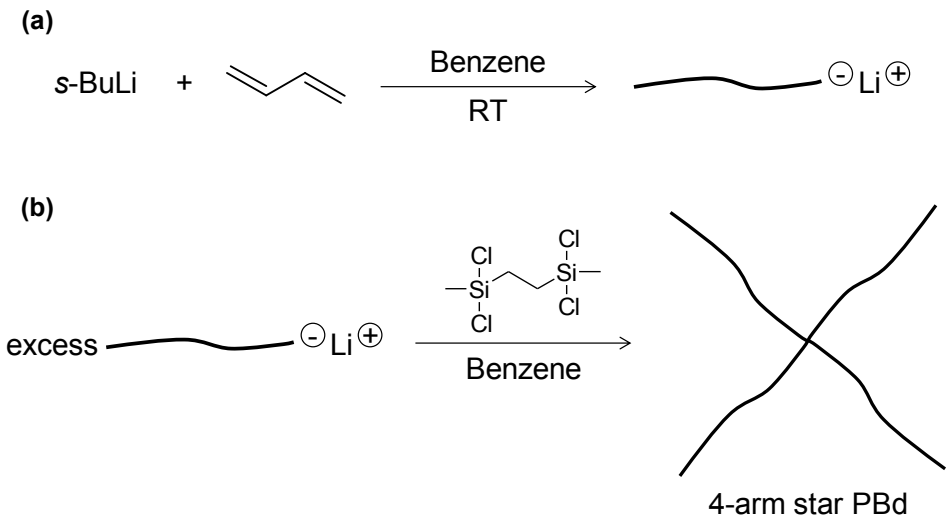

Scheme 5.1. Synthetic route for 4-arm star PBd (24KS) **(Scheme provided by Beom-Goo Kang)**

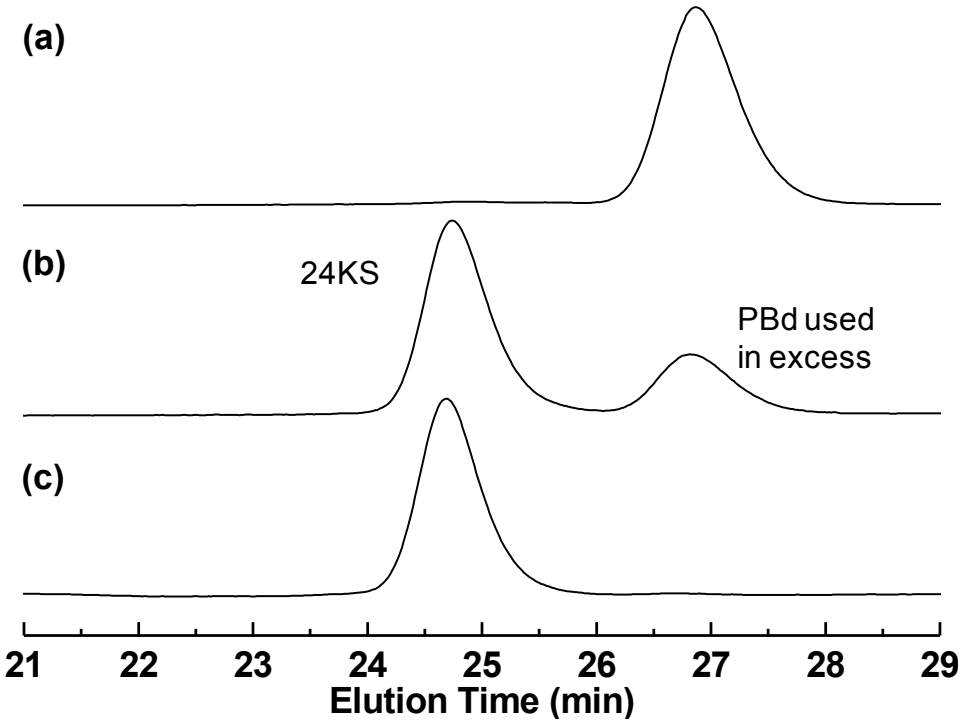

Figure 5.2. SEC curves of (a) PBd (i.e., the linear arms), (b) the polymer mixture obtained from the linking reaction, and (c) 24KS after fractional precipitation. **(SEC curves provided by Beom-Goo Kang)**

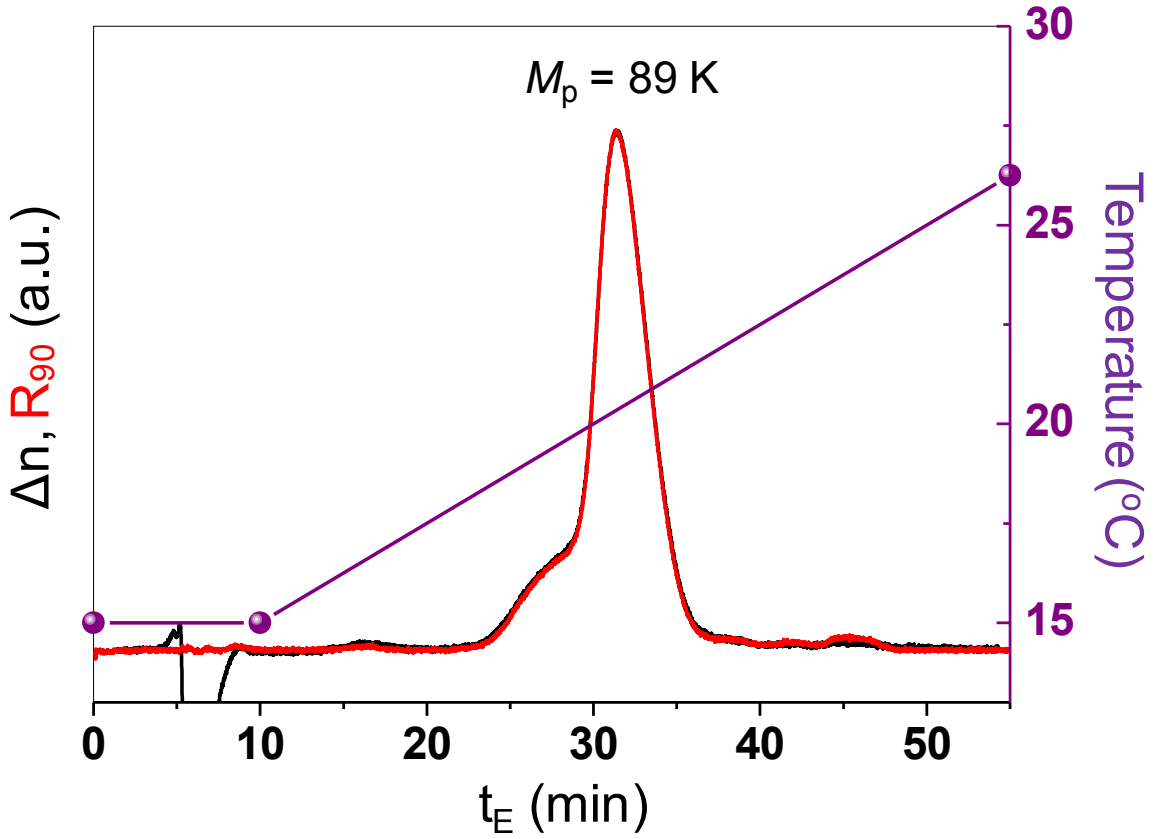

Figure 5.3. RP-TGIC chromatogram of 24KS (after fractional precipitation) recorded by a RI detector (black line) and a LS detector (red line). Peak MW (M_p) is determined by LS detection. Column temperature program is also shown in the plots. **(TGIC plot provided by Sanghoon Lee)**

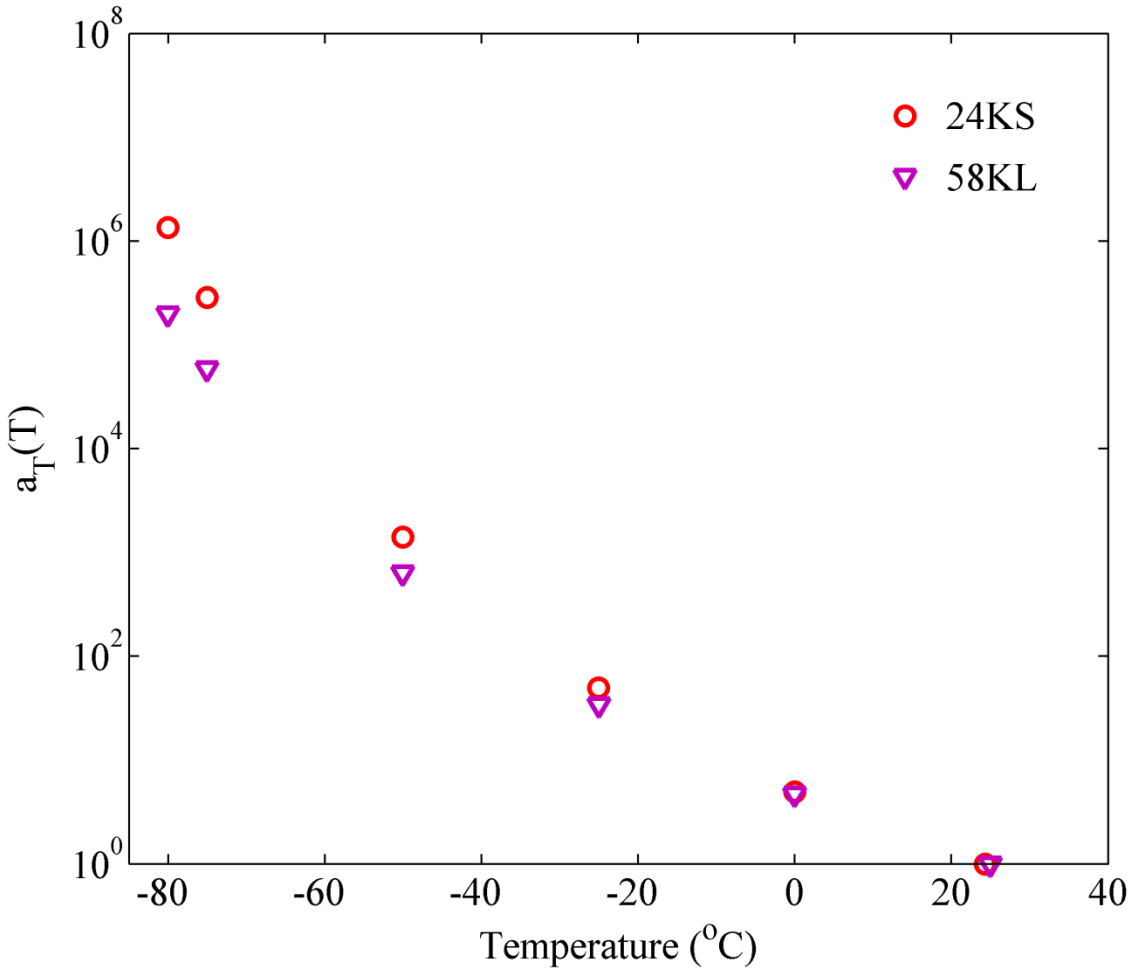

Figure 5.4. Comparison of the WLF shift factors for 24KS star and 58KL linear 1,4-PBds having the same reference temperature of T = 25 °C.

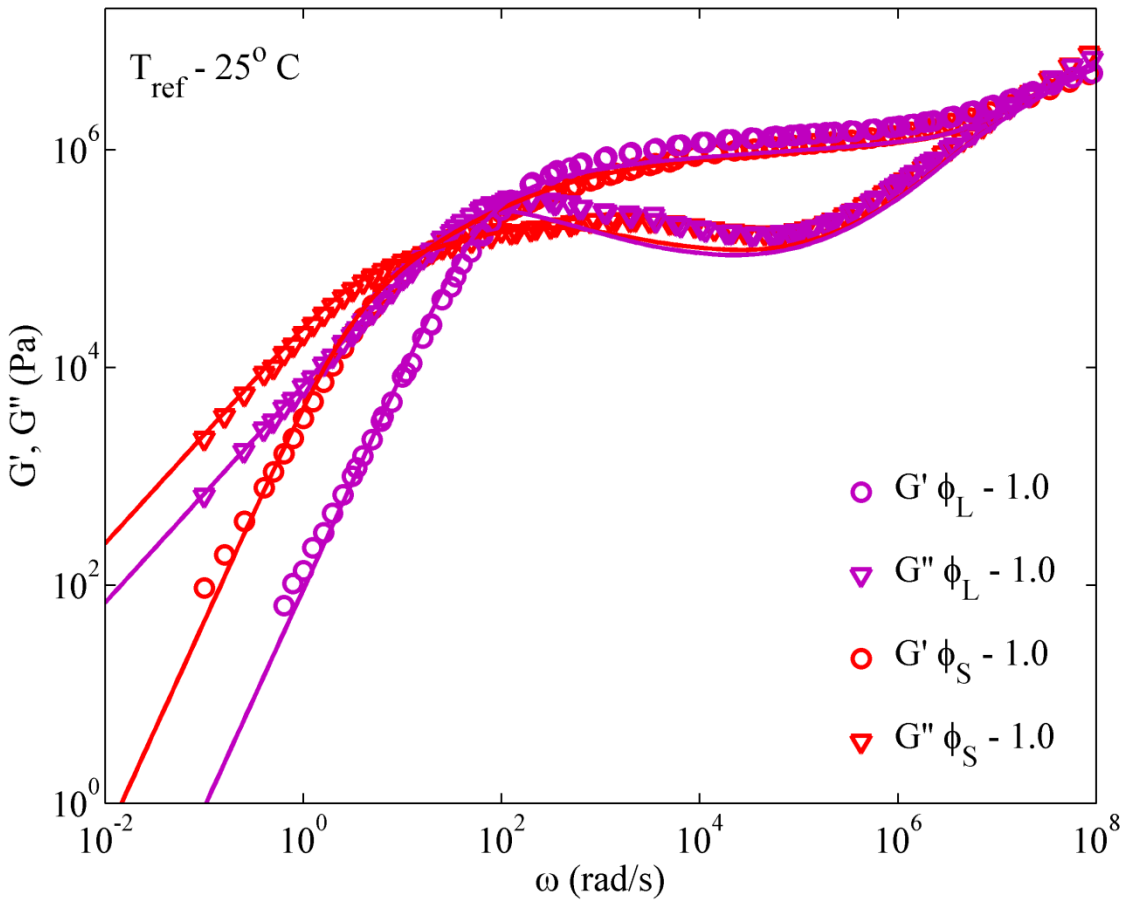

Figure 5.5. Master curves for storage, G' (circles) and loss, G" (inverted triangles) moduli for pure 24KS star and pure 58KL linear 1,4-PBds. The experimental data are time-temperature shifted using the WLF equation and the shift factors from Figure 5.4 to a reference temperature of T=25°C. Solid lines are tube model predictions (Hierarchical 3.0 model) with arm-retraction in a "thin" tube in the CR-Rouse regime using the 'Park' input parameters given in Table 5.2.

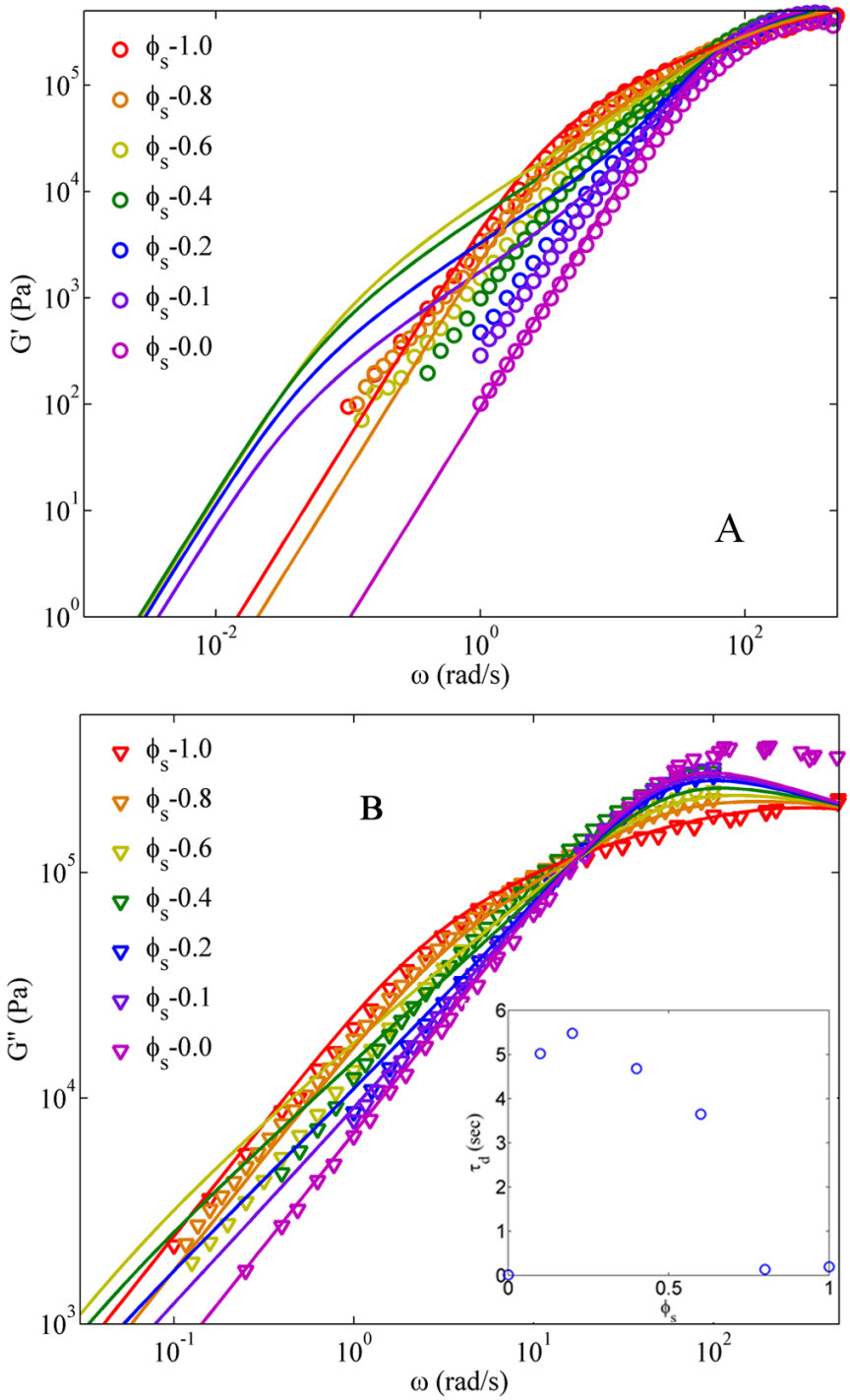

Figure 5.6. A: Storage, G' (circles) and B: Loss, G" (inverted triangles) moduli for PBd 24KS-58KL blends at different star volume fractions as shown. The symbols are experimental data at T=25°C. Solid lines are tube model predictions for the same Hierarchical model and parameters described in Figure 5.5. The inset in 5.6B shows the variation of terminal time, τ_d extracted from model predictions as a function of star volume fraction, ϕ_s .

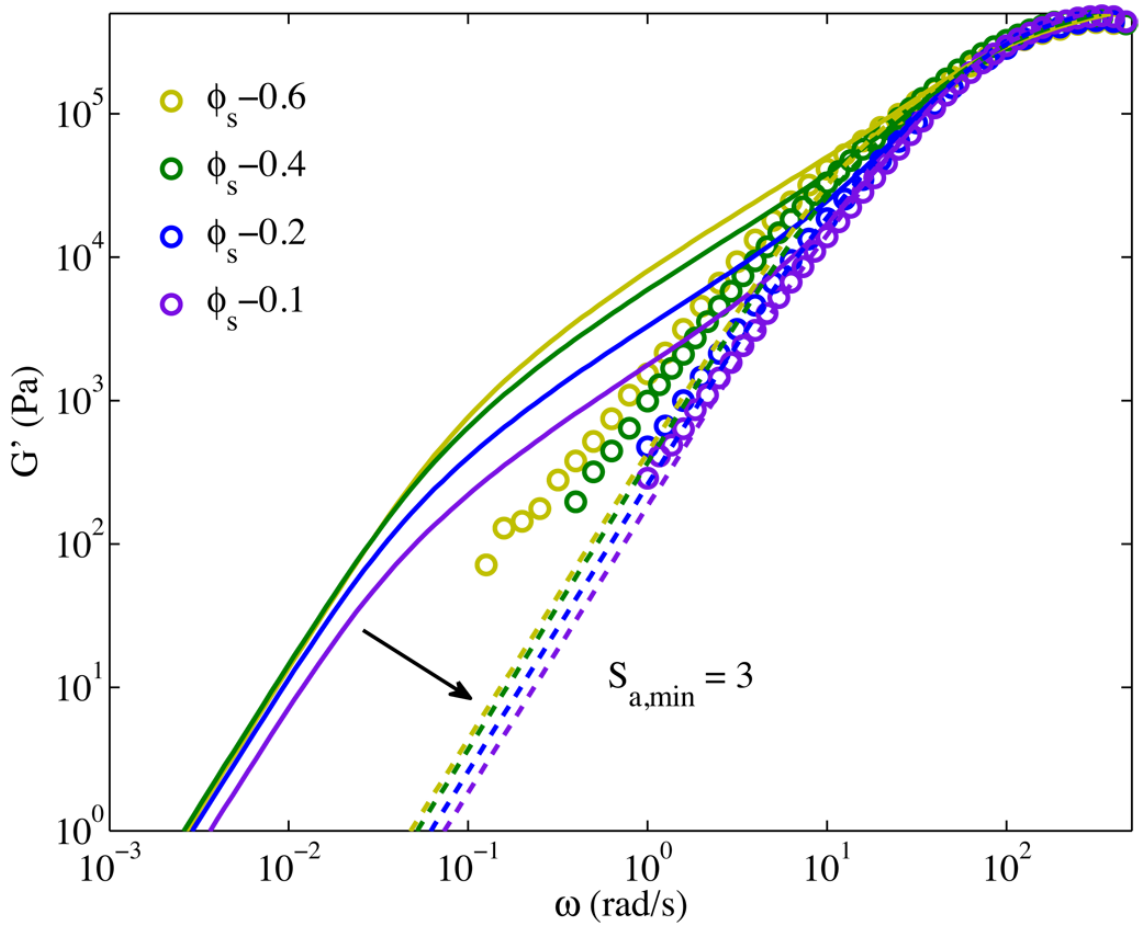

Figure 5.7. The data (symbols) and predictions for arm-retraction in a "thin" tube (solid lines) taken from of Figure 5.6A for four blends, with dashed lines giving the predictions with disentanglement relaxation process activated at the entanglement threshold value of $S_{a,\min} = 3$.

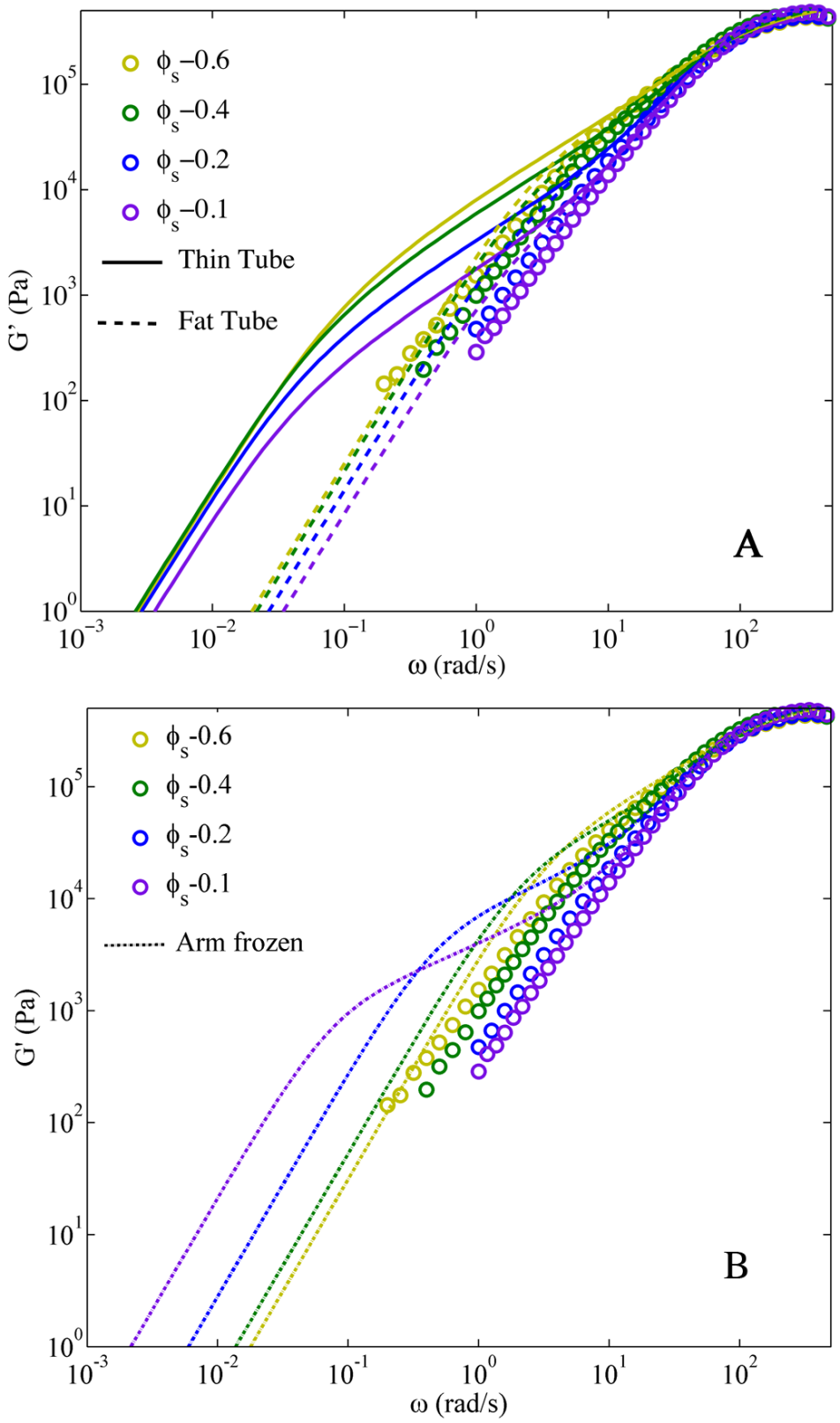

Figure 5.8. The same as Figure 5.7, except in A, the dashed lines show arm-retraction in the fat tube, while in B, the dotted lines show predictions with the 'arm frozen' algorithm in the CR-Rouse regime.

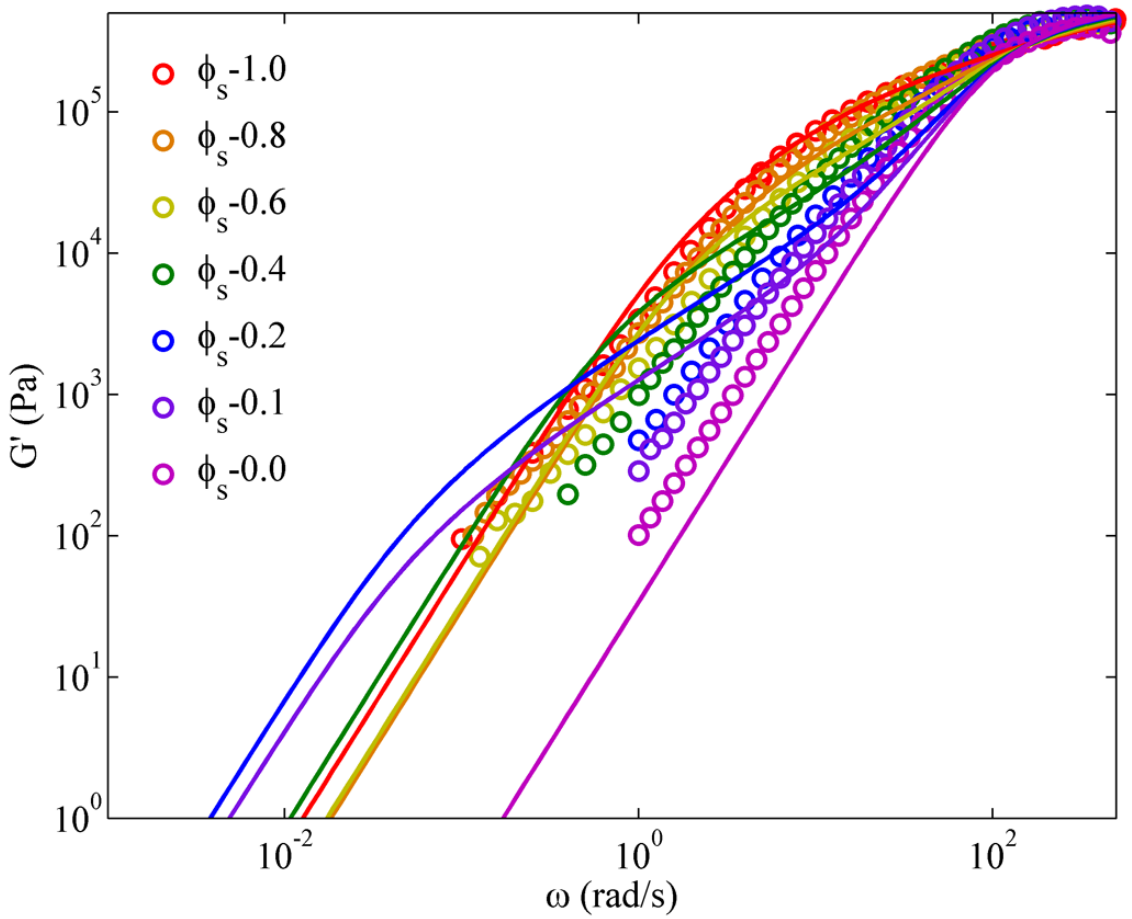

Figure 5.9. The same as Figure 5.6A, except the solid lines are BoB tube model predictions using the 'Das' input parameters.

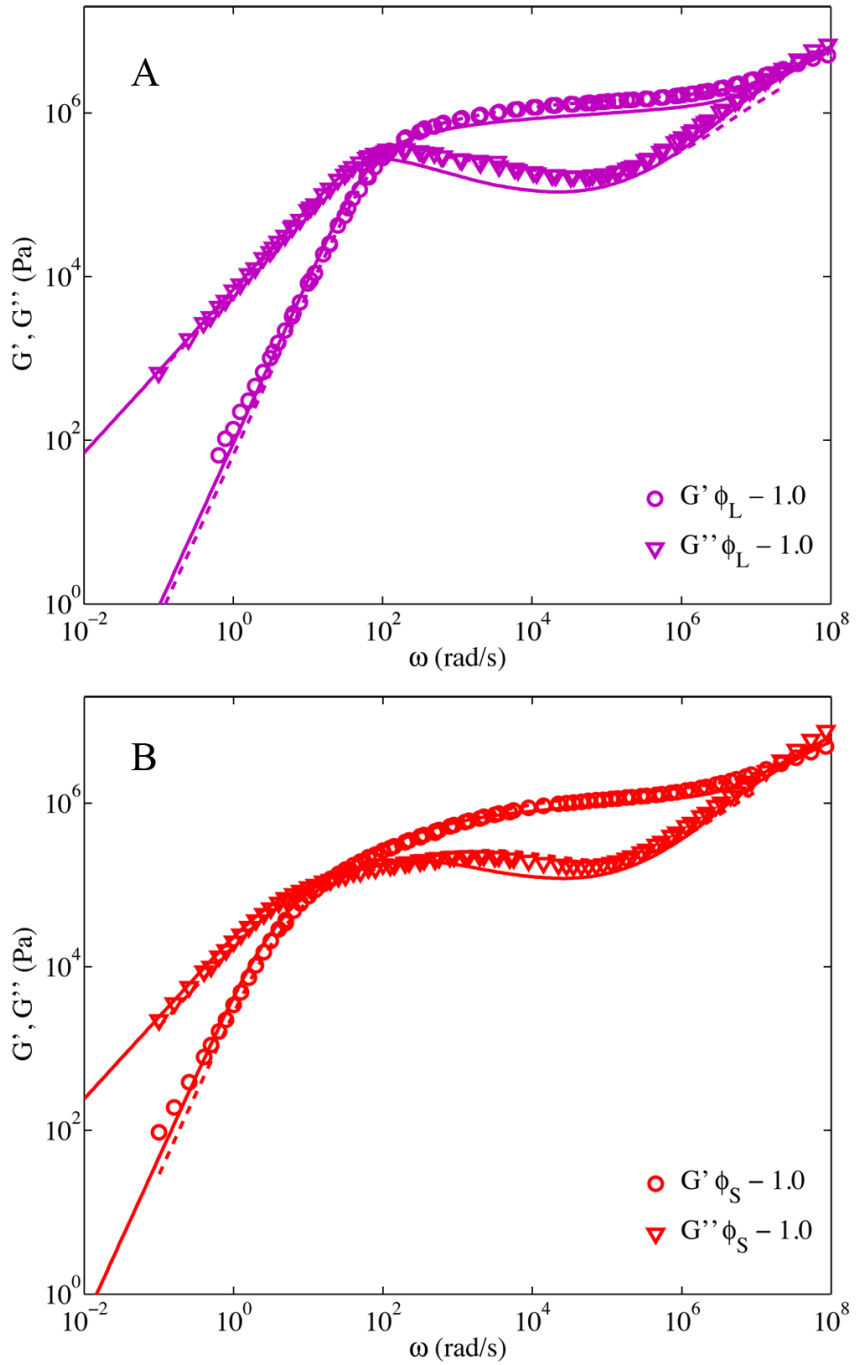

Figure 5.10. Storage, G' (circles) and loss, G" (inverted triangles) moduli for pure 24KS star and pure 58KL linear 1,4-PBds. A shows the CFSM predictions (dashed lines) based on matching the low frequency crossover for pure 58K linear chains data with M_c = 618 Da, τ_c = 0.15 μs. For the star-branched chains, N_c^{sb} /arm = 39, and for the linear chain, N_c^{lc} = 94. B shows the same CFSM predictions (dashed lines) for pure 24K star using the same parameters as in A. Tube (Hierarchical) model predictions are shown as solid lines**. (CFSM predictions in this plot are generated by Maria Katzarova)**

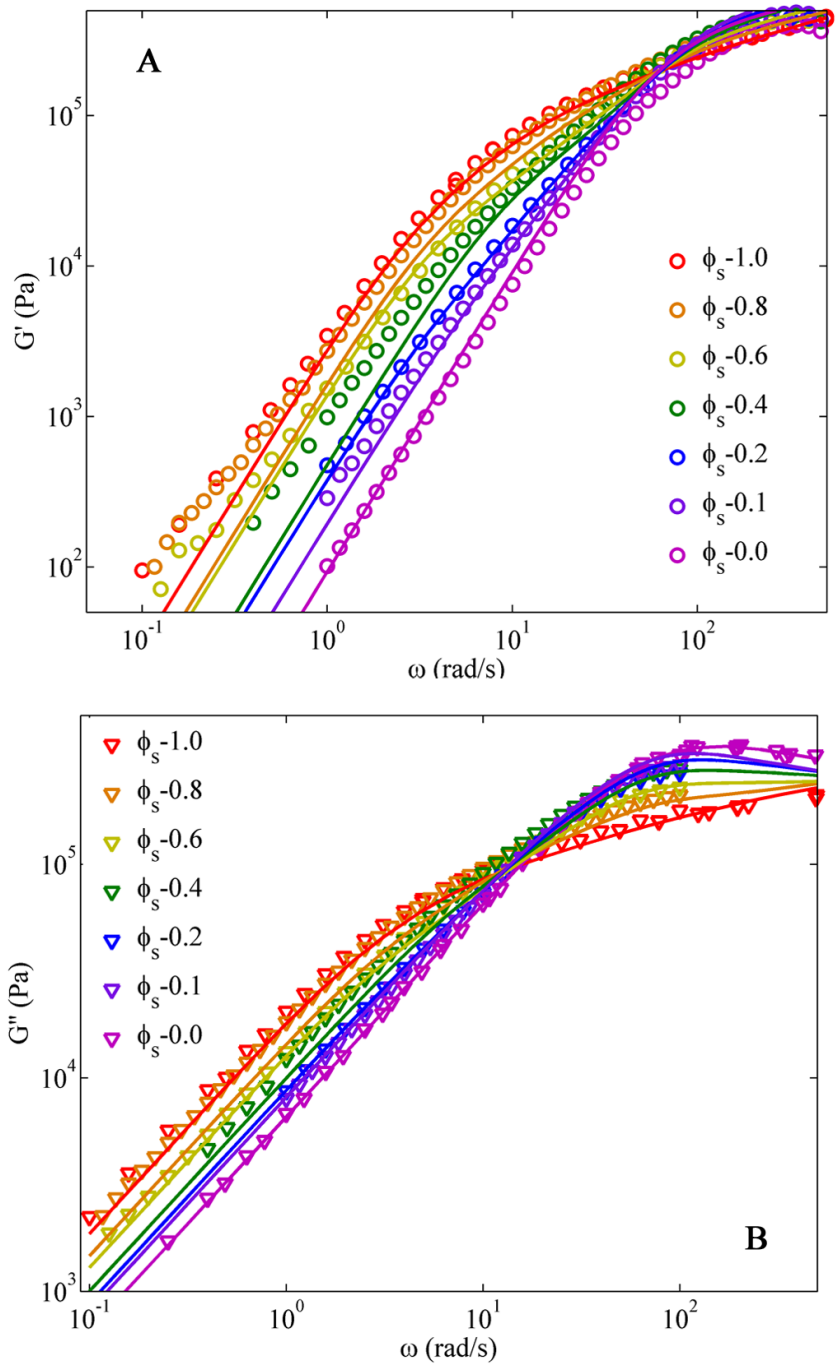

Figure 5.11. A: Storage, G' (circles) and loss, B: G" (inverted triangles) moduli for 1,4-PBd 24KS-58KL blends with decreasing fraction of star-branched chains from *left* to *right* as shown. The symbols are experimental data at T = 25°C. Solid lines are CFSM predictions. The CFSM parameters used were obtained in Section 5.5.2.1.For the star-branched chains, N_c^{sb} /arm = 39, and for the linear chain, N_c^{lc} = 94. A self-consistent τ_c= 0.15 μs, was used for both architectures. **(CFSM predictions in this plot are generated by Maria Katzarova)**

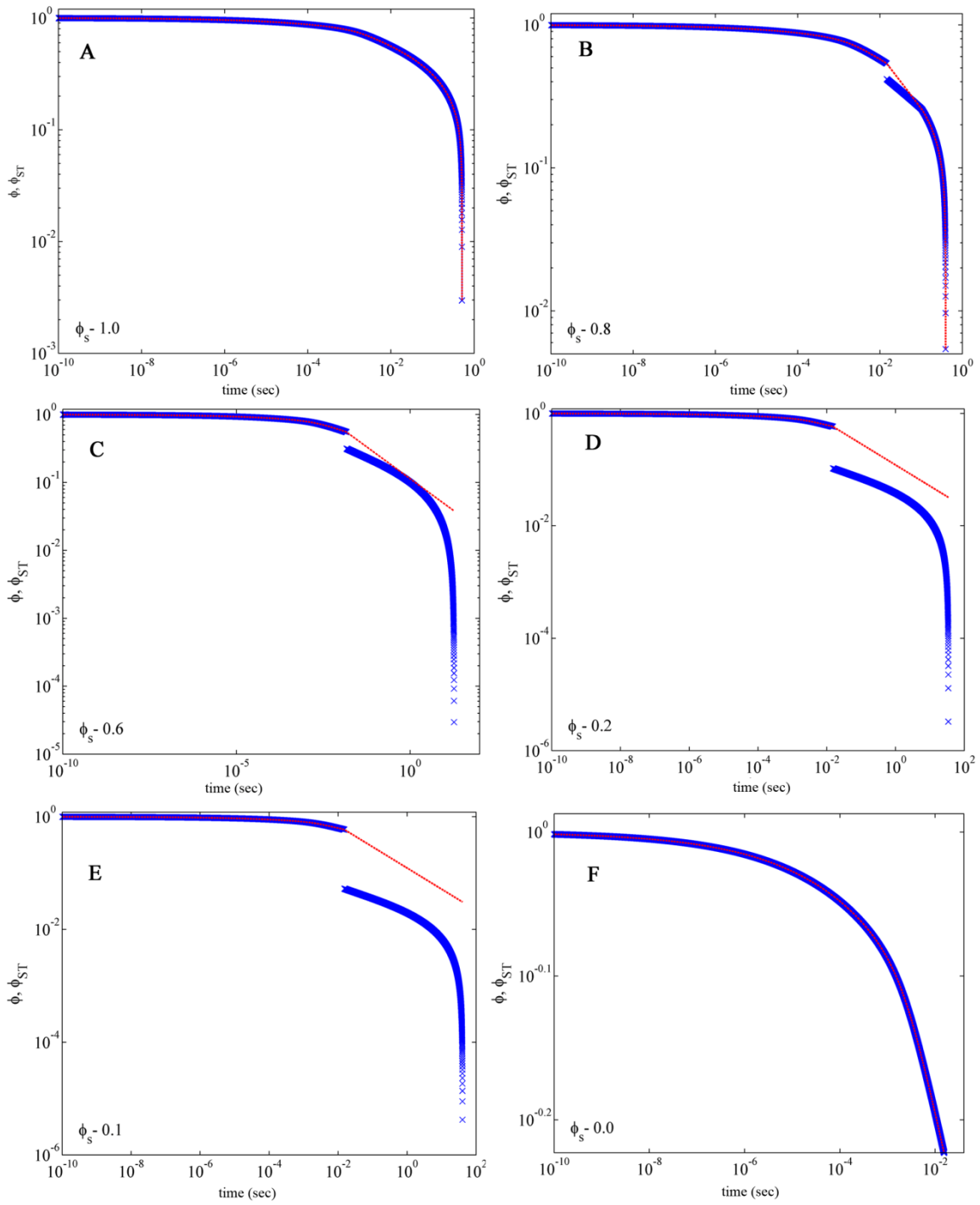

Figure 5.12. Hierarchical model predictions (with parameters described in the caption to Figure 5.6) for un-relaxed volume fraction ϕ (blue symbols) and supertube volume fraction ϕ_{ST} (red dotted lines) as a function of time for 1,4-PBd 24KS-58KL blends with star volume fractions ϕ_s - 1, 0.8, 0.6, 0.2, 0.1, 0 (A, B, C, D, E, F respectively).

CHAPTER 6

Conclusions and future work

6.1. Conclusions

In this dissertation, we have systematically addressed three of the most troubling problems in entangled polymer rheology in both the linear viscoelastic and non-linear viscoelastic regime from the perspective of tube based models and coarse-grained molecular slip-link simulations in additions to using model driven synthesis and design of experiments. These are:

1. In non-linear viscoelasticity, tube model failure to describe extensional rheology difference between entangled polymer solutions and melts

2. In linear viscoelasticity, uncertainties and high variability in tube model input parameters

3. Tube model failure in linear viscoelasticity of binary blends of 1,4-polybutadiene star-shaped and linear polymer melts

The key findings obtained from the results presented in this thesis are summarized below.

Chapter 2 presented a comprehensive review of the advances in tube theory based constitutive modeling of polymer melts and solutions focusing on model prototypes, for example, the FENE-P model used for un-entangled systems and the tube based, DEMG model, for entangled systems focusing on changes in the rheological behavior and its effect on material functions like steady viscosity as concentration increases from dilute solutions to entangled solutions and finally, to melts. For both dilute and entangled solutions, steady extensional viscosity was found to increase with extension rate and that the plateau value of its high-extension rate viscosity was higher than the low-extension rate value. Moreover, the high extension rate plateau in viscosity was same for both the DEMG and the FENE-P model. In other words, at extension rates high enough that the stretch Weissenberg number Wi_s exceeds unity,

the DEMG theory at steady state reduced to the FENE-P model. This is expected, because at high rates, at steady state, the polymer molecules are nearly fully aligned and stretched out, and entanglements become irrelevant to their rheology. However, for melts in extension, their high-extension rate viscosity was found to be lower than their low-extension rate value leading to extension viscosity thinning. In shear, on the other hand, shear thinning increased dramatically with entanglement density as we progressed from dilute solutions to melts.

First, in Chapter 3, to explain the observed qualitative difference between melts and solutions in extensional flows, we developed a simple tube based constitutive model that can accurately discriminate the steady-state extensional viscosity behavior between entangled polymer solutions and melts. Here we developed functional forms based on the concept of Kuhn segment alignment and tested its effect on two mechanisms, 1. tube diameter increase and 2. local friction reduction. In the first mechanism, these formulas gave the dependence on Kuhn segment alignment of tube diameter, and through this on the terminal relaxation time τ_d and plateau modulus G_N. When done self-consistently, this mechanism failed to capture the observed extensional viscosity thinning for melts at $\dot{\varepsilon} > \tau_R^{-1}$. This is because tube widening caused an increase in the maximum extensibility of the tube, $\lambda_{\max}$ which then allowed a reduction of Kuhn segment alignment and orientation. In the second mechanism, we worked on the hypothesis that friction ζ is dependent on stretch/orientation parameter, F_{so} and developed specific functional forms for $\zeta(F_{so})$. These functional forms when included in the DEMG model accelerated both the terminal reptation relaxation as well as fast Rouse relaxation processes but did not cause $\lambda_{\max}$ to change as a function of orientation. This led to significant stretching and orientation between melt subchains, and caused the local friction to decrease in fast flows. Thus, we showed that we can describe the experimental data for both, PS melts and PS solutions, reasonably well.

Second, in Chapter 4, we developed a universal tube model parameter set namely, τ_e, G_N^0, M_e and prescribed their acceptable variability limits for 1,4-polybutadiene which is one of the widely used model polymer for rheology predictions. All of the three parameters were extracted by comparing high frequency linear viscoelastic G' and G" mastercurves for linear,

star, H, and comb architecture 1,4-polybutadienes from literature. The high frequency data for all of the samples compared superposed very well, irrespective of their molecular weight and architecture, indicating universality in high frequency behavior of 1,4-polybutadienes. A value of $\tau_e = (3.7 \pm 0.93) \times 10^{-7} (s)$ for the equilibration time at T=25 ^{o}C was extracted by fitting Rouse predictions to the high-frequency transition frequency data, after subtracting effects of glassy modes represented by the Kohlrausch-Williams-Watts (KWW) expression. We also compared variation of the plateau modulus, G_N^0 with the glass transition temperature, T_g for polybutadienes with varying 1,2 content. The plateau modulus was found to be linearly correlated to the glass transition temperature for polybutadienes with 1,2 content up to 30%. Thus, if we measure the glass transition temperature of polybutadiene, the value of the plateau modulus could be inferred from this correlation more accurately than from the measured 1,2 content, and from it get the entanglement molecular weight, M_e. The plateau modulus, G_N^0 for 1,4-PBd with 1,2 content of 6-12% was found to be $1.20 \pm 4\%$ MPa and the entanglement molecular weight, M_e was calculated using equation, $G_N^0 = \frac{4}{5}\frac{\rho RT}{M_e}$ to be $1478 \pm 4\%$. Thus, all three canonical parameters of the tube model were fixed within a tight range using just the high frequency transition data alone. This removes the freedom of adjustment of the tube parameters made in literature to fit various versions of the tube model to low- and moderate-frequency data.

Third, in Chapter 5, we found massive failure of two of the most advanced tube models, viz., the Hierarchical and the BoB model, to describe linear viscoelastic G' and G" data for binary blends of a well synthesized and well characterized 1,4-PBd star of arm molecular weight 24,000 g/mol and linear 1,4-PBd of molecular weight of 58,000 g/mol, despite their success in predicting the rheology of the pure star and pure linear. This failure was more extreme when the star volume fraction was low enough for the star arms to be sparsely self-entangled i.e less than 3 entanglements per arm after the relaxation of linear chains. This highlighted the inability of the tube models to accurately describe constraint release events in situations where rather abrupt relaxation of a portion of the entanglement network occurs by reptation of linear chains, but the remainder relaxes gradually by arm fluctuations. We also successfully tested the data against the Cluster Fixed Slip-link Model (CFSM) which incorporates both sliding dynamics (SD) of individual chains through the entanglement mesh by reptation and contour length fluctuations,

and constraint dynamics (CD), which captures both the "dynamic dilution" and "constraint-release Rouse" mechanisms of the tube model. However, a one-to-one correspondence of the details of the constraint release processes within the two models requires a more careful interrogation.

6.2. Future work

There are several important issues related to the work presented in this dissertation that need to be resolved in future investigations, both in linear and non-linear rheology. Further work needs to be done in different directions for each of the problems discussed here, to validate the conclusions presented here and to gain a further understanding of these systems.

In non-linear extensional rheology of polymer melts and solutions, we have developed a simple constitutive model which accounts for monomeric friction reduction in the tube model and describes the behavior of linear monodisperse PS solutions and melts. Further modeling efforts need to be invested in describing the new data on extensional rheology of bidisperse PS blends[1] and polydisperse systems, perhaps, by using some form of a mixture rule which takes into account the molecular weights and molecular weight distributions. It will also be interesting to see how important a role monomeric friction reduction plays in describing the elongational rheology of multi-arm, branched systems like pom-pom PS and asymmetric PS[2]. Finally, there are new data sets (blends of PS with oligomeric PS solvent) reported by Huang *et al.*[3] for which consideration of the nematic interaction parameter between the oligomeric solvent and the polymeric molecules, in addition to monomeric friction reduction, becomes important in order describe their elongational rheology. Some progress on modeling their extensional rheology has been achieved by Ianniruberto[4].

In linear viscoelasticity, we were not able to clearly discern the exact values of the dilution exponent, α and fluctuation potential pre-factor, ν. In chapter 5, however, we demonstrated successful slip-link (CFSM) model predictions for binary blends of star and linear polymers. Because slip-link models do not impose a value of either α and ν a priori, best-fit values of α and ν can be extracted from slip-link simulations of star/linear blends that we use to test the tube model. Additional star-linear blends need to be tested using slip-link simulations for this purpose. This will lead to an independent assessment of the values of α and ν.

Finally, rheology is not the only, or even always the best, method for determining constraint release dynamics. A method that provides additional information on the entanglement state, including the apparent tube diameter, is neutron spin echo measurements[5]. However, so far, these measurements have been extended only to microsecond time scales long enough to track the entanglement dynamics of linear and short-arm star polyethylene melts. Another method that provides considerable insight into constraint release dynamics, and is not limited to short time scales, is dielectric spectroscopy. When applied to polymers with type A dipoles, such as cis-polyisoprene, the relaxation of the polymer end-to-end vector is directly obtained. This relaxation is much less sensitive to constraint release than is the stress. As a result, by comparing measurements of dielectric spectroscopy and rheology on the same melts, valuable information can be gained on the contribution of constraint release to the relaxation of stress. We can deploy a combination of rheology and dielectric spectroscopy to obtain deep insight into constraint release processes in linear and star polymers, and into blends of linear polymers of differing molecular weight. Dielectric relaxation is only influenced by the relaxation of the end-to-end vector of the chain, and hence it is very sensitive to long-distance, long-time correlations in chain configuration. In blends, the terminal relaxation of a component stands out sharply in dielectric relaxation, while in mechanical relaxation it is partly obscured by relaxation of the other component. Watanabe[6] has skillfully deployed this combination of rheology and dielectric spectroscopy to obtain deep insight into constraint release processes to a large body of data of monodisperse star and linear polyisoprenes, as well as blends. These results demonstrate that constraint release effects are not completely described by the existing paradigms that rely on simple choices between CR-Rouse motion or full dynamic dilution, or even some simple combination of the two[6]. Existing models do not explain even these "simple" blend data.

One can compare predictions of the tube (Hierarchical) model for branched and linear polymers for dielectric relaxation as well as mechanical relaxation. Since dielectric relaxation of type A polymers tracks relaxation of the end-to-end vector, the hierarchical 3.0 model developed for predicting the rheology of mixtures of branched and linear polymers can be used, essentially without modification, to compute dielectric relaxation, simply by plotting the relaxation of the function, ϕ which accounts for chain relaxation without the contribution of "supertube" or constraint release relaxation, ϕ_{ST} as described in the model description[7,8]. This will enable us to

compare predictions of the tube (Hierarchical) model *for both mechanical and dielectric relaxation* to the dielectric and mechanical relaxation data for cis-polyisoprenes and enable a more rigorous and holistic picture of constraint release.

6.3. References

1. Nielsen, J. K., Rasmussen, H. K., Hassager, O., McKinley, G. H., "Elongational viscosity of monodisperse and bidisperse polystyrene melts," *J. Rheol.* 50, 453 (2006)
2. Nielsen, J. K., Rasmussen, H. K., Denberg, M., Almdal, K., Hassager, O., "Nonlinear branch-point dynamics of multiarm polystyrene," ," *Macromolecules* 39, 8844 (2006)
3. Huang, Q., Hengeller, L., Alvarez, N. J., Hassager, O., "Bridging the gap between polymer melts and solutions in extensional rheology," *Macromolecules* 48, 4158 (2015)
4. Ianniruberto, G., "Extensional flows of solutions of entangled polymers confirm reduction of friction coefficient," *Macromolecules* 48, 17, 6306 (2015)
5. Wischnewski, A., Monkenbusch, M., Willner, L., Richter, D., Likhtman, A. E., McLeish, T. C. B., Farago, B., "Molecular observation of contour-length fluctuations limiting topological confinement in polymer melts," *Phys. Rev. Lett.* 88, 058301 (2002)
6. Watanabe, H., "Slow dynamics in homopolymer liquids," *Polym. J.* 41, 929 (2009)
7. Larson, R. G., "Combinatorial rheology of branched polymer melts," *Macromolecules* 34, 4556 (2001)
8. Wang, Z., Chen, X., Larson, R. G., "Comparing tube models for predicting the linear rheology of branched polymer melts," *J. Rheol.* 54, 223 (2010)